# PREPARATION AND CHARACTERIZATION OF POLY-L-LACTIDE-NATURAL SILICA COMPOSITES

**A Thesis Submitted to the**
**Graduate School of Engineering and Science**
**of İzmir Institute of Technology**
**in Partial Fulfillment of the Requirements for the Degree of**

**MASTER OF SCIENCE**

**in Chemical Engineering**

**by**
**Berna ŞİRVANLIOĞLU**

**October 2023**
**İZMİR**

We approve the thesis of **Berna ŞİRVANLIOĞLU**

**Examining Committee Members:**

**Prof. Dr. Funda TIHMINLIOĞLU**
Department of Chemical Engineering, İzmir Institute of Technology

**Prof. Dr. Mustafa Muammer DEMİR**
Department of Material Science and Engineering, İzmir Institute of Technology

**Assoc. Prof. Dr. Nilay GİZLİ**
Department of Chemical Engineering, Ege University

**18 October 2023**

**Prof. Dr. Funda TIHMINLIOĞLU**
Supervisor, Department of Chemical Engineering, İzmir Institute of Technology

**Prof. Dr. Aysun SOFUOĞLU**
Head of Department of Chemical Engineering, İzmir Institute of Technology

**Prof. Dr. Mehtap EANES**
Dean of the Graduate School of Engineering and Science

# ACKNOWLEDGEMENTS

This thesis was dedicated to firstly to Mustafa Kemal ATATÜRK who is the leader of Turkish people and gave us everything what we had.

I want to express my sincere thanks to my advisor, Prof. Dr. Funda TIHMINLIOĞLU, for all of her advice, support, and encouragement during my MSc studies. I would like to extend a particular thank you to my coworkers Dr. Elif GÜNGÖRMÜŞ DELİİSMAİL, Damla YALÇIN GÖL, Dr. Dildare METİN and Dr. Sedef TAMBURACI for their friendship, support, and assistance.

Additionally, I want to share my gratitude to my family, Yağmur DAĞA ÖZDEN, Tuğberk YAĞDI for their constant encouragement, inspiration, and tolerance during not only my academic career but whole life. I always feel so lucky to be with you all.

I'd like to recognize the assistance and understanding of my friend and supervisor Dr. Özgün DELİİSMAİL and my manager Başak TUNCER from SOCAR R&D.

# ABSTRACT


## PREPARATION AND CHARACTERIZATION OF POLY-L-LACTIDE-NATURAL SILICA COMPOSITES

Tissue engineering research has been primarily focused on the development of customizable 3D scaffolds capable of promoting natural tissue regeneration while providing robust structural support. Synthetic polymer-based composites have garnered significant attention in recent years for biocompatibility and biodegradability, particularly in hard tissue engineering. In this study, we have chosen to combine the synthetic polymer PLA with natural silica as Diatomaceous earth for creating a customizable biomaterial tailored for bone tissue engineering applications.

To create the PLA-Diatom composites, we employed melt mixing and hot-press methods, using two different types of diatoms: calcinated and raw diatoms. To enhance the compatibility of PLA, PEG and PEG/POSS were introduced as plasticizers/compatibilizers. Various concentrations of these plasticizers and reinforcing agents were meticulously applied to the PLA matrix to fine-tune the properties of the PLA biomaterial. Our comprehensive characterization involved SEM for morphology, mechanical testing, rheological analysis, AFM for roughness, contact angle analysis for surface wettability, swelling property, and FTIR for chemical structure.

Our findings revealed that 3% diatom addition into PLA significantly improved tensile strength (32,72±0,27 for PLA and 51,51±4,15 for calcinated to 55,33±0,97 MPa for raw diatom), slight decrease in modulus (2277±45,65 for PLA to 2183,11 MPa for calcinated and 2246,43±24,19 for raw diatom), and reduced strain with higher diatom concentrations. Rheological analysis indicated a shift towards more liquid-like behaviour in PLA-Diatom composites, further enhanced by plasticizers, ensuring stable viscosities. Surface roughness increased with pure and plasticized PLA with diatom application. Surface wettability and water uptake capacity improved significantly compared to pure PLA.

# ÖZET

## POLİ-L-LAKTİD –DOĞAL SİLİKA KOMPOZİTLERİNİN HAZIRLANMASI VE KARAKTERİZASYONU

Doku mühendisliği araştırmaları, doğal doku rejenerasyonunu desteklerken yapısal destek sağlayacak 3B doku iskeleleri geliştirmeye odaklanmıştır. Sentetik polimer-temelli kompozitler özellikle sert doku mühendisliği için biyouyumluluk ve biyobozunurluk özellikleri ile son yıllarda dikkat çekmiştir. Bu çalışmada kemik doku mühendisliğinde kullanılmak üzere tasarlanabilir biomalzeme olarak sentetik polimer PLA ile doğal silika kaynağı diatom kullanılmıştır.

PLA-diatom kompozitler iki farklı tip diatom (kalsinlenmiş ve ham) ile eritilip karıştırılmış ve sıcak press ile basılmıştır ve malzeme uyumluluğunu iyileştirmek için plastikleştirici olarak PEG ve PEG/POSS ile muamele edilmiştir. Plastikleştirici ve güçlendirici katkı farklı konsantrasyonlarda uygulanarak, en iyi malzeme özelliklerini sğlayan kompozisyon araştırılmıştır. Yüzey morfolojisi (SEM), kimyasal yapı (FTIR), yüzey pürüzlülüğü (AFM), ıslanabilirlik (Kontak açı), mekanik ve reolojik analiz, su tutma kapasitesi kapsamlı olarak karakterize edilmiştir.

Elde edilen bulgulara göre iki farklı diatom için de 3% konsantrasyon en iyi sonuçlar gözlemlenmiştir. Mekanik dayanım artmış (PLA 32,72±0,27 MPa, PLA-3CD 55,33±0,97 MPa ve PLA-3RD 51,51±4,15 MPa), modül de (PLA 2277,26±45,65 MPa, PLA-3CD 2183,11±78,81 MPa ve PLA-3RD 2246,47±24,19 MPa) ve uzama değerlerinde (PLA 5,60±0,73 %, PLA-3CD 4,94±0,54 % ve PLA-3RD 3,76±0,10 %) düşüş tespit edilmiştir. Reolojik analiz diatom katkının ve katkı konsantrasyonundaki artışın akışkan davranışı arttırdığını göstermiş veplastikleştiricilerle bu özelliğin iyileştiği tespit edilmiştir. Yüzey pürüzlülüğü, ıslanabilirliği ve su tutma kapasitesi diatom katkıyla artmıştır.

Dedicated to my father

*Dr. Muammer ŞİRVANLIOĞLU*

# TABLE OF CONTENTS

# LIST OF FIGURES

**Figure** **Page**

# LIST OF TABLES

# LIST OF ABBREVATIONS

| | |
|---|---|
| **PLA** | Poly Lactide |
| **CD** | Calcinated Diatom |
| **RD** | Raw Diatom |
| **PEG** | Poly Ethylene Glycol |
| **PEG/POSS** | Poly Ethylene Glycol – Polyhedral oligomeric silsesquioxanes |
| **PLA-3CD** | PLA – 3% Calcinated Diatom |
| **PLA-5CD** | PLA – 5% Calcinated Diatom |
| **PLA-10CD** | PLA – 10% Calcinated Diatom |
| **PLA-3RD** | PLA – 3% Raw Diatom |
| **PLA-5RD** | PLA – 5% Raw Diatom |
| **PLA-10RD** | PLA – 10% Raw Diatom |
| **PLA-5PEG** | PLA – 5% Poly Ethylene Glycol |
| **PLA-10PEG** | PLA – 10% Poly Ethylene Glycol |
| **PLA-5PEG/POSS** | PLA – 5% Polyhedral oligomeric silsesquioxanes |
| **PLA-5PEG-3CD** | PLA – 5% Poly Ethylene Glycol – 3% Calcinated Diatom |
| **PLA-5PEG-5CD** | PLA – 5% Poly Ethylene Glycol – 5% Calcinated Diatom |
| **PLA-5PEG-10CD** | PLA – 5% Poly Ethylene Glycol – 10% Calcinated Diatom |
| **PLA-5PEG-3RD** | PLA – 5% Poly Ethylene Glycol – 3% Raw Diatom |
| **PLA-5PEG-5RD** | PLA – 5% Poly Ethylene Glycol – 5% Raw Diatom |
| **PLA-5PEG-10RD** | PLA – 5% Poly Ethylene Glycol – 10% Raw Diatom |
| **PLA-10PEG-3CD** | PLA – 10% Poly Ethylene Glycol – 3% Calcinated Diatom |
| **PLA-10PEG-5CD** | PLA – 10% Poly Ethylene Glycol – 5% Calcinated Diatom |
| **PLA-10PEG-10CD** | PLA – 10% Poly Ethylene Glycol – 10% Calcinated Diatom |
| **PLA-10PEG-3RD** | PLA – 10% Poly Ethylene Glycol – 3% Raw Diatom |

| | |
|---|---|
| **PLA-10PEG-5RD** | PLA – 10% Poly Ethylene Glycol – 5% Raw Diatom |
| **PLA-10PEG-10RD** | PLA – 10% Poly Ethylene Glycol – 10% Raw Diatom |
| **PLA-5PEG/POSS-3RD** | PLA – 5% Poly Ethylene Glycol – 3% Calcinated Diatom – 3% Raw Diatom |
| **PLA-5PEG/POSS-5RD** | PLA – 5% Poly Ethylene Glycol – 3% Calcinated Diatom – 5% Raw Diatom |
| **PLA-5PEG/POSS-10RD** | PLA – 5% Poly Ethylene Glycol – 3% Calcinated Diatom – 10% Raw Diatom |
| **TGA** | Thermal Gtravimetric Analysis |
| **DSC** | Differential Scanning Calorimetry |
| **AFM** | Atomic Force Microscope |
| **SEM** | Scanning Electron Microscopy |
| **FTIR** | Fourier Transform Infrared Spectroscopy |
| **PE** | Poly Ethylene |
| **PP** | Poly Propylene |
| **ROP** | Ring opening Polymerization |
| **GAG** | Glycosaminoglycans |
| **PGA** | Poly Glycolic Acid |
| **PLGA** | Poly Lactic Glycolic Acid |
| **PPF** | Poly Propylene Fumarate |
| **ECM** | Extra Cellular Matrix |
| **Tg** | Glass transition Temperature |
| **Tm** | Melting Temperature |
| **Tc** | Crystallization Temperature |
| **Tcc** | Cold Crystallization Temperature |
| **HA** | Hydroxyapatite |
| **TCP** | Tri Calcium Phosphate |
| **CaP** | Calcium Phosphate |
| **MMT** | Montmorillionite |
| **Gly** | Glycerol |

| | |
|---|---|
| **PG** | Polypropylene Glycol |
| **Sor** | Sorbitol |
| **MLO** | Maleinized Linseed Oil |
| **ESAO** | Epoxy Styrene Acrylic Oligomer |
| **PBAT** | Poly Butylene Adipate |
| **HSF** | Hybrid Sisal Fiber |
| **SF** | Sisal Fiber |
| **FESEM** | Field emission Scanning Electron Microscopy |
| **ABS** | Acetonitrile Butadiene Styrene |
| **PCL** | Poly Caprolactone |
| **PHB** | Poly Hydroxy Buterate |
| **PDO** | Poly Dioxane |
| **ZnO** | Zinc Oxide |
| **DE** | Diatomaceous Earth |
| **PDLLA** | Poly D,L Lactide |
| **PDLA** | Poly D Lactide |
| **PLLA** | Poly L Lactide |
| **PET** | Polyethylene terephthalate |
| **Xc** | % Crystallinity |
| **MW** | Molecular weight |
| **n** | Flow Behaviour |
| **$TiO_2$** | Titanium Dioxide |
| **HNT** | Halloysite Nanotube |
| **Suc** | Sucrose |
| **TAIC** | Triallylisocyanurate |
| **FDM** | Fused Deposition Molding |

| | |
|---|---|
| **GLY** | 3-glycidyloxypropyl- trimethoxy silane |
| **$SiO_2$** | Silicon dioxide |
| **PBS** | Phosphate Buffer Solution |
| **RPM** | Round per minute |
| **Min** | Minute |
| **YM** | Young Modulus |
| **G'** | Storage Modulus |
| **G''** | Loss Modulus |
| **η*** | Complex viscosity |

# CHAPTER 1

# INTRODUCTION

Polymer composite materials are useful for a variety of industrial applications because they combine various advantages such as lightweight, better physical-chemical properties, high specific stiffness as well as durability [1]. Given the environmental worries, including global warming and plastic wastes, it has become crucial to replace petroleum-based polymers with biodegradable polymers. Therefore, biodegradable polymer composites for medical, packaging, and other related applications have been the main subject in the last two decades of the 20$^{th}$ century [2].

Aliphatic polyesters are a class of synthetic polymers that have gained popularity. They include poly(lactide) (PLA), poly(caprolactone) (PCL), poly (glycolic acid) (PGA), polyhydroxybuterate (PHB), poly(dioxanone) (PDO), and a number of their co-polymers that are synthesized from bio-based origin [3]. Due to its excellent mechanical and biochemical performance among the aforementioned polymers, PLA has been noted and frequently used in the biomedicine field and has received FDA approval [4]. PLA has similar properties to conventional plastics like nylon, polypropylene and polyethylene terephthalate Although it has various advantages, the limitations of PLA's brittleness, hydrophobic surfaces, slow degradation, acidic degradation products, and other intrinsic weaknesses prevent PLA from being used practically any further biomaterial applications [5]. It truly is very challenging to create a reliable biomaterial using only PLA, hence additional studies of hybrid or composite biomaterials based on PLA are necessary to address the aforementioned drawbacks. In literature, various plasticizers/compatibilizers have been employed to improve processability, and flexibility by lowering the glass transition temperature, and increase ductility. These plasticizers for PLA such as polyethylene glycol (PEG), polypropylene glycol, and citrate esters [6]. The most popular of these are PEGs. These polyethers (molar mass in the range of 6000 g/mol) exhibit exceptional physico-chemical characteristics, water solubility, and low toxic effects, making them appropriate for interaction with living things. PEG is incorporated into PLA using a variety of methods, including physical blending, copolymer synthesis (end functionalized, branching or block copolymers), coatings, etc. Due to its simplicity,

physical blending is the method of choice in this case [7]. Recently, new hybrid nanoparticle, Polyhedral oligomeric silsesquioxane (POSS), a class of distinct three-dimensional building blocks with a clear framework and adaptable physicochemical properties, was used as a compatibilizer, through physical blending or chemical bonding to achieve the desired performance in PLA composites. Organic side groups (alkyl, aryl, or any of their derivatives) are joined to the silicon atoms by covalent bonds in POSS molecules, which resemble Si-O cages. [8].

Although PLA possesses sufficient properties for some applications, enhancing its mechanical and thermal, and biological properties through the use of micro and nanoparticles can result in even further improvements for biomaterial applications. Our motivation in this thesis mainly focused on development of PLA based composites for bone tissue engineering applications. Therefore, in particular, the mixing with inorganic and organic additives, such as bioceramics [9], $SiO_2$, nanoclays, silver nanoparticles, ZnO, and biopolymer nanoparticles was reported to be a useful method to address the aforementioned shortcomings of PLA for hard tissue engineering applications [10].

Among those additives, hydroxyapatite (HA) was one of the earliest bioceramics that was investigated. HA is the most stable ceramic and has a low solubility in physiological environments that are influenced by factors like temperature, pH, body fluids, etc. The organism's HA surface has high osteoconductive qualities and encourages cell osteogenesis by inducing the production of mineralized matrix and activating on the replication of genes and proteins involved in the formation of bone tissue [11]. Bioglass (BG) is another exciting ceramic material. It is often employed as a filler for bony defects. After implantation, BG forms a tight relationship with bone tissue, causing it to regenerate and produce new blood vessels. [12]. Halloysite nanotube, has generated a considerable lot of interest in the creation of polymer nanocomposites due to its distinctive tubular microstructure, mechanical characteristics, flame retardancy, greater thermal stability, and adaptable surface chemistry [13]. Montmorillonite (MMT) is a highly effective nanofiller in polymer composites for the intended effects and in biopolymeric composite systems, montmorillonite (MMT), a member of the smectite group of minerals, is the most often utilized nanoclay filler [14].

Being mechanically, thermally and biocompatible stable, immune to microbial attack, and optically apparent silica has several benefits over other inorganic materials. By demonstrating notable gains in structure, modulus, strength, and toughness that cannot be obtained by utilizing the polymer alone, silicate nanoparticles have been widely

exploited to enhance the mechanical properties of synthetic and natural polymers. Consequently, silicate nanoparticles are frequently used as reinforcements in biomedical applications [15]. Silica plays a crucial role in the biomineralization process, which involves the deposition of minerals onto organic matrices to form bone as a bio-safe additive. Silica nanoparticles have been investigated for their potential to mimic the biomineralization process and promote bone mineralization in literature in many polymer composites [16]. Recently, Kaseem et al (2021) have studied the rheological, thermal, mechanical, and biodegradation properties of PLA/silica nanocomposites [17].

Diatomaceous earth (DE) or diatomite, is a natural amorphous silica material made of skeletons of diatoms. It is created by the 'micro-shells' of marine eukaryotic unicellular organisms, or phytoplankton, settling out. Because of the numerous porous patterns that make up the structure of these silica shells, they are ideal for transporting low molecular weight materials. Their huge surface area of almost 200 $m^2/g$ is a result of their nano-porous nature [18]. They have low density, a porous structure, an abrasive quality, chemical inertness, biocompatibility, a high capacity for absorption, low thermal conductivity, strong acid resistance, and permeability, among other characteristics [19]. Due to its surface silanol groups, they are suitable to react organic compound/functional groups, therefore, it is a suitable candidate to be filled with or release active substances that have the potential to have antibacterial or antioxidant effects [20]. In addition, since they are cheap and abundant, they are used as reinforcing fillers, filter aids, membranes abrasives, and insulating materials [21].

Only a few studies have utilized the potential biomedical applications of diatom frustules in literature.  as natural silica particles. The first study was related to the bone tissue engineering applications. Tamburaci and Tihminlioglu (2017) investigated the effect of diatomite loading on the mechanical, chemical, and swelling properties, morphological and surface properties of chitosan composites. These composites were suggested as a potential candidate with desired physical-chemical properties as well as biological activities for bone tissue engineering applications [22].

In this thesis study, therefore, our aim is to combine the useful biomaterial properties of both polylactide and diatomite as a natural silica source as biodegradable composite for bone tissue engineering applications and to investigate the effect of diatomite type (calcinated and raw diatom) and loading on the mechanical, morphological, chemical, rheological, water sorption and surface wettability of composites. In addition, since our motivation is to use these findings later for 3D printing

applications of PLA composites for bone replacement materials, processability of the PLA based materials is important. Therefore, effects of two different plasticizer/compatibilizers, PEG and PEG/POSS, on the properties of PLA-diatom composites were also investigated.

The thesis is structured as follows: An overview of this research is provided in Chapter 1 as introduction. Background information on the literature on synthetic biodegradable polymer PLA, and the impact of silica reinforcement and PEG, PEG/POSS compatibilizers with PLA is provided in Chapter 2. In Chapter 3, the applied methods and characterization techniques that were used in the experiments are discussed along. The results of the study are given and discussed in Chapter 4. Chapter 5 consists of the conclusion and future work.

# CHAPTER 2

# LITERATURE REVIEW

## 2.1. Biodegradable Polymers

A wide range of petroleum-derived synthetic polymers are manufactured globally, and large volumes of these polymers are discharged into the environment as substantial industrial waste. Given the environmental worries, including global warming and plastic contamination, it has become imperative to substitute petroleum-based plastic with biodegradable polymers.

Biodegradable polymers for medical, packaging, and other related applications have been the main subject in the last two decades of the 20$^{th}$ century [1]. According to the European Bioplastics (European Bioplastics and Nova-Institute, 2019)[23], polymers are classified into four main classifications (Figure 2.1). Among those, bio-based biodegradable polymers are considered more sustainable alternatives to fossil-based and non-biodegradable ones. Although raw material source and biodegradability are the main important factors from the environmental point of view, production methods of these polymers are also important for classification point. Figure 2.2 shows the classification according to these production methods.

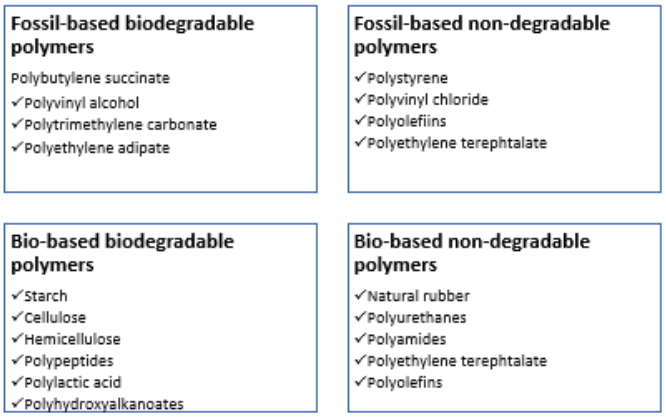


Figure 2.1. Plastic classification due to the source of raw material and degradability [24]

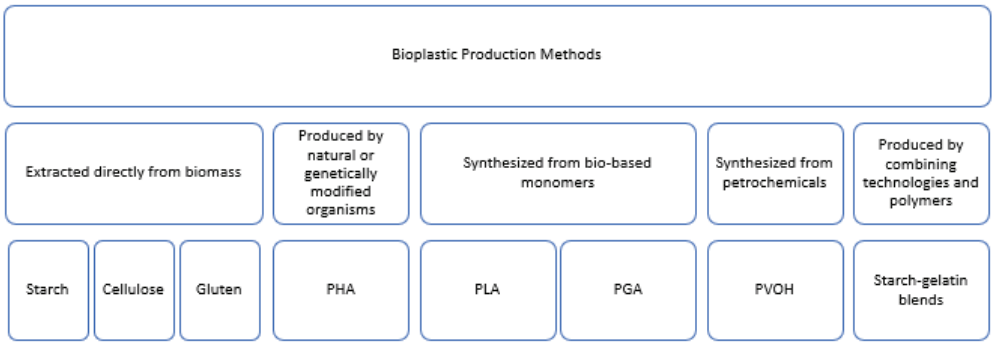


Figure 2.2. Production techniques of bioplastics [24]

Polylactic acid or poly-Lactide (PLA), polyglycolic acid (PGA), PLGA are the most commonly used biodegradable polymers that are synthesized from bio-based origin. These polymers as well as their copolymers or blends, are commonly utilized as biomaterials [25]. Among them, polylactide polymer has gained much attention not only biomedical applications as well in industrial packaging applications due to desired properties [26].

## 2.2. PLA

Poly (lactic acid) or polylactide (PLA) is the most used biodegradable linear aliphatic thermoplastic polyester polymer. It is promising due to the fact that the monomers can be produced from renewable raw materials as well as derived from organic lactic acid [27]. Lactic acid can be produced from high yields of microbial fermentation of sugars that are recovered from sustainable or renewable plant feedstocks. It is the first industrial polymer produced from renewable resources [28].

PLA has enormous value since it can be generated from renewable carbon and is biodegradable, in contrast to other high volume conventional synthetic polymers like polyethylene and polypropylene, they are not biodegradable [29]. PLA can be synthesized by different polymerization processes from lactic acid including: poly-condensation, ring opening polymerization and by direct methods like azeotropic dehydration and enzymatic polymerization. However direct lactic acid polymerization and ring opening

polymerization of L-lactide are the most commonly used [5]. Figure 2.3 shows the main synthesis routes of PLA.

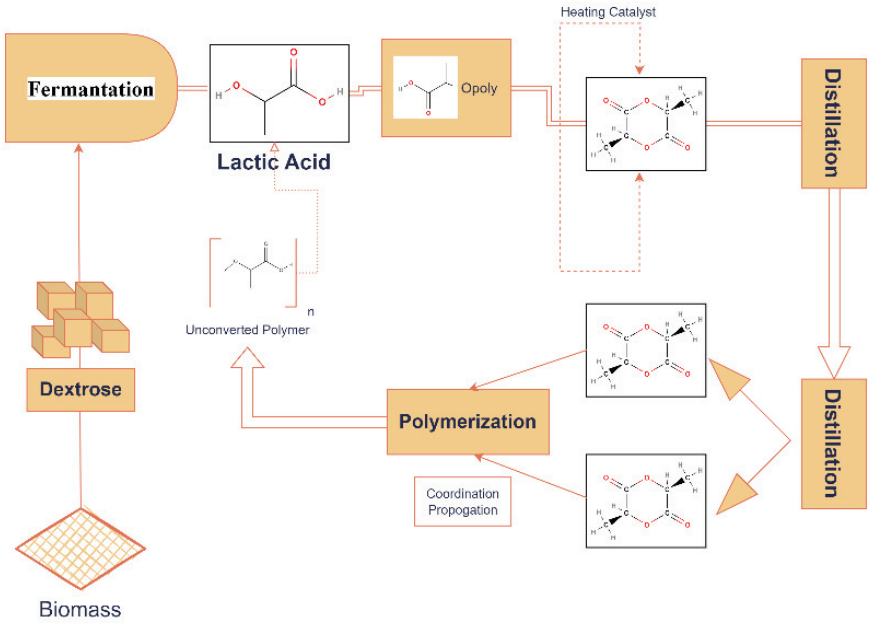


Figure 2.3. PLA synthesis routes [30]

The primary method for producing high-molecular-weight PLA is ROP of lactide which is frequently carried out with a catalyst based on stannous octoate. However, different catalysts or polymerization techniques are also used for laboratory demonstration [31].

PLA is one of the few polymers that may readily modify its stereochemical structure by polymerizing a controlled mixture of L and D isomers to create high molecular weight, crystalline or semicrystalline polymers. It is transparent by nature and may be coloured to achieve different levels of opacity and transparency [2] This polymer usually exists in the stereoisomeric forms of PDLA, PLLA, and PDLLA, as illustrated in Figure 2.4 below.

PLA has similar properties (e.g. elongation, tensile modulus and tear resistance) to conventional plastics like nylon, PP and PET. It has various advantages for production including biodegradability, environmentally friendly, processability and energy savings. However, some disadvantages exist such as toughness, hydrophobic, and slow

degradation time that limits its use in some applications. Although it has good tensile strength and modulus, elongation at break values is low. Slow degradation time and high contact angle of PLA again limits its use in both biomaterial and packaging applications [5].

PLA and the related copolymers were mostly developed as biomedical materials because of their biocompatible and bioabsorbable qualities. They have been employed in a range of therapeutic and medical disciplines, including the manufacture of microspheres and hydrogels, scaffolds, protein encapsulation and distribution, and drug carriers. Good biodegradability, biocompatibility, elasticity, bio stimulatory, and mechanical characteristics are displayed by semi-crystalline, L-Lactide form of PLLA and it is also combined with other polymers and additives to create high-performance composite scaffolds for tissue regeneration applications [32]. Additionally, PDLA is a semi-crystalline polymer, which offers much higher degradation rate than PLLA polymer. This polymer possesses low biocompatibility compared to PLLA, however, PDLA polymer is vastly applied in biomedical applications. PDLLA is an amorphous lactide-derived polymer that has fastest biodegradation time, and high biocompatibility. This polymer is excellent for making porous, biocompatible scaffolds for very short life time applications or drug carriers [33].

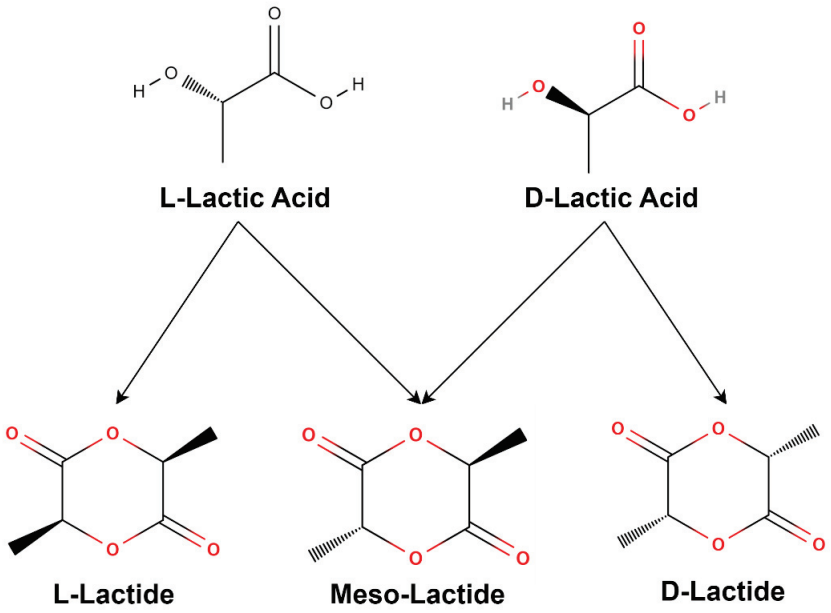


Figure 2.4. Isomeric forms of PLA [2]

PLA's stability, processability, degradation, immiscibility with other polymers, aging, and recyclability are all impacted by its mechanical and physical qualities. Next section gives the important properties of PLA in detail.

### 2.2.1. Crystallinity of PLA

The isomers of PLA's chemical groups, processing temperature, annealing period, and Mw all affect PLA's properties [34]. The crystallinity of PLA and, by consequence, its general characteristics are directly influenced by the stereochemistry and thermal history. The rate of crystallinity, which indicates the proportion of crystalline regions to amorphous content in a polymer, is a crucial characteristic of polymers. Many polymer features, including as hardness, modulus, tensile strength, stiffness, crease, and melting temperatures, are influenced by crystallinity. Three structural configurations known as α, ß, γ are available for PLA crystal growth. The α form forms during melt or cold crystallization, the ß form occurs when the more stable α form is mechanically stretched, and the γ form, which has recently been discovered to occur on hexamethylbenzene substrate [35]. PLA's glass transition temperature ($T_g$) and melting temperature ($T_m$) both gets higher values with increasing levels of PLLA units D-content is also an important parameter that changes properties of PLA. The higher D-content in PLA can cause a decrease in the rate of crystallization and therefore $T_m$ can be lowered [36].

### 2.2.2. Thermal properties of PLA

Characteristic temperatures of a polymer such as glass transition temperature(($T_g$), melting ($T_m$) and crystallization ($T_c$) temperatures, can be determined by differential scanning calorimetry (DSC). The $T_g$ is one of the most critical variables for amorphous PLA since it is at and above this value when there are significant variations in polymer chain mobility. Flexibility is reduced when it is below the $T_g$. PLA can be either amorphous or semicrystalline. $T_g$ and $T_m$ are crucial physical factors for determining behaviour for semi-crystalline PLA [36]. A more significant characteristic is $T_m$ for crystalline polymers. Above it, complete polymer chain mobility takes place, thereby

reducing the mechanical characteristics to zero. The process temperatures should also be determined by considering melting temperature. Since viscosity is dramatically lowered at these higher temperatures to facilitate processability, they are by nature considerably higher than the melting point (Table 2.1).

Table 2.1. Physical properties of PLA and isomers[5]

| | PLA | L – PLA | DL – PLA |
|---|---|---|---|
| $T_g$ [$^oC$] | 45-60 | 55-65 | 50-60 |
| $T_m$ [$^oC$] | 150-162 | 170-200 | Amorphous |

According to literature studies, PLA has a melt enthalpy of 93 J/g at 100% crystallinity ($\Delta H°_m$) [37] The molar mass, thermal history, and purity of the polymer all affect the $T_m$ and the level of crystallinity [38]. Amorphous poly (L-lactic acid) and crystalline PLLA have been shown to have densities of 1.248 g/ml and 1.290 g/ml, respectively. According to reports, crystalline and amorphous PLA have densities of 1.36 g/cm$^3$ for L – lactide, and 1.33 g/cm$^3$ for meso-lactide [39].

## 2.2.3. Mechanical Properties

Lactic acid-based polymers' mechanical characteristics can range greatly, from flexible and soft plastics to rigid and highly durable materials. When greater mechanical qualities are desired, semi-crystalline PLA is favoured over amorphous polymer. Regular repeating units in semi-crystalline polymers enable the chains to fold into crystallites, which are dense areas. In comparison to an amorphous counterpart, they serve as crosslinks to provide the polymer better tensile strengths and higher modulus. Semi-crystalline polymers still contain amorphous regions since no polymer can entirely organize into a crystalline substance [29] When amorphous polymers are dropped below $T_g$, their flexibility is substantially diminished. Segmental motion is non – existent at temperatures below $T_g$, and any dimensional variations in the polymer are caused by short distortions of the fundamental valence bonds. Elastomers must be employed above the brittle threshold, although amorphous polymers, such as all those containing D, L – PLA,

work best below $T_g$[40]. Semi-crystalline PLA displays a tensile modulus of approximately 3 GPa with a tensile strength of 50-70 MPa and an elongation at break of around 4%. Table 2.2. gives the mechanical properties of PLA's. Depending on the MW and the steorochemistry, mechanical properties can be tailored. As known, mechanical strength and modulus increase when is MW is higher [5].

Table 2.2. Mechanical properties of PLA [5]

| | Tensile Strength [MPa] | Young Modulus [GPa] | Elongation of break [%] |
|---|---|---|---|
| PLA | 21-60 | 0,35-3,5 | 2,5-6 |
| PLLA | 15,5-150 | 2,7-4,14 | 3-10 |
| PDLA | 27-50 | 1-3,45 | 2-10 |

## 2.2.4. Rheological Properties

Rheology is a key characterization technique for developing polymeric materials with the desired physical properties and for controlling the processing. In the case of rheological characterization, the type of deformation is determined by the condition of the material, which might behave elastically or viscously. In general, elastic materials—also referred to as ideal solids—store energy like a spring. However, viscous materials like water, which is sometimes referred to as an ideal liquid, disperse energy. As seen in Figure 2.5, there is a linear relationship between shear rate and stress. Non – Newtonian fluids, on the other hand, are those that typically do not behave in an ideal manner in anyway. Even though at higher shear rates, the viscosity of the matter might exhibit decreasing (shear-thinning) or growing (shear thickening) behaviour due to shear rate. Certain materials behave like Newtonian liquids at lower shear rates. Pseudoplastic and dilatant fluids are the names of these substances, respectively. When shear stress and strain have a linear relationship with yield stress, a material is referred to as a Bingham plastic, and Herschel-Bulkey fluid exhibits shear thinning behaviour with yield stress (Figure 2.5) [41].

Due to their ability to store and release energy, polymer melts are viscoelastic materials and frequently exhibit shear thinning behaviour, which may be explained by the Power Law model.

$$\tau = K * \gamma^n \qquad \textbf{(Eqn. 2.1)}$$

where n represents flow behaviour and K represents flow consistency. The classification of the fluid type is based on the flow behaviour index. Where n<1 The viscosity of the pseudoplastic fluid is constant at very low shear rates, decreasing with shear rate at middle shear rates, and appearing constant at extremely high shear rates [42].

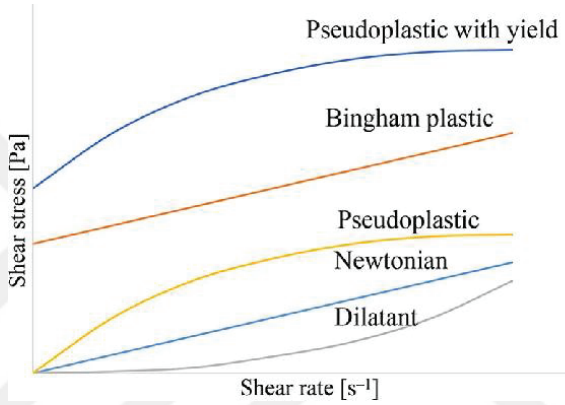


Figure 2.5. Rheological behavior of matters [43]

Table 2.3. Flow behavior [43]

| |
|---|
| n<1 Pseudoplastic |
| n=1 Newtonian |
| n>1 Dilatant |

The viscoelastic behaviour of the sample is roughly described by the storage modulus G' which stands for the elastic component of the viscoelastic behaviour. The viscous component of the viscoelastic behaviour, which is thought of as the sample's behaviour in the liquid state, is characterized by the loss modulus G". Internal friction between the parts of a flowing fluid, and consequently between molecules and particles, is the mechanism that causes viscous behaviour. The formation of frictional heat in the sample and the conversion of the energy generated by deformation into heat energy,

always proceed with this friction. The sample absorbs this portion of the energy; it is then used by its own internal friction mechanisms and is not available to the sample material for further behaviour anymore. This energy loss is also known as "energy dissipation.". The elastic part of energy, on the other hand, is retained in the deformed material by expanding and stretching the internal structures avoiding overstressing the interactions or overstretching or degrading the material. Storage moduli are greater than loss moduli in viscoelastic solids where G' > G". This is a result of linkages inside the substance, such as chemical bonding or physical-chemical interactions[43].

As a viscoelastic fluid PLA, shear thinning behaviour and viscosity changes between the range of a 40 to 2000 Pa.s at 1000 to 10 $s^{-1}$ were observed, as well as the shear viscosities of pure Polylactide and its blends [44].

## 2.3. Reinforcements

Polylactic acid (PLA) is a class of thermoplastic polymers that is frequently employed in biomaterial technology because of its superior processability, biocompatibility, and biodegradability [45]. Besides these benefits, PLA's mechanical and biological properties still need to be improved. The other applications of PLA can be found mainly in packaging technology due to the similar properties of conventional synthetic plastic and eco-friendliness [46]. Our motivation in this thesis mainly focused on development of PLA based composites for bone tissue engineering applications. Therefore, reinforcements used in this field are mostly discussed.

Although PLA possesses sufficient properties for some applications, enhancing its mechanical and thermal, and biological properties through the use of micro and nanoparticles can result in even further improvements for biomaterial applications. In particular, the mixing with inorganic and organic additives, such as nanosize $SiO_2$, nanoclays, carbon nanotube, $TiO_2$, ZnO, and biopolymer nanoparticles was reported to be a useful method to enhance the performance of PLA [47].

In orthopaedics and dentistry, the usage of second generation (biocompatible, bioactive, and biodegradable) calcium salts, such as calcium hydroapatite, tricalcium phosphate TCP, ($Ca_3(PO_4)_2$), CaSi-based ceramics, and bioactive glass, has increased significantly [47]. Especially, synthetic HA ($Ca_{10}(PO_4)_6(OH)_2$) bio-ceramics are a very

interesting biomaterial because they offer good osteoconductivity, osteoinductivity, and biocompatibility. The hydroxyapatite growth on its surface shares a structural composition with bone tissues and chemistry with the mineralized phase of bone, which accounts for the material's strong bonding with bone tissue [48]. The ability of the HA structure to contain a variety of ions, including $K^+$, $Na^+$, $Mg^{2+}$, $Sr^{2+}$, $Cl^-$, and $F^-$, increases both its mechanical capabilities and its capacity for healing [49]. Bio-ceramics made of phosphate are frequently employed in biomedical applications. Due to the nonstoichiometric, poly-substituted, inorganic CaP apatite that makes up 70% of the natural bone matrix. CaP facilitates calcification and enhances the bone resorption procedure [50].

The extracellular matrix, which normally provides the essential strength and acts as a substrate for cell adhesion, motility, and tissue growth, is being imitated by a variety of nano scaffolds [51]. The perfect scaffold should be suitable and biodegradable in order to eventually be replaced with functioning tissue.

In addition to the aforementioned inorganic additives to boost the material's total mechanical strength, cell adhesion abilities, and bone-forming potential, some metallic nanoparticles have frequently been used such as titanium, aluminoxane, and iron [52].

### 2.3.1. Silica based Reinforcement

Silica has been used as an additive in coating, food and biomedical applications. Silica nanoparticles (SiNPs) stand out among the nanoparticulate systems for their exceptional qualities for biological applications. Because of its high surface area, biocompatibility, and durability in acidic tissues, inorganic SiNPs improve the thermal and physicochemical properties of other substances while also shielding them from erosion and thermal deterioration [53]. Non-porous silica nanoparticles, a type of amorphous silica nanoparticles without a distinctive structural shape and in an irregular form, exhibit excellent biocompatibility and are frequently used in therapeutics (as stabilizing agents), drug carriers, imaging, enzymatic encapsulation, and other applications [54].

Its structure contains silanol groups (Si-OH), which make it simple to form covalent bonds with other substances and enable processes like the attachment of

antibodies, nucleic acids, and fluorescent compounds [55]. Typically, Si is absorbed as metasilicate, which is widely distributed in connective tissue. Si is beneficial for increasing bone density and preventing osteoporosis since it is necessary for the metabolic process involved in bone calcification [56]. Likewise, Si contents in nascent bone can generate a considerable degree of osteogenesis during the early stages of bone matrix formation and aqueous Si was able to cause the inorganic phase of bone, hydroxyapatite, to precipitate [57]. According to Nielsen et. al (2004) [58], skeletal collagen and extracellular matrix molecules including sialic acid, such as osteopontin, are impacted by the biochemical action of silicon on bone development processes prior to the creation of bone crystals. According to a study by Reffitt et. al (2003) [59] physiological quantities of soluble Si can stimulate the production of collagen type 1 in human osteoblast-like cells.

Polylactic acid (PLA)/silica composites have received considerable attention in recent years as highly functional and high-performance materials. Kaseem et al (2021) have studied the rheological, thermal, mechanical, and biodegradation properties of PLA/silica nanocomposites [17]. They found that dispersion of silica nanoparticles is playing a critical role in the determination final properties the composites. In another study of L-lactic acid (PLLA) was polymerized in an environment of silica by Yan et al (2007) without using any of catalysts, but rather in solution, PLLA oligomers are grafted onto silica. In comparison to PLLA composites made with non-grafted silica, the mechanical characteristics of the grafted silica were improved by the PLLA's effective dispersion [60].

Another promising reinforcement used in polymer composite system is Halloysite (HNT). HNT is an aluminosilicate clay mineral with a structural formula of $Al_2(OH)_4Si_2O_5 \cdot nH_2O$. Due to its unique tubular microstructure, mechanical characteristics, flame retardancy, variable surface chemistry, and greater thermal stability, HNT has received a lot of interest in the creation of polymer nanocomposites [61]. The impact of HNT on the thermal characteristics of PLA/HNT nanocomposites was noticed by Alakrach et al (2018) [62]. The impact of halloysite quantity on the mechanical and thermal characteristics of electrospun PLA/HNT composite mats were examined by Dong et al (2015) [63] and Prashantha et al (2012) [64]. Venkatesh et al. (2019) proposed a study for the development of PLA with a nano-clay Halloysite Nanotubes (HNT) for 3D printing of biodegradable fstents for different anatomical purposes which may be specially customized for implants for medical use [65]. Halloysite

nanotubes (HNT) powder, which are reported to be biodegradable and have good mechanical qualities individually, were employed to strengthen Poly Lactic Acid (PLA), which was used as the basis for the investigation. By using the twin screw extrusion technique, HNT loadings of 3% and 5% weight concentration were applied to PLA before being pelletized. - The twin screw extruder with a specific die fixed to it was successfully used to extrude the produced homogenous pellets into filaments with a diameter of 1.750 mm for method that results 3D printing filament.

Uniaxial tensile testing was used to characterize the mechanical characteristics of the 3D printed tensile test bars. HNT addition to PLA matrix increased Young Modulus up to % 3 HNT/PLA on the other hand % 5 HNT/PLA showed lower Young Modulus and even lower than pure PLA, as well. This characteristic was also observed for tensile strength. Elongation values are approximately same for pure PLA and %3 HNT / PLA but more addition of HNT lower the elongation at break as well. Mechanical test results are given in Table 2.4 below [65].

Table 2.4. Mechanic Test results of PLA/HNT composites [65]

| | Young Modulus | Tensile strength | Elongation at Break |
|---|---|---|---|
| PLA | 391,22 | 33,37 | 14,71 |
| PLA/% 3 HNT | 443,58 | 37,44 | 14,7 |
| PLA/%5 HNT | 357,10 | 29,97 | 12,75 |

The thermal characteristics of the 3D printed nanocomposites were evaluated using the DSC technique and the results showed that the addition of HNT to the PLA matrix does not significantly alter the glass transition temperature ($T_g$). However, as the amount of HNT is increased, the cold crystallization temperature ($T_{cc}$) considerably drops, indicating that the HNT has a nucleating impact on the PLA. The reduction in the cold crystallization temperature suggested that nanocomposites were more likely to crystallize and also that heterogeneous nucleation was more likely to occur when thinner crystalline lamella was generated than in virgin PLA [65].

Bioactive glass (calcium sodium phosphosilicate) is also a silica-based additive used in biomedical field as a fiber or particulates in polymers [66]. In the study of Roether et al. (2002), they suggested employing highly porous poly (DL-lactide) (PDLLA) foams covered with and impregnated with bioactive glass (Bioglass®) particles to create innovative bioactive and bioresorbable composites by freeze-drying technique [67]. The foam prepared has two different pore sizes, macropores with an average size of around 100 μm, and microporosity with an average size of about 20–30 μm, which together create a network. It has seen that Bioglass® particles homogeneously dispersed into PDLLA matrix and *in vitro* degradation in simulated body fluid experiments indicated that HA production was seen on the composites' surface. Therefore, it is suggested that the developed composites have potential as scaffolds for guided bone regeneration [67].

With the aid of microcompounding and polymer/particle leaching, Ozkoc et al (2009) created porous PLA-montmorilonite (MMT) nanocomposites. The polymer nanocomposites' compressive properties were increased by the addition of MMT. The surface hydrophilicity of the polymer nanocomposite had a direct impact on how well cells adhered. The hydrophilicity of the PLA surface was improved with the addition of nanoclays. This is caused by a reduction in the interfacial tension between the polymer and water, which increases the hydrophilicity of PLA.[68].

In the study of Kodal and his co-workers (2018), they prepared polyhedral oligomeric silsesquioxane (POSS)/ poly (lactic acid) (PLA) nanocomposites by twin-screw microcompounder. It was reported that crystallization rate of PLA enhanced by the incorporation of POSS particles. POSS induced nucleation of crystals. In plasticized PLA/POSS nanocomposites, a significant association was found between the interfacial chemistry and the nucleation rate. The nucleation activity of the POSS particles was shown to be primarily controlled by polar interactions [69].

### 2.3.2. Diatom as Natural Silica

Diatoms belong to the algae family. Their characteristic feature is the decorated silica shells (frustules) with various shapes and sizes (10–200 μm). Diatoms are considered microorganisms due to their small size. It has relatively low price and abundant. Diatomaceous earth, which is made of diatom shells, covers the bottoms of all

types of water bodies as a result of the abundance of diatoms in water [70]. Diatom shells have a range of pore systems that vary depending on the species as well as within each individual diatom. The ability to capture nutrients and filter out harmful elements is made possible by the pores' various shapes and sizes. Diatoms are a source of three-dimensional nanoparticles silica (60-95%) that is renewable and can be employed in various pathogen-filtering devices (bacteria or viruses) [71].

Diatom frustule, or cell walls, have attracted significant interest in bone tissue engineering in recent years, mostly because of its distinctive morphological structure and chemical makeup. Diatom biosilica has been shown by Thi et al (2016), [72] to dissolve and release silicon ions in aqueous conditions. Diatoms are considered microorganisms due to their small size. Diatomaceous earth, which is made of diatom shells, covers the bottoms of all types of water bodies as a result of the abundance of diatoms in water [73]. It is an important component utilized in the food and chemical sectors as well as construction because of its appealing qualities, such as high sorption capacity, abrasiveness, insecticide activity, and nontoxicity. Diatom shells have a range of pore systems that vary depending on the species as well as within each individual diatom. The ability to capture nutrients and filter out harmful elements is made possible by the pores' various shapes and sizes. Diatoms are a source of three-dimensional nanoparticles silica that is renewable and can be employed in various pathogen-filtering devices (bacteria or viruses) [21]. It has low density, a hierarchical porous structure, a high surface area, abrasiveness, insulating qualities, inertness, absorptive capacity, brightness, and a high silica content. It is frequently used in the food industry. It can be used as a sealant, absorbent, functional addition, natural pesticide, dental filling, and roofing material [71]. It has low density, a hierarchical porous structure, a high surface area, abrasiveness, insulating qualities, inertness, absorptive capacity, brightness, and a high silica content. It is frequently used in the food industry. It can be used as a sealant, absorbent, functional addition, natural pesticide, dental filling, and roofing material [74].

Diatom frustule, or cell walls, have also attracted significant interest in bone tissue engineering in recent years, mostly because of its distinctive morphological structure and chemical makeup. Thi et al (2016), [70] showed dissolution of diatom biosilica in water. Release silicon ions in aqueous conditions has been determined.

These frustules can be used to reinforce biomaterials having micro and nanoscale porosity, and non-toxic structure [75].Only a few studies have utilized the potential biomedical applications of diatom frustules in literature.  as natural silica particles. The

first study was related to the bone tissue engineering applications. Tamburaci and Tihminlioglu et al (2017) investigated the effect of diatomite loading on the mechanical, chemical, and swelling properties, morphological and surface properties of chitosan composites. These composites were suggested as a potential candidate with desired physical-chemical properties as well as biological activities for bone tissue engineering applications [22].

## 2.4. Compatibilizer/Plasticizer

Compatibility refers to a blend's phase morphology and property role in the field of a particular application. Immiscible polymer blends can be made more compatible and have better qualities via the process of compatibilization. Compatibility plays two key roles in stabilizing the produced phase morphology: first, it reduces the size of the dispersed phase by lowering interfacial tension; and second, it prevents the dispersed phase from coalescing. The use of compatibilizers, which are often macromolecular species exhibiting interface activities in heterogeneous blends, can also enhance the interfacial contacts between the dispersed phase and matrix. Useless incompatible mixes can be transformed into useful compatible materials that combine the great qualities of the blend components thanks to the establishment of distinct phase morphology and better interfacial contact [74].

On the other hand, plasticizers, which have low molecular weights, are added to polymer matrix to make polymer films more flexible and processable. The effectiveness of plasticizer depends on its molecular weight, polarity and stability. Plasticizers decrease hydrogen bonds between polymer chains, hence increasing the free volume or molecular mobility of polymers [76]. In literature various plasticizers have been employed to improve processability, and flexibility by lowering the glass transition temperature, and increase ductility. These plasticizers for PLA such as polyethylene glycol (PEG), polypropylene glycol, and citrate esters. One of the most effective PEGs for PLA plasticization has been observed to be polyethylene glycols (PEG), particularly low molecular weight PEG. Moreover, PEG is a hydrophilic, non-toxic, and biocompatible polymer which has been applied in a variety of fields, including biotechnology and industrial manufacture [77]. Srithep and Pholharn (2017) have investigated plasticizing

effect of PEG on PLLA and PDLA. It was found that the addition of plasticizer to the PLA reduced the glass transition temperature of the stereo complex, indicating increased flexibility and improved crystallization rate [78].

Since PLA filaments were used in 3D printing applications recently, processability of the PLA based materials is important. Two ways are generally accepted for maintaining the proper viscosity of PLA-printing; either raising the processing temperature or adding a plasticizer. The best plasticizer to use is one that prevents thermal degradation of the polymer and allows functioning at low temperatures. In one of the related studies in literature, they studied the printability of PLA-PEG blends. The addition of PEG to the PLA solution alters the scaffolds' structure and physico-chemical composition in addition to that, making the scaffold printing process easier due to its plasticizing action [7]. The glass transition temperature, ductility, and processing of PLA have all been improved by using various biodegradable and non-biodegradable plasticizers [76].

The other plasticizers that are used in PLA can be given as examples that Glycerol (Gly), propylene glycol (PG), sorbitol (Sor), and sucrose (Suc) with different compositions, sizes, and forms [79].

Another example is that in order to enhance the interactions between the polymer and the filler, a number of compatibilizer/coupling agents were utilized, including (3-glycidyloxypropyl) trimethoxy silane, epoxy styrene acrylic oligomer, and maleinized linseed oil [18].

## 2.5. Silica Functionalized Hybrid Materials as PEG/POSS

POSS particles, which have inorganic-organic nanosized cage architectures, have the potential to be regarded as a significant contender. The organic groups of the cage may improve compatibility with the polymer matrices, while the inorganic core may offer molecular reinforcement when introduced into them. By modifying the organic groups affixed to the corners of the cage, POSS's chemistry can be adjusted according to its intended use. POSS particles can be combined directly with the matrix to create polymer nanocomposites, or they can be bonded to the polymers during the polymerization process.

Although plasticizing of PLA enhanced its flexibility the tensile strength decreases depending on the plasticizer type and content [80]. It was observed that POSS nanoparticles enhanced the toughness properties of PLA in a more balancing toughness [69]:stiffness ratio. It also improved dispersion with plasticized and non-plasticized PLA composites with higher mechanical properties [69]. It was also reported that rheology of PLA/POSS composites can be affected by the (R) groups attached to the POSS, these groups could cause the interaction between POSS and PLA and therefore could improve mechanical properties It is also suggested to be possibly used in biomedical and tissue engineering because of the non-toxic and cytocompatibility of POSS [80].

Poly(ethylene glycol)-functionalized POSS (PEGPOSS) is one of the POSS nanofillers that can be used to change the properties of PLA since its PEG groups have the ability to make PLA more miscible and, because of their plasticizing impact, to increase PLA's flexibility [81]. Jung et al. (2014) reported that PLA/PEG-POSS nanocomposites were effectively manufactured by combining melts and subjecting them to electron beam radiation. According to the tensile test results, the PLA/PEG-POSS nanocomposites were made more flexible by adding at least 15% weight percentage of PEG-POSS. Additionally, the tensile strength of the nanocomposites was increased to 44.5 MPa by electron beam irradiation at an absorbed dosage of 100 kGy when TAIC was present [82].

## 2.6. PLA – Diatom Composites

Few studies exist in the literature recently related to the reinforcing effect of diatoms in polymers. They are good candidates for reinforcing PLA – based composites due to the excellent properties of diatom frustules explained above. It was reported that dispersion of silica within the PLA matrix during fabrication of composites is the key parameter to enhance the mechanical, thermal, and rheological properties of PLA. Studies on composite systems revealed that, as compared to pure PLA, PLA – composites demonstrated distinctly better mechanical, thermal, and physicochemical qualities. Effect of diatom content on properties of PLA composites was summarized in the following sub-sections.

### 2.6.1. Mechanical Properties of PLA – Diatom Composite Systems

Dobrosielska et al. (2020) investigate the printability of PLA –diatomite composites using diatomite as an enhancer and structural filler. The composites were prepared by fused deposition moulding (FDM) process. Particle size effect on the composite properties were also studied. The composites obtained as filaments, then they were used for 3D printing. An increase in tensile strength and an improved elongation at break were observed in some compositions. Mechanical and rheological properties of the composites were affected by particle size of diatoms [83]. As comparison to the value for pure PLA (37.7 3 MPa), the samples of PLA composites containing diatom shells produced using the same technique demonstrated nearly twice as strong tensile strength (highest value of 63.7 2 MPa). The samples with 1% diatomaceous earth had the highest mechanical strength, it was discovered. Because there are too many discontinuities in the polymer, higher filler concentrations lead to a reduction in tensile strength [21]. As a result, the results showed that eco-friendly, biodegradable, and multipurpose polymers for the FDM process were demonstrated using the acquired materials, which were then shaped into 3D - printed filament and demonstrated satisfactory printability.

In another study related to PLA-diatom composites, Aggarwal et al. (2019) used diatomaceous earth in PLA for 3D printing. Diatomaceous Earth (DE) and PLA pellets were gradually combined using an Xplore® extruder while being kept at a temperature of 175°C and 120 rpm. Following compounding, filaments were extruded to undergo additional processing. The consistency and quality of the created filaments were evaluated for their suitability for 3D printing. On the other hand, the tensile performance of the filaments slightly decreased when diatomaceous earth was added to PLA. About 19% reduction in yield strength was observed with 5 wt% DE. However, modulus of elasticity, which is very identical to all specimens and represents an object's propensity to deform along its axes, a significant decrease in all the attributes with the 15-weight percent DE sample [84].

In the last study regarding on PLA-diatom composites, Aguera et al. (2019) have prepared PLA-diatomite (DE) composites by extrusion and followed injection moulding. Numerous compatibilizer/coupling agents (epoxy styrene acrylic oligomer (ESAO), maleinized linseed oil (MLO), and 3-glycidyloxypropyl- trimethoxy silane (GLY) were used to enhance the interactions between the polymer and the filler. The brittle

biopolymer neat PLA, which is utilized as a matrix, has a low elongation at break of 6.4%. Using DE as filler, the bio composite displays a stiffer behaviour. Due of the stiffening brought on by the DE filler, the PLA-DE elastic modulus rises by 7.2% but the elongation and tensile strength at break are somewhat reduced. The elastic modulus rises by 28% when DE has previously undergone a silanization process (PLA-DE-GLY). As the elongation at break improves from 4.9% (PLA-DE) to 5.7% (PLA-DE-GLY), a modest coupling effect may be seen for these composites, suggesting a small drop in brittleness. The tensile characteristics of PLA-DE are largely unchanged by the coupling agent ESAO addition. However, the application of MLO makes it possible to produce a material that is significantly more ductile because of numerous overlapping processes, including PLA plasticization, chain extension, and compatibilization. Tensile strength for PLA-DE-MLO bio composite drops from 62.5 MPa for PLA-DE with no coupling agent or compatibilizer to 40 MPa. The PLA-DE-MLO bio composite behaves less delicately. According to several studies, the dual activity of maleinized vegetable oil is what causes this effect. MLO works as a compatibilizer between the silica DE filler and the polymeric matrix on the one hand. This compatibilization effect, which has also been reported in other polyester composites, is directly connected to the reaction/interaction between both the maleic anhydride attachment groups in MLO and the hydroxyl groups present in both PLA (end-chains) and siloxane/silanol groups in DE [18].

### 2.6.2. Thermal Properties of PLA – Diatom Composite Systems

Thermal characterization of composites is very important parameters which directly tells about important information such as transition points, thermal stability, and processability of the material.

Dobrosielska et.al (2020) reported the thermal properties of PLA-diatom composites. It was found that decomposition of pure PLA and composites occurs in a single stage. Addition of diatoms decreased the $T_g$'s of composites compared to pure PLA (57,7°C). At about 120°C, an exothermic peak on the heating curve known as $T_{cc}$, or "cold crystallization," was reported. The decrease in $T_{cc}$, however, a slight increase in melting temperature, $T_m$, was observed with diatom incorporation in the range of 150-154 $^oC$. They also found that melting peak area increased by the diatom content. This is

explained by the possibility that diatom shells serve as crystallization nuclei and promote the creation of crystallites [21].

In this study of Aggarwal and coworkers (2019), they also investigated thermal properties of PLA-diatom filaments. They demonstrated that nucleation and chain mobility phenomena in the presence of diatomaceous earth particles. It was explained that diatomaceous earth can behave as nucleating agents in the PLA matrix, which improves crystallization and provides an explanation for the observed phenomena [84].

Aguera and coworkers (2019) have prepared PLA-diatomite (DE) composites by extrusion and followed injection moulding. Effects of compatibilizers on thermal behaviour were investigated. Thermal analysis results showed that there is no change on the thermal decomposition behaviour for the compatibilized PLA-DE samples compared to the uncompatibilized PLA-DE. The exothermic peak, which is located between 110 and 130 ºC, is related to the cold crystallization temperature of PLA ($T_{cc}$). Pure PLA exhibits a peak (highest crystallization rate) during the cold crystallization process at 119.4°C and decreases with the DE content. The endothermic peak, which is located between 160° and 175°C ($T_m$), represents the melting process of crystalline PLA domains. The baseline can show a step change at moderate temperatures between 60° and 70°C, which corresponds to the PLA glass transition temperature ($T_g$). The $T_g$ of PLA, which stays at about 63°C, is unaffected by the addition of DE. The highest $T_g$ falls to the value of 60.4°C clearly demonstrates the plasticizing action of MLO compatibilizer [18].

Among various compatibilizers, MLO molecules increased the mobility of PLA polymer chains and have a lower melting point for crystallization. In principle, a plasticizer raises the free volume and hence lowers the interactions between polymers. The $T_{m1}$ and $T_{m2}$ values changed slightly when 10 wt% DE is added to the PLA matrix (PLA-DE), the peak temperatures were 165°C and 172°C, respectively. The use of MLO as a compatibilizer in PLA-DE-MLO composites, however, demonstrates a distinct melting process, defined by a single melting peak centred at 170°C, indicating that all crystalline zones have the same morphological structure and melt temperature range [18].

### 2.6.3. Rheological Properties of PLA – Diatom Composite Systems

To assess the thermal, morphological, mechanical characteristics of PLA composites, a variety of characterisation approaches are applied and rheological analysis were investigated as well. In order to indicate melting behaviour and select better processing type for polymer matrix, rheological analysis must be done. Several researchers investigated the rheological behaviour of PLA and their composites.

Ding et al. (2021) investigated the rheological properties with using a rotational rheometer with a plate diameter of 25 mm and a gap of less than 1 mm, melt-rheological behaviours were assessed. To prevent thermal damage, the frequency dependence was observed at 190°C, 5% stain, under nitrogen flow. The complex viscosity vs frequency and the elastic modulus G′ were assessed. [85]

The diatomite blend's G′, G″, and η* values were comparable to those of PLA/PBAT. The inclusion of talc and diatomite enhanced PLA/PBAT blends compatibility and reduced the mixes' viscosity [85].

In the study of Aguero et al. (2019), they investigated rheological behaviour with an oscillatory rheometer that has a clamp mechanism for solids functioning in a mixture of torsion and shear was used to conduct dynamic mechanical& thermal characterization. Strong stiffness at moderate temperatures is indicated by the G′ result calculated for neat PLA and, in specifically, with the addition of DE. When the temperature rises, especially when it approaches $T_g$ (about 65 °C), this strong storage modulus rapidly declines. This is because the polymer's visco-elastic behaviour has changed. The low storage modulus values (approximately 2 MPa, between 70 and 90 °C) are consistent with PLA's visco-plastic behaviour [18].

In particular, on the addition of just 10 weight percent DE to PLA, G′ increases from 604 MPa (neat PLA) to 1733 MPa. This results in a 287% increase in the overall rigidity at 40 °C, which is a moderate temperature. The various compatibilizing methods used in the study result in a striking modification of the thermomechanical behaviour. Ductility of composites was enhanced by ESAO and MLO resulted in a noticeable decrease in stiffness. The silanized method (PLA-DE-GLY), which was DE was subjected to silanization in aqueous solutions containing 1.3 weight percent GLYMO, exhibits the similar behaviour; however, the drop is somewhat more pronounced for MLO and ESAO. G′ changes for PLA-DE-MLO and PLA-DE-ESAO from 1733 MPa (PLA-

DE) to 1293 and 978 MPa, respectively. Note that ESAO and MLO create composites with reduced storage modulus (G′), even below PLA typical values, at temperatures above 100°C [18].

### 2.6.4. Morphological Properties of PLA – Diatom Composite Systems

Diatom has unique structural properties and adsorption capacity, almost all researches which is on diatom frustules with PLA investigated the morphological features of composites. Han et al (2021) reported that the circular band that connects the two overlapped diatom valves is clearly visible. From the top valve, a few small pores with an irregular radial pattern are also apparent. Aggarwal et al (2019) indicated that it was clearly observed the interphase and boundaries of diatoms in the PLA-DE matrix. Interestingly the diatoms frustules seem to be filled by PLA evidencing potential for good adhesion in the matrix structure [84].

Dobrosielska et al. (2020) have investigated the morphological properties by SEM. It was found that diatom shells in various sizes and shapes are depicted in PLA matrix. SEM photographs of raw fossilized diatomaceous earth revealed that it had a mixture of broken and unbroken shells, including shell agglomerates that ranged in size from 20 to 80 nm and had a diameter of 8 to 20 nm. Regardless of the proportion, the size of the agglomerates grows as the number of diatoms in the matrix increases. Only a small number of the diatom shells are constructed of smooth walls; the rest of them were apparent in the SEM pictures, taking on the configuration of a cylinder and having multiple apertures. This distinguishing trait of diatom shells allowed live diatoms to better absorb and discharge metabolic waste. These pores can be thought of as pores in the context of their impact on the characteristics of diatom shells as a filler. SEM imaging investigations have demonstrated that the pores are crucial to the filler's ability to attach to the polymer matrix [21]. In the study of Aguero’s research (2019), they investigated effects of different compatibilizers on the morphological properties of PLA-Diatom composites. FESEM was used to detect fractured surfaces left over from PLA-DE biocomposites' impact tests. A brittle material's usual smooth and homogenous shape can be seen in the topography of the PLA matrix. Particles of diatomite are visible in the matrix. The micro-gap that surrounds the DE particles shows that there is some loss of

particle-matrix continuity. The results indicated that, in contrast to uncompatibilized PLA-DE composites, there is less interface gap and some interaction between the PLA matrix and the DE particles when MLO produces a biocomposite with superior mechanical balance, enhanced ductility, and a minor resistance loss without sacrificing the biocomposite's good environmental performance [18].

## 2.7. PLA Composites in 3D Printing Applications

For the production of polymer-based composites, traditional techniques like compression moulding and injection moulding are particularly popular. Both manufacturing processes combine temperatures and pressures to create composite materials with improved mechanical qualities. Studies on more modern manufacturing techniques, such as FDM, indicate that they may be able to compete with conventional techniques in terms of usability and minimal human interaction. Yet, due to their inability to create things for mass production, techniques like FDM have been restricted to the creation of prototypes and mock-ups. These production process and design considerations, such as tool rotational speed, raster angle, layer orientations, wall thickness, etc., have an impact on the mechanical characteristics of 3D printed products. To get the greatest increase in both tensile strength and modulus, these variables can be tuned.

In FDM, a heated extruded plastic end melts polymer onto a substrate surface. This process offers several benefits, including ease of use, good printing quality, and ease of adjusting and controlling the structure [86]. Nonetheless due to the layering brought on by the printing technique, the mechanical characteristics of printed goods are heavily influenced by the printing direction [87]. Although 3D printing technology has advanced significantly, there are still a number of noteworthy obstacles to be overcome before it can be accepted as a standard bio fabrication technique in medicine and be used on the medical market. These obstacles include reproducibility, performance by configuration, biomaterials characterization, regulatory hurdles, software design, the capabilities of the 3D printers, and standardization and integration of whole bio fabrication platform. In order to effectively address these problems, the main constraint is the dearth of heterogeneous biomaterials [88].

Because to its low cost, biocompatibility, biodegradability, and ease of processing compared to ABS, PLA is the most popular polymer used for FDM [89]. While being challenging to manipulate because of its rapid cooling and solidification, it may be easily extruded between 190 and 230 °C (melting temperature 175 °C). Because to the generation of lactic acid intermediates during degradation, which could cause tissue irritation (in the case of orthotics) or cell death (in the case of scaffolds), one of the main issues with PLA is its long-term biocompatibility [90]. PLA can easily deform under high temperatures, especially when stressed. The brittle nature of 3D printed PLA pieces makes them more suitable for aesthetic than mechanical uses. This is due to the fact that the layers in the print have small pores and spaces between them related to the 3D printing process. It exhibits weak impact resistance, limited tensile elongation, brittle behaviour, poor heat resistance, and a slower crystallization rate [91]. In order to handle these limitations of PLA, there are some fillers used, because they have the potential to buffer within the normal pH range and to neutralize acidity, organic and inorganic fillers, carbonated calcium phosphates etc. and PLA can be coupled to address this problem [92].

Several of the biomaterial are embedded with inorganic biomaterials because of the inorganic/organic makeup of bone, including hydroxyapatite [93], bioactive glass [94], carbon nanotubes [95], nano clays [96], calcium silicates [97], and calcium phosphates [98].

Due to its involvement in bone remodelling, silica has gained increased attention in recent years [99]. In vivo and in vitro studies with silicon-containing implants and ceramics, such as Si-substituted hydroxyapatites and Bioglass 45S5® [100] give data to support the therapeutic efficacy of silicon in bone. When compared to implants without silicon, silicon-containing bone enhancers and scaffolds were found to attach to bone more strongly. Bone tissue engineering has showed promise using Bioglass 45S5®, which has a $SiO_2$ content of 45%. The main benefits of Bioglass 45S5® are its capacity to bind with bones, release therapeutic ions, and promote cell development and differentiation [101]. But because it was added to polymer scaffolds, the mechanical strength and fracture toughness were reduced [102].

Diatom frustule, or cell walls, have attracted significant interest in the field of bone tissue engineering in recent years, mostly because of its distinctive morphological structure and chemical makeup. Diatom bio silica has been shown by Thi et al (2016), to dissolve and release silicon ions in aqueous conditions. Also, they stated that an in vitro

experiment utilizing Swiss mouse embryonic fibroblast cells showed diatom biosilica particles to have little to no harmful effect (3T3) [70].

There are few researches on the literature about PLA-Diatom 3D printed composites which are helpful to get the idea behind using diatom as inorganic silica source with PLA. Dobrosielska et al (2020) states that in comparison to polylactide (PLA), the composites produced by diatomaceous earth modification of PLA exhibited superior thermal stability and a higher degree of hydrophobicity [21]. Also, it was shown that the composites had a greater WCA after being exposed to water and had a smaller mass change than clean PLA. Regarding the mechanical strength characteristics, the analyses for the composites showed, in certain instances, an improvement in elongation at rupture and a tensile strength increase. The samples additionally displayed enhanced flexural durability. When diatomaceous earth is used to modify polylactide, the melt flow increases proportionately to the modifier's content. Several mechanical and rheological properties of the composites, in addition to the density of the filaments, are affected by the use of various mesh fractions of the filler. With processing in water, the composites made with the diatomite size fraction of 40 μm exhibit stronger hydrophobicity, a higher melt flow index, and higher values for the majority of mechanical strength measures [21].

Aggarwal indicated that to make a composite for 3D printing filaments, diatomaceous earth could be added to PLA as a filler. The finished PLA-DE composite material exhibits minimal material quality deterioration following 3D printing, demonstrating its potential to reduce the price of PLA filaments by 5–10%. Diatomaceous earth was found to behave as nucleating reagents in the PLA matrix, which enhanced crystallization. More diatom concentration appeared to limit chain mobility, and they noticed lower crystallization nucleating efficiency. Future research will examine the reported crystallization phenomena to see whether it is possible to further enhance the material's properties, such as by reducing the possibility of surface water impacts and enhancing the diatoms' dispersion in the PLA-DE matrix [84].

Han et al. (2021) a little different work about PLA-Diatom composites but with 3D Printing method. To evaluate their Si release and compressive strength during in vitro degradation, Diatom biosilica and Bioglass 45S5® PDLGA scaffolds were examined in PBS buffer. The findings indicated that adding diatoms to PDLGA scaffolds slows down their deterioration, with structural decomposition starting up to four weeks later compared with pure PDLGA scaffolds. $Si^{4+}$ ions were released at a much higher concentration from the 5% wt. Bioglass 45S5®-PDLGA scaffold than they were from the 1 and 5 weight

percent diatom-PDLGA scaffolds at the same period. Quick bursting release at week 2 for the Bioglass 45S5® composite could put bone repair at danger. Diatom Biosilica 45S5® incorporation showed a slower release rate of $Si^{4+}$ ions from scaffolds than Bioglass 45S5®. Moreover, compression experiments showed that diatom-PDLGA scaffolds' compressive strength could be maintained for a longer period of time than pure PDLGA scaffolds and 5 wt% Bioglass-PDLGA scaffolds, which is advantageous for bone repair. The silica ions' ability to prevent the PDLGA's deterioration is primarily responsible for the material's sustained compressive strength. Strength must be maintained in scaffolds until tissue has generated and established structure to the extent where scaffold support is no longer necessary [103].

# CHAPTER 3

# EXPERIMENTAL STUDY

## 3.1 Materials

PLA polymer from Naturework company (Ingeo™ 4340D) in pellet form was used as matrix material for the preparation of composites. Two different types of diatoms, natural diatoms or raw (RD) and calcined diatoms (CD), were used as silica-based reinforcing agents. RD was purchased from Sigma Aldrich and CD (Celatoms FW-60 grade) was purchased from Eagle Picher Filtration&Mineral, USA). Polyethylene glycol (PEG) in pellet form with a molecular weight of 4000 and Polyhedral oligomeric silsesquioxanes (POSS) modified with PEG (PEG/POSS, (Hybrid Plastics, USA) were used as plasticizers/additives in composites. PBS (10X) tablets (Sigma Aldrich) were used for swelling studies of the composites.

## 3.2. Methods

### 3.2.1. Preparation of PLA-Diatom composites

Experiments were conducted in two steps as firstly melt mixing of polymer, filler and plasticizer in "Haake- Rheomixer 600" and then compression moulding of composites in Carver Hot-press.

PLA polymer was mixed as matrix material with raw and calcined diatoms in order to prepare PLA/Diatom composites. Melt mixing of polymeric matrices and diatoms were performed with the "Haake Rheomix 600 as shown in Figure 3.1. An excellent dispersion of fillers/additives in the matrix of polymer can be possible with the aid of its design. There are two rotors in the rheomixer that revolve in opposing directions to provide optimal additive dispersion in the polymeric matrix material. For the best mixing, processing parameters of the rheometer; speed of rotor, temperature in the

rheometer and time should be well adjusted. Therefore, in this study, these parameters were initially optimized for PLA polymer according to the design of experiments. The details of the design are given in the next section (3.2.2).

Before compounding process, PLA and diatoms were dried to remove the residual moisture of the materials at 60°C for 12 hours in vacuum oven. The composites were prepared at the optimized processing conditions selected based on the design of experiment results as the mixing temperature of 175°C, the speed of the rotors of 30 rpm and the mixing time of 10 minutes. PLA was initially added to the rheomixer. The torque signal was followed and approximately 2 minutes later PLA melted properly and diatoms were then added to disperse inside of the matrix. For PEG or PEG/POSS incorporated samples, they were added to the matrix just before diatom addition. The composites were prepared with both raw and calcined diatoms at 3, 5 and 10 wt % diatom content. The concentrations of plasticizer/additives were changed between 5 to 10 wt%. Then, the samples taken from the rheomixer were compressed within 150x150x1 $mm^3$ rectangular sheet in Carver Hot-press (Figure 3.2). In order to prevent the void formation, plates were pressed without pressure for 4 minutes, then were pressed at 1500 psi for 6 minutes at 175°C. All specimens were cooled to 60°C in 8 minutes under the same pressure. Table 3.1 lists all the samples prepared at different compositions of PLA, diatoms and plasticizer/additives with the abbreviated codes.

Figure 3.1. General view of Haake Rheomixer


Figure 3.2. Carver Hot Press

Table 3.1. Sample codes and compositions of PLA/Diatom composites

| **Sample Code** | **Content** |
|---|---|
| PLA | Pure PLA |
| PLA-3RD | PLA - %3wt Raw Diatom |
| PLA-5RD | PLA - %5 Raw Diatom |
| PLA-10RD | PLA - %10 Raw Diatom |
| PLA-3CD | PLA - %3 Calcinated Diatom |
| PLA-5CD | PLA - %5 Calcinated Diatom |
| PLA-10CD | PLA - %10 Calcinated Diatom |
| PLA-5PEG-3RD | PLA/%5PEG - %3 Raw Diatom |
| PLA-5PEG-5RD | PLA/%5PEG - %5 Raw Diatom |

**(cont. on next page)**

Table 3.1 (cont.).

| Sample Code | Content |
|---|---|
| PLA-5PEG-10RD | PLA/%5PEG - %10 Raw Diatom |
| PLA-5PEG-3CD | PLA/%5PEG - %3 Calcinated Diatom |
| PLA-5PEG-5CD | PLA/%5PEG - %5 Calcinated Diatom |
| PLA-5PEG-10CD | PLA/%5PEG - %10 Calcinated Diatom |
| PLA-10PEG-3RD | PLA/%10PEG - %3 Raw Diatom |
| PLA-10PEG-5RD | PLA/%10PEG - %5 Raw Diatom |
| PLA-10PEG-10RD | PLA/%10PEG - %10 Raw Diatom |
| PLA-10PEG-3CD | PLA/%10PEG - %3 Calcinated Diatom |
| PLA-10PEG-5CD | PLA/%10PEG - %5 Calcinated Diatom |
| PLA-10PEG-10CD | PLA/%10PEG - %10 Calcinated Diatom |
| PLA-5PEG/POSS-3RD | PLA/%5PEG/POSS/ - %3 Raw Diatom |
| PLA-5PEG/POSS-5RD | PLA/%5PEG/POSS - %5 Raw Diatom |
| PLA-5PEG/POSS-10RD | PLA/%5PEG/POSS - %10 Raw Diatom |

### 3.2.2. Optimization of Process parameters of Melt Mixing

Optimization of mixing process parameters were performed with the aid of Minitab software by Box – Behnken Design method. Melt mixing process depends on the parameters as temperature, RPM and time. Significance of these 3 parameters as process input factors, as well as interactions between them, were examined using a Box-Behnken Design and response surface methodology (RSM).

Process output was mechanical properties (tensile strength) as response variable. Melt mixing of PLA was done at three different temperatures as 165$^{o}$C, 175$^{o}$C and 185$^{o}$C and three different mixing speed as 20 RPM, 30 RPM and 40 RPM with three different melting time as 8 minutes, 10 minutes and 12 minutes. The levels of the factors were coded as -1, 0 and +1, corresponding to the low, medium and high levels, respectively. Table 3.2 lists the experiments done according to the design of experiments. All statistical analyses were performed by MINITAB 21 Statistical Software.

Prepared molten PLA were pressed in Carver Hot-press at 175°C for 10 minutes. Then, they were cut with Ceast hollow die punch according to ASTM 638. Tensile strength was determined using Testometric mechanical test instrument. Based on the optimization results, PLA diatom composites were prepared at the optimum melt compounding conditions.

Table 3.2. Experiments performed according to the design of experiment for the optimization of melt mixing process

| Batch Number | Temperature [C] | RPM | Time [min] |
|---|---|---|---|
| 1 | 165 | 20 | 8 |
| 2 | | | 10 |
| 3 | | | 12 |
| 4 | | 30 | 8 |
| 5 | | | 10 |
| 6 | | | 12 |
| 7 | | 40 | 8 |
| 8 | | | 10 |
| 9 | | | 12 |
| 10 | 175 | 20 | 8 |
| 11 | | | 10 |
| 12 | | | 12 |
| 13 | | 30 | 8 |
| 14 | | | 10 |
| 15 | | | 12 |
| 16 | | 40 | 8 |
| 17 | | | 10 |
| 18 | | | 12 |
| 19 | 185 | 20 | 8 |
| 20 | | | 10 |
| 21 | | | 12 |
| 22 | | 30 | 8 |
| 23 | | | 10 |
| 24 | | | 12 |
| 25 | | 40 | 8 |
| 26 | | | 10 |
| 27 | | | 12 |

### 3.2.3. Characterization of Composites

The characterizations of the composites were performed in order to obtain the morphological, mechanical, thermal and rheological properties, as well as swelling % and surface topography & wettability characters of composites.

### 3.2.3.1. Morphological Properties

Scanning electron microscopy (SEM) was used to examine the morphology of PLA/Diatom composites. The surfaces of fractured side of tensile tested specimens were examined by Philips XL 30 SFEG SEM. Diatoms morphology as well as its dispersion into the matrix and the interface between polymer and diatoms were investigated with the surface images of fractured surface. Before the analysis, samples were coated with a gold thin layer by Emitech K550X under Argon gas.

### 3.2.3.2 Surface Characterization of Composites

Atomic force microscopy (AFM) imaging was performed by using Nanoscope IV MMSPM (Digital Instruments Inc., USA). A three – dimensional picture of the surface is often created in AFM imaging modes by scanning cantilever over the surface. The cantilever tip is in contact with the surface, and the cantilever and sample interaction are being measured. AFM imaging modes offer a variety of information about the surface of the material under investigation. Point probe cantilever tip was used in contact mode to determine the surface morphology and roughness of PLA/Diatom composite plate samples. Three scanned regions, each measuring 10x10 μm were used to investigate the roughness character of each sample.

Surface wettability property of the composites was measured using the KSV Attension Theta Optical Tensiometer. 6 μl of ultrapure water was dropped on the composite surface during the analyses. Ten duplicates of the analyses were performed for each sample, and the resulting average values of the repeated measurements were

reported. The contact angles of the analysed composite were computed digitally by a computer program, and the mean value was calculated for each composite sample.

### 3.2.3.3. Mechanical Properties

Mechanical properties were measured according to ASTM 638 standards. Compression moulded plates were cut as a shape of dog bone according to the standard size using a Ceast Hollow Die Punch. Testometric mechanical testing equipment was used to determine tensile mechanical properties such as tensile strength, stress and strain at break, Young Modulus from the stress-strain data. Cross tip speed was 50 mm/min and the maximum load of mechanic test equipment was 100 kN and the results were obtained using Testometric Co. WINTEST software. The conditioning of the samples was conducted at 25$^{o}$C and 50% relative humidity for 24 hours according to the standard before mechanical testing. The data was reported as the average of at least five samples of each composite sample.

### 3.2.3.4. Thermal Properties

In order to investigate thermal properties of composites, differential scanning calorimetry (DSC), and thermal gravimetric analysis (TGA) analyses were performed by using TA instruments Q10 and Perkin Ermer Diamond TG/ DTA.

DSC analyses were carried out to determine the glass transition and melting temperature of pure PLA and PLA-Diatom composites under nitrogen atmosphere with flow rates of 20 L/min at a heating rate of 10$^{o}$C/min from room temperature to 600$^{o}$C, Crystallization temperature of composites were determined by initially heated to 600$^{o}$C with a heating rate of 20$^{o}$C/min, then, cooled to 0$^{o}$C with a cooling rate of 20$^{o}$C/min, and then heated to 600$^{o}$C with a heating rate of 20$^{o}$C/min again using nitrogen flow of 20 L/min.

Thermal stability of the composites was examined by Perkin Elmer Diamond TG/ DTA analysis from room temperature to 600$^{o}$C with a heating rate of 30$^{o}$C/min. The analyses were carried out in a nitrogen-free, dry atmosphere.

### 3.2.3.5. Fourier Transform Infrared (FTIR) Analysis of Composites

Chemical structure of PLA-Diatom composites was evaluated by FTIR analysis. Effect of plasticization on the chemical interaction between PLA polymer and diatom silicas were also investigated. FTIR analysis was made with Schimadzu 8601 Infrared Spectroscopy at a resolution of 4 $cm^{-1}$ in the wavenumber range of 400-4400 $cm^{-1}$ and 20 scans between the specified wavelengths.

### 3.2.3.6. Rheological Properties

Effects of diatom type and loading and plasticizers/additives on rheological properties of PLA were investigated by TA Rheometer Trios V4.5.1.4249. The measurements were carried out using a parallel plate rheometer. Two identical 25 mm plates were used for measurements with 1 mm thickness of each sample. Dynamic strain sweep tests at 175$^{o}$C and average frequency of 10 rad/$s^{-1}$ were done to determine the upper limit of linear viscoelastic properties of PLA and PLA-Diatom composites. To minimize non-linear response and to get reasonable signal intensities even at high temperatures, the strain intensity was maintained at 1%.

Dynamic frequency tests were carried out at 175$^{o}$C which was chosen as process temperature of composites. Complex viscosities, loss modulus and storage modulus were all examined.

### 3.2.3.7. Water Sorption Capacity of Composites

Samples were cut out from the plates of PLA and PLA-Diatom composites with 1cmx1cm dimensions. The dried specimens were then placed in static 25$^{o}$C Phosphate Buffer Solution (PBS) bath for 4, 12, 24 and 48 hours to obtain water sorption capacity of samples. After the incubation periods, samples were weighted ($W_t$) after removing extra surface water on the surface by using paper towels. Water uptake or swelling % of composites was calculated using the equation below (Eqn.4.1)

$$Water\ Uptake\ [\%] = \frac{W_t - W_0}{W_0} * 100 \qquad \textbf{(Eqn 3.1)}$$

Where $W_o$ and $W_t$ are the weight of dried and wet samples, respectively.

# CHAPTER 4

# RESULTS AND DISCUSSION

In this study, PLA composites containing natural silica, diatoms, were prepared by melt blending method. The effects of diatom type, concentration and type of plasticizer and its concentration on the mechanical, structural, thermal, rheological and water uptake properties of the composites were investigated. Optimization of process parameters (temperature, mixing time and time) of melt mixing was done by design of experiment statistical analysis. PLA-diatom composites were then prepared at this optimum process conditions and characterized.

## 4.1. Optimization of Process Parameters of Melt Mixing

Design of experiment was performed in order to investigate the optimum mixing conditions on tensile strength of PLA. Three process variables were temperature, mixing time, and mixing speed (RPM). The values of these parameters with low, medium and high levels were set and given in Table 4.1.

In this study, Box-Behnken Design is used which is a nonlinear model of Response Surface Methodology, and an experimental design and necessary experimental matrix is produced by the Box-Behnken Design to combine the process parameters and conditions. The quadratic response surface model, which is used to estimate or anticipate the response values, is developed with the aid of design[104].

Minitab software 21 was used for comparing results with Response Surface Regression: Strength versus Temperature; RPM; and Time analysis. Table 4.1 summarizes P-values of binary interactions for Temperature-Temperature, Temperature-Time, Temperature-RPM, Time-Time, Time-RPM and Time-Time. Temperature is referred as (A); RPM is referred as (B) and Time is referred as (C).

Results indicated that the key parameters that had dominant effect on tensile strenght of PLA as time of mixing, second order interactions of time and RPM, and pure

quadratic terms of temperature and RPM. RPM and Time binary interaction was observed as dominant operating variables regarding the P-Value as the lowest (0,02).

Table 4.1. Minitab Results with respect to Response Surface Regression: Strength versus Temperature; RPM; Time

| Term | Coef | SE-Coef | T-Value | P-Value | VIF** |
|---|---|---|---|---|---|
| **Constant** | 70,90 | 0,80 | 87,97 | 0,00 | |
| **Temperature [A]** | -0,28 | 0,49m | -0,56 | 0,59 | 1 |
| **RPM [B]** | 0,73 | 0,49 | 1,48 | 0,19 | 1 |
| **Time [C]** | 1,32 | 0,49 | 2,69 | 0,04* | 1 |
| **A*A** | -2,41 | 0,72 | -3,31 | 0,02* | 1,01 |
| **B*B** | -2,97 | 0,72 | -4,10 | 0,01* | 1,01 |
| **C*C** | -1,75 | 0,72 | -2,41 | 0,06 | 1,01 |
| **A*B** | 0,21 | 0,69 | 0,30 | 0,77 | 1 |
| **A*C** | 0,88 | 0,69 | 1,26 | 0,26 | 1 |
| **B*C** | -2,24 | 0,69 | -3,22 | 0,02* | 1 |

*The P value less than or equal to 0.05 has been considered as significant

**The variance inflation factor (VIF) is a measure of the degree of convergence in regression analysis.

The regression equation for the tensile strength was as follows:

$$Strength = -687 + 7{,}90\,T + 2{,}62\,RPM + 5{,}07t - 0{,}02408\,T^2 - 0{,}02976\,RPM^2 - 0{,}438\,t^2 + 0{,}00209\,T * RPM + 0{,}0441\,T * t - 0{,}1123\,RPM * t \quad \textbf{Eqn. 4.1}$$

*T: Temperature, t: time*

Box-Behnken design result was given as contour plot of Strength vs Time-RPM at constant temperature in Figure 4.1. As the green colour gets darker, the strength increases. Results indicated that mechanical strength values of PLA changed between 29-32 MPa. Therefore, optimum RPM-Time conditions were selected from the darker green regions where the mechanical strength is maximum. (Figure 4.1). The tabulated form of the results of experiments performed according to statistical design for the melt mixing of PLA was also given in Table 4.2.

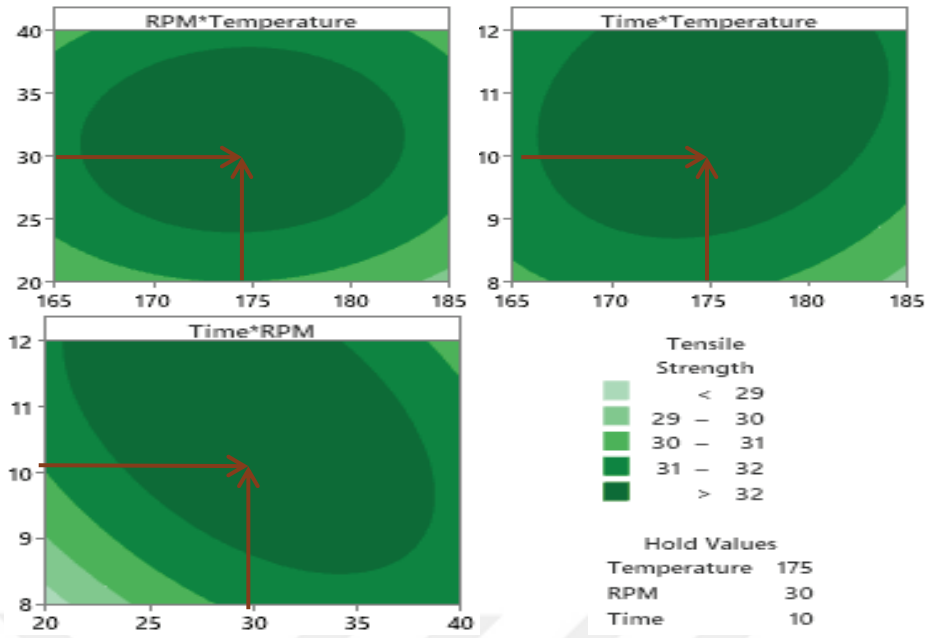


Figure 4.1. Contour plots by plotting Strength versus time-RPM.

Figure 4.1 showed that 30 RPM with around 10-minutes operation time gave the highest strength values for PLA around 32 MPa. Figure 4.2 also illustrates factorial plots of tensile strength with respect to binary interaction parameters. As can be seen from the figure, as mixing speed has a positive effect on tensile strength value of PLA, however the highest mixing speed of 40 RPM directly decreased tensile strength result compared to the 30 RPM result. Time of mixing also positively effects on the strength, however at 40 rpm mixing speed and 12minute mixing time at constant mixing temperature decreased the strength. As temperature of mixing increased from 165 to 175°C, the strength values increased, however the higher mixing temperature of 185 ° C decreased the strength. values.

Figure 4.2 also illustrates factorial plots of tensile strength with respect to binary interaction parameters. As can be seen from the figure, as mixing speed has a positive effect on tensile strength value of PLA, however the highest mixing speed of 40 RPM directly decreased tensile strength result compared to the 30 RPM result. Time of mixing also positively effects on the strength, however at 40 rpm mixing speed and 12-minute mixing time at constant mixing temperature decreased the strength. As temperature of mixing increased from 165°C to 175°C, the strength values increased, however the higher mixing temperature of 185°C decreased the strength. values.

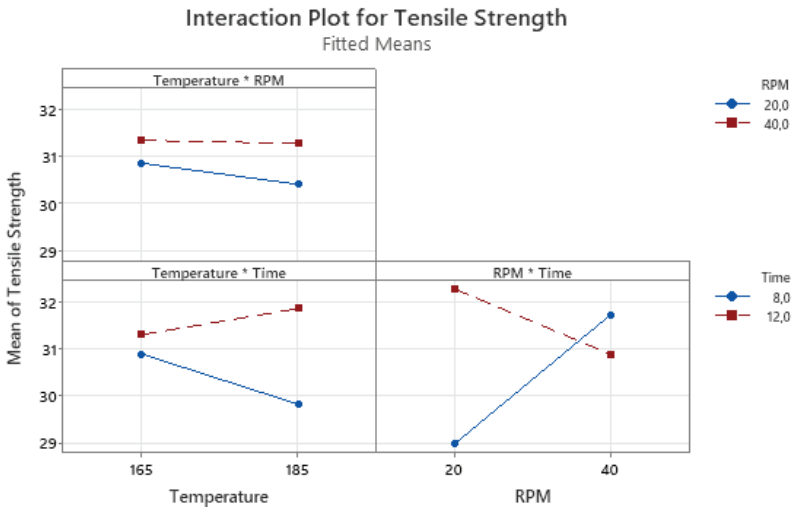


Figure 4.2. Factorial plots of strength with respect to binary parameters

Table 4.2. The results of experiments performed according to statistical design for the melt mixing of PLA.

| | Temperature [C] | Time [min] | RPM | Tensile Strength [MPa] |
|---|---|---|---|---|
| PLA | 165 | 8 | 20 | 27,654 |
| | | | 30 | 30,729 |
| | | | 40 | 30,520 |
| | | 10 | 20 | 30,555 |
| | | | 30 | 31,555 |
| | | | 40 | 30,495 |
| | | 12 | 20 | 30,954 |
| | | | 30 | 30,816 |
| | | | 40 | 32,400 |
| | 175 | 8 | 20 | 28,122 |
| | | | 30 | 31,657 |
| | | | 40 | 31,877 |
| | | 10 | 20 | 31,390 |
| | | | 30 | 32,723 |
| | | | 40 | 31,729 |
| | | 12 | 20 | 31,265 |
| | | | 30 | 30,188 |
| | | | 40 | 30,888 |
| | 185 | 8 | 20 | 31,358 |
| | | | 30 | 29,468 |
| | | | 40 | 31,717 |
| | | 10 | 20 | 30,297 |
| | | | 30 | 31,546 |
| | | | 40 | 31,866 |
| | | 12 | 20 | 30,432 |
| | | | 30 | 29,940 |
| | | | 40 | 31,400 |

As a result, the optimum mixing conditions based on the design of experiment statistical analysis was given in given in Table 4.3.

Table 4.3. The optimum mixing conditions of PLA

| Temperature [C] | Time [min] | RPM |
|---|---|---|
| 175 | 10 | 30 |

After selection of the optimum mixing process parameters for PLA polymer, PLA-diatom composites were prepared at this constant process operating conditions in Haake rheomixer and characterized.

## 4.2. Characterization of Composites

### 4.2.1. Morphological Properties

Effects of diatom and plasticizer incorporation on dispersion of diatoms in the PLA matrix, interfacial adhesion between diatom and PLA and fracture modes of the PLA composites were studied by examining fracture surface of the PLA and PLA-diatom composites by SEM.

Figure 4.3 shows the fracture surface of pure PLA at 500x magnification. Smooth surface of PLA was clearly seen in the figure and cracking regions denoted as arrows were obtained.

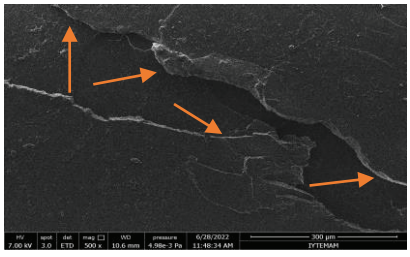

Figure 4.3. SEM micrograms of PLA with 500x magnification

Figure 4.4 below illustrates the different morphologies of raw and calcinated diatom frustules with microstructural characteristics at three different magnifications (500x, 1000x, 2500x and 5000x). Calcinated diatoms has found mostly regular centric type cylindrical diatoms in shape with an average particle size of 10,83±1,22 µm using Image J software. However, Raw diatom frustules mostly consist of irregular shapes with pennate and centric types of diatoms with the average particle size of 35,69±2,57 µm as illustrated in Figure 4.4(d-f). It is also seen that a few of the frustules were broken.

SEM analysis of PLA/Diatom composites were also carried out after mechanical test to observe the fracture surfaces of composite samples to investigate the polymer matrix-particle interaction and distribution of diatoms [18]. Figure 4.5 below illustrates the different morphologies of raw and calcinated diatom frustules with microstructural characteristics at 2500x magnifications The results clearly indicated diatom particles were generally well distributed and embedded e in PLA matrix and Diatom frustules were observed in fracture area.

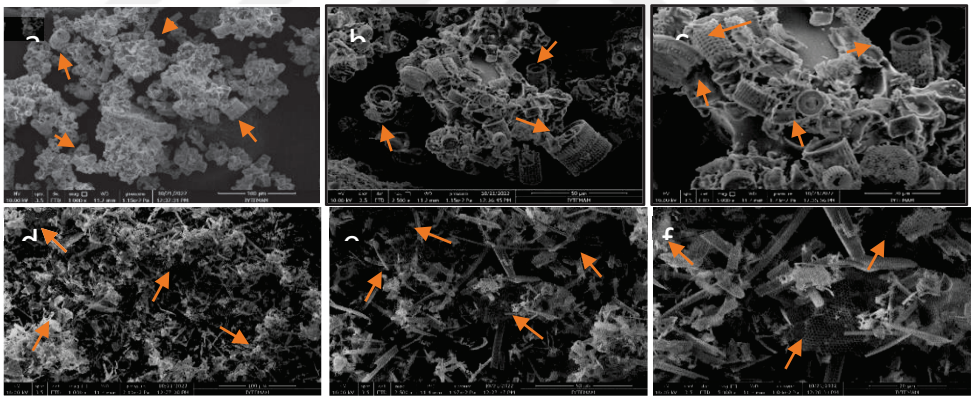

Figure 4.4. SEM images of pure calcinated (a,b,c) and raw diatom (d,e,f) 1000x, 2500x and 5000x magnification.

Fractured region of PLA-CD composites had dd diatom frustules in the cross-sectional area. Calcinated diatom particles were clearly observed in the SEM images and had particle sizes of 11.70 ± 0.581 µm, 11.210 ± 0.75 µm and 11.10 ± 0.76 µm for PLA-3CD, PLA-5CD and PLA-10CD, respectively. It is also noted that calcinated diatom particles exhibited good wetting by PLA polymer matrix. CP particles were covered with a PLA layer. This clearly shows that there is good adhesion between them. Fractured

region of PLA-CD composites had dd diatom frustules in the cross-sectional area. Calcinated diatom particles were clearly observed in the SEM images and had particle sizes of 11.70 ± 0.581 μm, 11.210 ± 0.75 μm and 11.10 ± 0.76 μm for PLA-3CD, PLA-5CD and PLA-10CD, respectively. It is also noted that calcinated diatom particles exhibited good wetting by PLA polymer matrix. CP particles were covered with a PLA layer. However, there are some voids observed between PLA and diatom particles. In the same manner, raw diatom particles were also detected with much larger sizes in the cross section for PLA-3RD, PLA-5RD and PLA-10RD composites with particle sizes of 22.38±2.56 μm, 27.40±5.20 μm and 29.61±2,61 μm respectively. An interesting result was that pure raw diatom particles had a higher value than the sizes in PLA-RD composites. The organic content of the raw diatom particles had shown fibrous shapes and the high temperature processing most probably decomposed the organic content of the raw diatom frustules. Consequently, the particle sizes of diatoms in PLA-RD composites had a lower particle size value than pure raw diatom frustules. It is seen that CD incorporated PLA composites has better dispersion characteristic behaviour. The comparison of the both diatom concentration showed slightly different dispersion There is a major fact that the presence of characteristic porous structure and particle sizes of diatom shell affect its distribution in polymer matrix. The calcinated diatoms were more uniformly dispersed in the PLA matrix than the raw diatoms because the particle sizes and shapes of the calcined diatoms were more similar to each other and much lower in size compared to those of the raw diatoms. At low diatom concentrations for PLA-3CD and PLA-3RD composites, polymer matrix was observed as uniform structure at the fracture region. Only a small number of diatoms are seen. However, above 3wt% diatom concentrations, the diatoms were observed more apparently in the matrix and tends to agglomerate. The most appropriate distribution was obtained for both 3wt% diatom content for both raw and calcined groups. Diatom frustules, that had particle size greater than 20 μm, showed tendency to agglomerate [18].

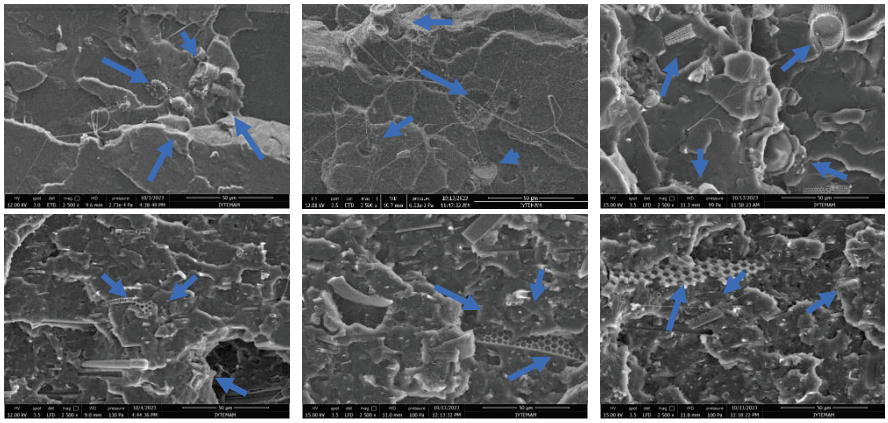

Figure 4.5. SEM images of PLA-3CD, PLA-5CD and PLA-10CD (a,b,c) and PLA-3RD, PLA-5RD and PLA-10RD (d,e,f) with 2500x magnification

In plasticizer modified PLA groups, PLA was plasticized by PEG with two different concentrations (5 and 10 wt%) PEG is an excellent plasticizer for PLA because it has good miscibility with PLA. The surface of the pure PLA matrix was essentially smooth and Figure 4.6 indicated that the fracture surface of the pure PLA shows a brittle fracture morphology, but the PEG added PLA shows a ductile fracture morphology. SEM images showed that PLA/PEG blends had more fibrous and rough morphological structure. This structure was an indication of proper PEG dispersion within PLA matrix and increased ductility of polymer. The appearance of a thread-like structure in the PLA/PEG groups indicated that the PLA is well plasticized with PEG addition, which has already been supported by the increase of PEG concentration in PLA that caused an increase in elongation of break values of PLA due to good plasticization effect of PEG [105].

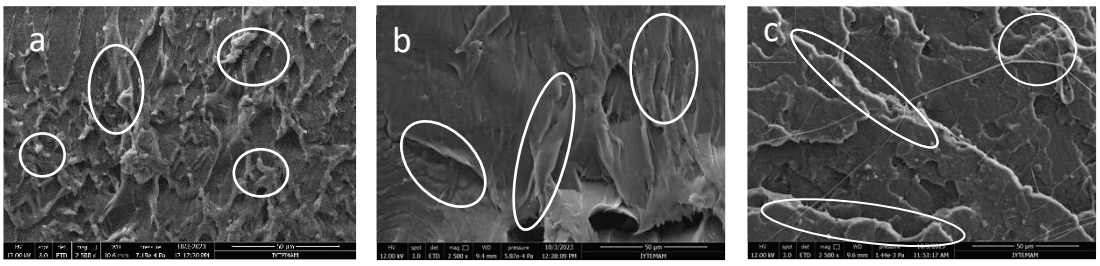


Figure 4.6. SEM images of PLA-5PEG (a), PLA-10PEG (b) and PLA-5PEG/POSS (c) with 2500x magnification

Effect of PEG plasticizer addition on the distribution of diatom particles in PLA matrix was also investigated. Figure 4.7 illustrates SEM images of PLA-5PEG composites containing 3, 5 and 10 wt % of diatoms.

It is observed that the roughness of the surface increases as the diatom concentration increases in PLA-5PEG composites, especially at high concentrations. It is also noteworthy that the addition of PEG improves the dispersion of diatoms as compared to the PLA composites without PEG. The particle size of raw diatoms in the PLA reduced compared the ones without plasticizer. As a result, the addition of PEG made it easier to disperse the raw diatoms in the PLA. The plasticizing effect of PEG allowed a good distribution and embedment of the diatom particles in the PLA matrix. literature, PEG has been also utilized as a compatibilizer in polymer composites to improve the interactions between reinforcement and matrix. PEG's chemical composition enables hydrogen bonding formation when mixed with diatoms therefore, improves the dispersion and compatibility between matrix and filler [105].

PLA-5PEG composites had increased roughness in surface, thus both diatom addition attached surface of PLA-5PEG more effectively. PLA-5PEG-3CD, PLA-5PEG-5CD and PLA-5PEG-10CD were measured 11,96±0,95 μm, 12,69±0,42 μm and 12,45±1,11 μm respectively and calcinated diatom particle sizes had similar values, as expected. PLA-5PEG-3RD, PLA-5PEG-5RD and PLA-5PEG-10RD had 24,32±3,36 μm, 28,92±3,69 μm and 30,07±4,35 μm respectively. PEG had no significant effect of particle size of diatoms. Dispersions of diatoms into PLA matrix increased, consequently diatom particles were shown clearer, but increasing concentration seemed to have a tendency to agglomerate.

As the concentration of PEG increased from 5 to 10 wt%, it was seen that except 5 wt % diatom incorporated PLA composites, (PLA-10PEG-5CD and PLA-10PEG-5RD) the fracture surfaces have more rough structure (Figure 4.8). For PLA-10PEG-3CD, PLA-10PEG-5CD and PLA-10PEG-10CD composites, diatoms had particle sizes found as 12,29±0,87 μm, 11,73±0,87 μm and 13,36±0,48 μm, respectively. For raw diatom incorporated ones, diatoms had particle sizes of 23.55±1.90 μm, 29.05±5.14 μm and 30.33±3.57 μm for PLA-10PEG-3RD, PLA-10PEG-5RD and PLA-10PEG-10RD composites, respectively. Dispersion was found to be much better in both CD and RD incorporated PLA-10PEG composites with smallest particle sizes of diatoms as shown in Figure 4.8. Previously, at low PEG amount, a good dispersion was achieved in composites containing 3wt % diatoms, but with the increase in PEG concentration to 10wt%, a good

dispersion was achieved in composites containing higher diatom content of 5 wt%. As a result, increasing the PEG concentration improved the dispersion at higher diatom ratios. However, agglomeration problem is still observed in composites with high diatom content in PLA.

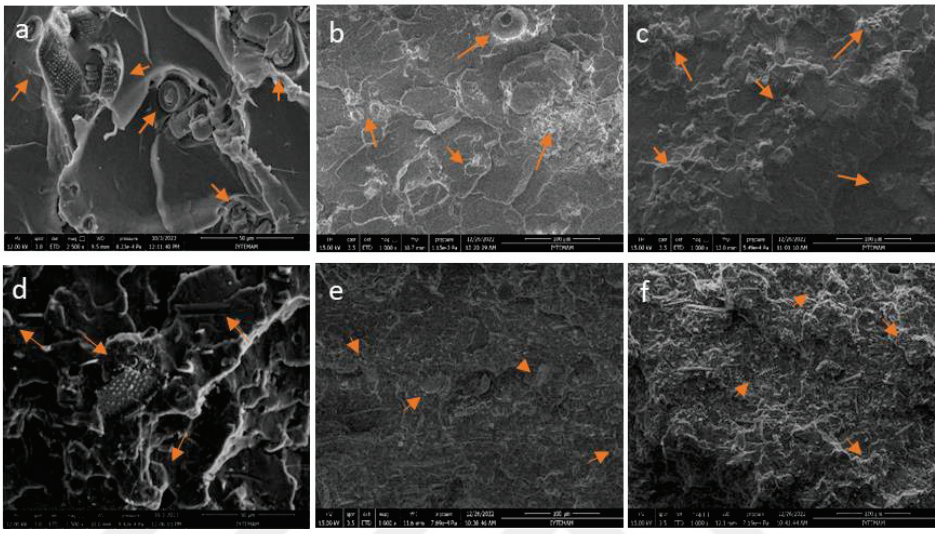


Figure 4.7. SEM images of PLA-5PEG-3CD, PLA-5PEG-5CD and PLA-5PEG-10CD respectively (a,b,c) and PLA-5PEG-3RD, PLA-5PEG-5RD, PLA-5PEG 10RD respectively (d,e,f) with 1000x and 2500x magnification (Arrows denote diatoms)

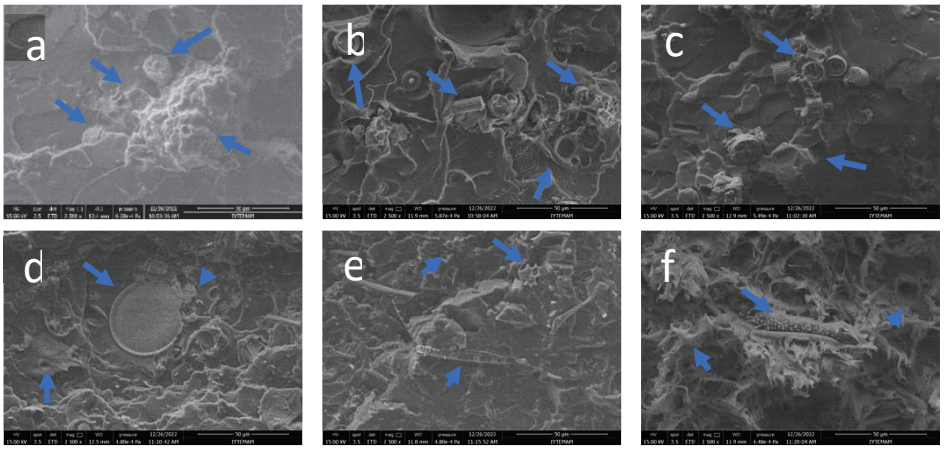


Figure 4.8. SEM images of PLA-10PEG-3CD, PLA-10PEG-5CD, PLA-10PEG-10CD respectively (upside) and PLA-10PEG-3RD, PLA-10PEG-5RD, PLA-10PEG 10RD respectively (downside) with 2500x magnification

In addition to the known plasticizer PEG, with unique cage structure PEG modified POSS (PEG/POSS) was used as a new plasticizer agent for PLA diatoms composites with 5 wt % concentration with respect to the PLA weight. Figure 4.9 indicates the fractured surface SEM images of PLA-5PEG/POSS, raw diatom incorporated PLA-5PEG/POSS composites.

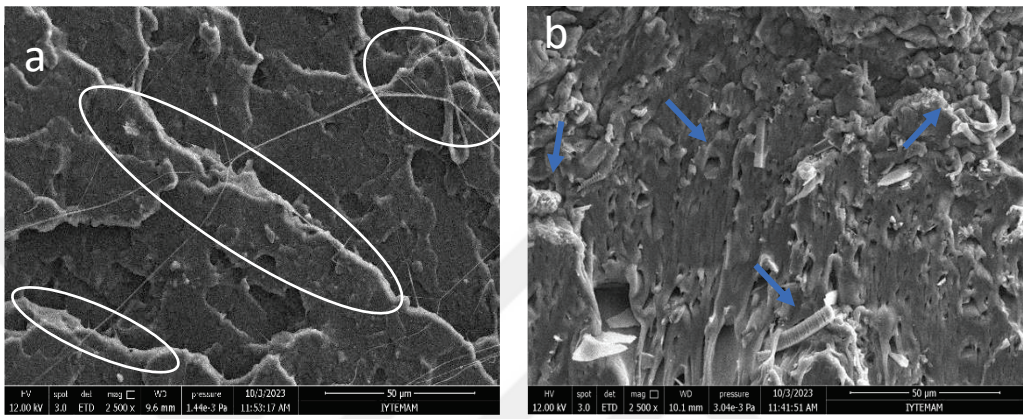


Figure 4.9. SEM images of PLA-5PEG/POSS, PLA-5PEG/POSS-3RD with 2500x magnification

As seen in Figure 4.9, the fracture surfaces of PLA-5PEG/POSS composites had more rough surfaces and raw diatom addition increased the surface roughness clearly. In the figure, whole raw diatoms are also visible. The formation of small aggregates of POSS particles indicates that there is compatibility between POSS and the PLA matrix, which may be due to the modification of the isobutyl group of POSS [106]. Since diatoms did not disintegrate after tensile testing, polymer fracture mostly occurs at the PLA-diatom interfaces instead of diatoms pull off. In addition, particle sizes of raw diatoms in PLA-5PEG/POSS matrix increased compared to PLA-5PEG matrix. The obtained particle sizes are determined as 36,94±4,78 µm, 38,50±3,72 µm and 37,65±5,04 µm, respectively for 3, 5 and 10 wt% RD incorporated PLA composites. When the grain size of the diatoms in the polymer was compared, it was found that the PEG plasticiser was better for the distribution of the raw diatoms in the PLA.

## 4.2.2. Surface Characterization of Composites

### 4.2.2.1 AFM

Atomic force microscopy analysis (AFM) was used to determine the topography of the surfaces and roughness of PLA composites.

AFM analysis was performed to investigate the surface structure differences with regard to surface area and roughness on PLA matrix with diatom addition. In order to see diatom frustules on the surface and get meaningful roughness measurements, atomic force micrographs of PLA-Diatomite composites were scanned at a 10µm-10µm scale. Figure 4.10 shows the surface topography and phase images of PLA with a 10µ*10µ scan size. The surface of pure PLA was relatively flat, with only a few topographic characteristics. The roughness value of the PLA, $R_q$, is the height deviation calculated from the mean of the image data plane's root mean square average. The $R_q$ value was 16,38±6,54 nm which was corresponded to literature [107]. Figures 4.11 and 4.12 show AFM images of both calcinated and raw diatom incorporated PLA composites. The Rq values of PLA-3CD, PLA-5CD and PLA-10CD were obtained as 27,23±9,52 nm, 26,47±6,98 nm and 29,13±9,79 nm, respectively (Table 4.4). Calcinated diatom addition into PLA matrix directly increased the surface roughness, as indicated with Rq values as compared to the pure PLA (Figure 4.11). AFM phase images of PLA-diatom composites showed that diatoms with porous structure in polymer matrix probably led to an increase in the roughness of composites. On the other hand, although raw diatom addition increased the surface roughness of PLA, the roughness value was not proportional to the diatom content, with roughness values ranging from 20.37±8.50 nm to 30.83±6.56 nm (Table 4.4). PLA-3RD, PLA-5RD and PLA-10RD had Rq values of 30.83±6.56 nm, 20.37±8.50 nm and 23.30±10.93 nm respectively. The reasons for this behaviour could be due to the uneven distribution of diatoms in the matrix and also the uneven particle size distribution of the raw diatoms used, which have organic and inorganic groups present [22]. The roughest surface character was obtained with PLA-3RD composite, which had the best distribution of diatoms in the PLA matrix as observed by SEM (Figure 4.5). Consequently, it was revealed that the diatom type and concentration affected the composites' surface roughness in different ways.

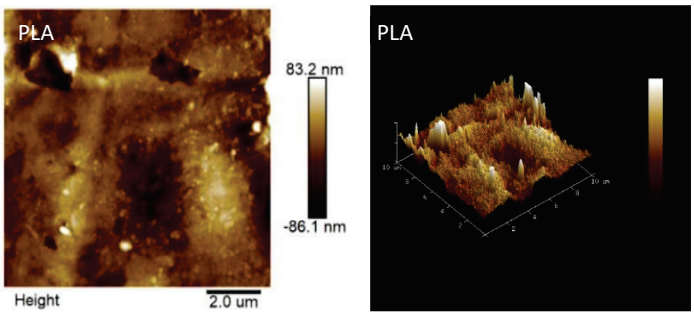


Figure 4.10. AFM images in 1-D and 3D of pure PLA

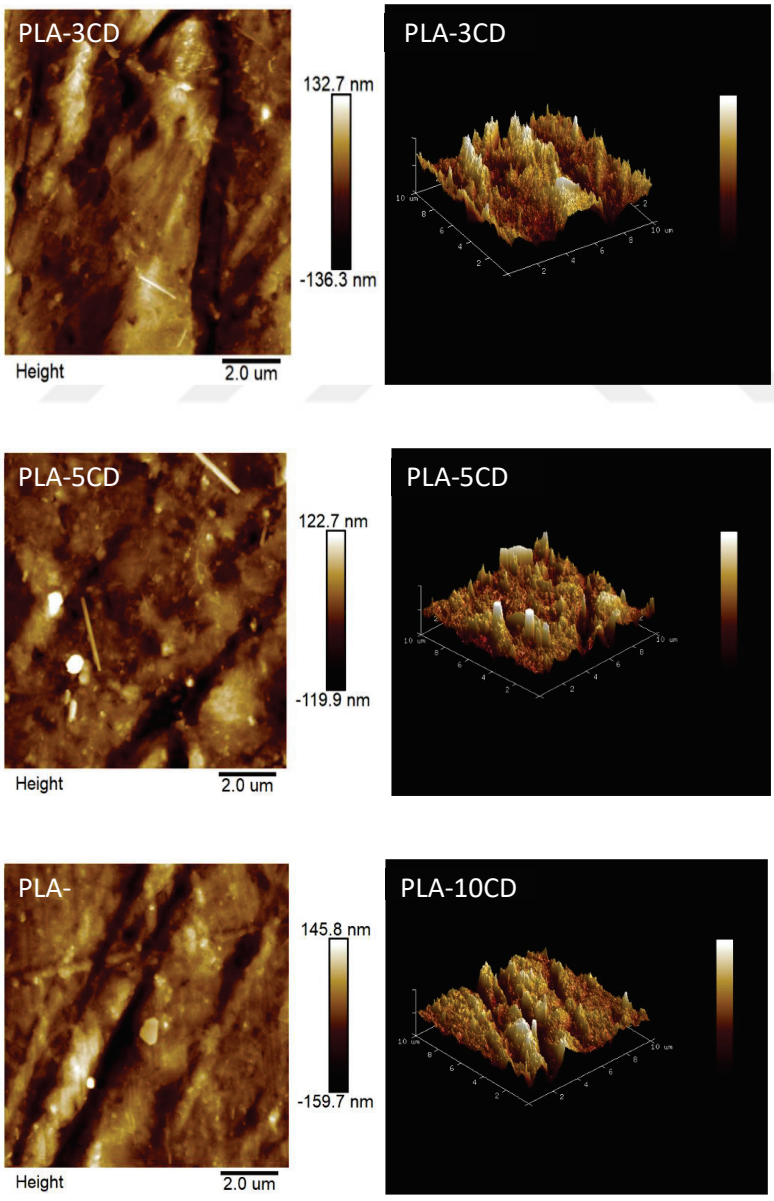


Figure 4.11. AFM pictures of PLA-CD composites

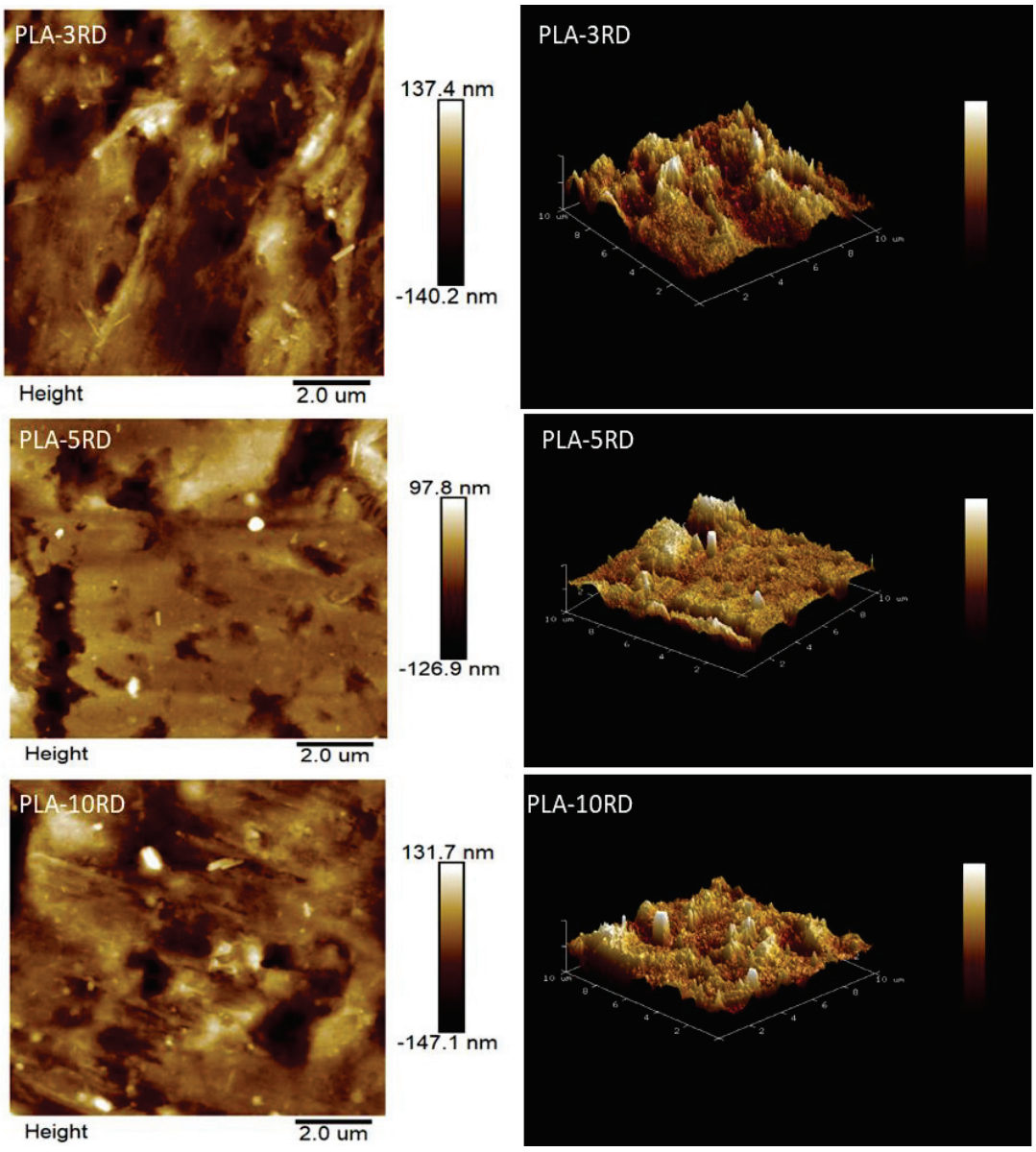


Figure 4.12. AFM images of PLA-RD composites

The surface topography images showed that at low diatom loadings, few small protruding regions were observed, however, at high diatom loadings, 10% wt, more concentrated protruding regions were obtained inducing higher roughness on the surface for calcinated diatom incorporated composites. AFM phase images indicated that diatom nanoparticles tend to agglomerate on surface with increasing concentrations. White regions indicated non-dispersed diatom contents due to agglomeration[21].

Table 4.4. Rq values of PLA and PLA-Diatom composites

| | |
|---|---|
| PLA | 16,38±6,54 |
| PLA-3CD | 27,23±9,52 |
| PLA-5CD | 26,47±6,98 |
| PLA-10CD | 29,13±9,79 |
| PLA-3RD | 30,83±6,56 |
| PLA-5RD | 20,37±8,50 |
| PLA-10RD | 23,30±10,93 |

### 4.2.2.2. Contact Angle

The wetting ability of a material is determined by contact angle measurements. The contact angle data for all composites were measured in order to determine the hydrophilicity. Table 4.5 shows static air-water contact angle data for PLA- composites. The results showed that all surfaces had hydrophilic surface characteristic. Diatom is a hydrophilic silica with a contact angle of 0° with water [21]. As the amount of diatom increases, the hydrophobicity of the polymer matrix should decrease. Incorporation of calcinated diatomite particles into the PLA matrix (82,5 $^{o}$) decreased the contact angle up to 5% (w/w) diatom (61$^{o}$) (Figure 4.13). A slight increase in the contact angle was observed for 10% diatom incorporated samples, due to the diatom agglomerations on the surface as observed by SEM analysis. However, for raw diatom incorporated samples, all composites showed better hydrophilic properties compared to pure PLA as shown in Figure 4.13 (b), but no correlation with raw diatom content was observed. This is due to the non-uniform distribution of the raw diatoms at high loading levels above 3% in the PLA matrix as demonstrated by SEM analysis.

Table 4.5. Contact Angle results of PLA-composites

| **Sample Code** | **Contact Angle** |
|---|---|
| PLA | 82,47±2,19 |
| PLA-3CD | 73,37±0,12 |
| PLA-5CD | 61,24±0,071 |
| PLA-10CD | 77,27±0,26 |

**(cont. on next page)**

Table 4.5 (cont.).

| Sample Code | Contact Angle |
|---|---|
| PLA-3RD | 78,55±0,74 |
| PLA-5RD | 84,84±0,66 |
| PLA-10RD | 73,82±0,39 |
| PLA-5PEG | 54,35±1,03 |
| PLA-5PEG-3CD | 73,12±0,09 |
| PLA-5PEG-5CD | 71,44±0,29 |
| PLA-5PEG-10CD | 67,63±0,53 |
| PLA-5PEG-3RD | 73,58±0,39 |
| PLA-5PEG-5RD | 61,63±0,07 |
| PLA-5PEG-10RD | 75,13±0,52 |
| PLA-10PEG | 47,93±0,09 |
| PLA-10PEG-3CD | 66,67±0,87 |
| PLA-10PEG-5CD | 43,74±0,09 |
| PLA-10PEG-10CD | 47,80±0,43 |
| PLA-10PEG-3RD | 40,81±0,07 |
| PLA-10PEG-5RD | 31,34±0,04 |
| PLA-10PEG-10RD | 37,21±0,04 |
| PLA-5PEG/POSS | 56,81±0,05 |
| PLA-5PEG/POSS-3RD | 79,23±0,06 |
| PLA-5PEG/POSS-5RD | 60,61±0,21 |
| PLA-5PEG/POSS-10RD | 68,87±0,07 |
| | |

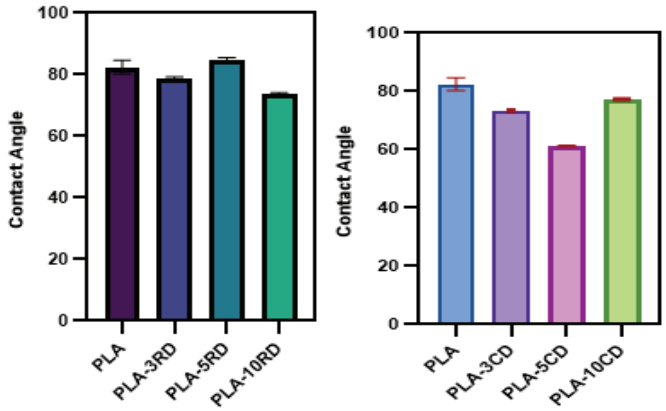


Figure 4.13. Contact angle results of a) CD-PLA b) RD-PLA

In addition to the Diatom addition as reinforcing agent, plasticizers were also utilized to PLA in order to improve PLA's characteristics. Figure 4.14 below showed change of contact angle with respect to plasticizer concentration.

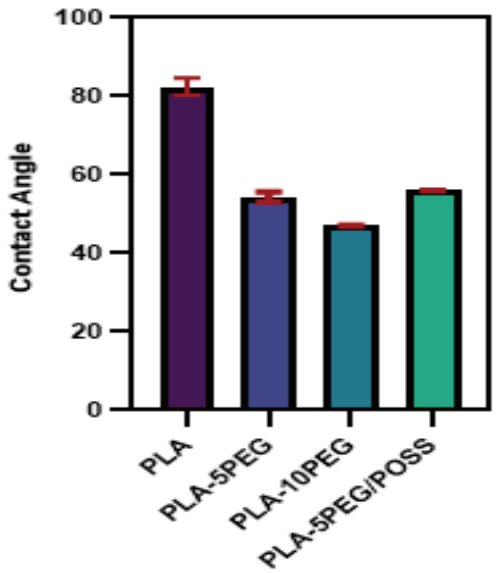


Figure 4.14. Effect of plasticizers addition on contact angle of PLA.

As seen in Figure 4.14, PEG and PEG/POSS addition with 5wt% concentration reduced the contact angle of PLA-PEG blend from 82 º to 57 º having moderately hydrophilic surface property with contact angle much lower than 90º. As PEG plasticizer concentration increased, wettability of PLA enhanced with a lower contact angle value from 54,35±1,03° to 47,93±0,09°. In the study of Serra et al. (2014), similar finding was obtained with PEG addition [77].

The contact angles of PLA-PEG-diatom composites were also investigated. The change of contact angles with diatom type and content was shown in Figure 4.15. Both type of diatom addition increased the contact angle of PLA-PEG-diatom composites up to 75 º which is still lower than pure PLA. This trend for PLA-PEG-diatom was opposite to the PLA-diatom composites. The reasons for increasing trend with diatom addition could be the interactions between PEG-diatoms or PEG adsorption in the pores of diatoms [108]. However, an increase in PEG concentration (10 wt%) again increased the wettability except for PLA-10PEG-3CD composites. Contact angle values are lower than the pure PLA-10PEG. This is most likely due to the fact that the PLA PEG interaction

becomes more dominant than PEG-diatom interactions, therefore, the contact angle has decreased [108].

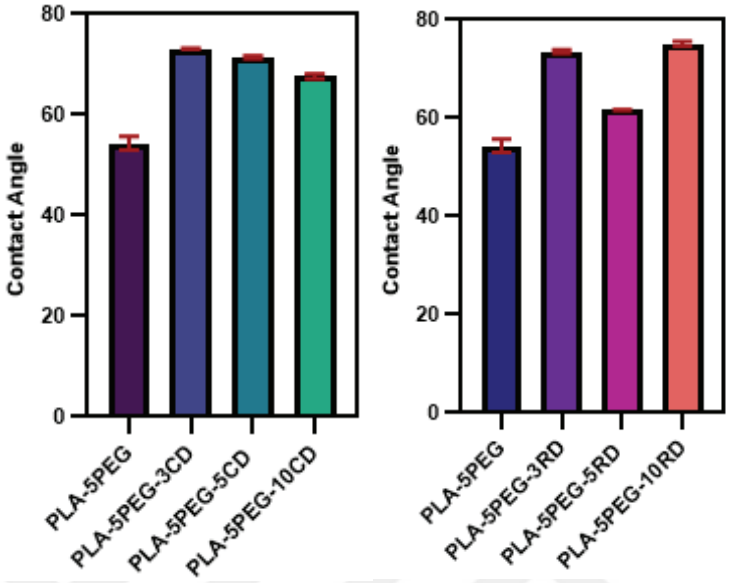


Figure 4.15. Contact angle PLA-5PEG-Diatom composites

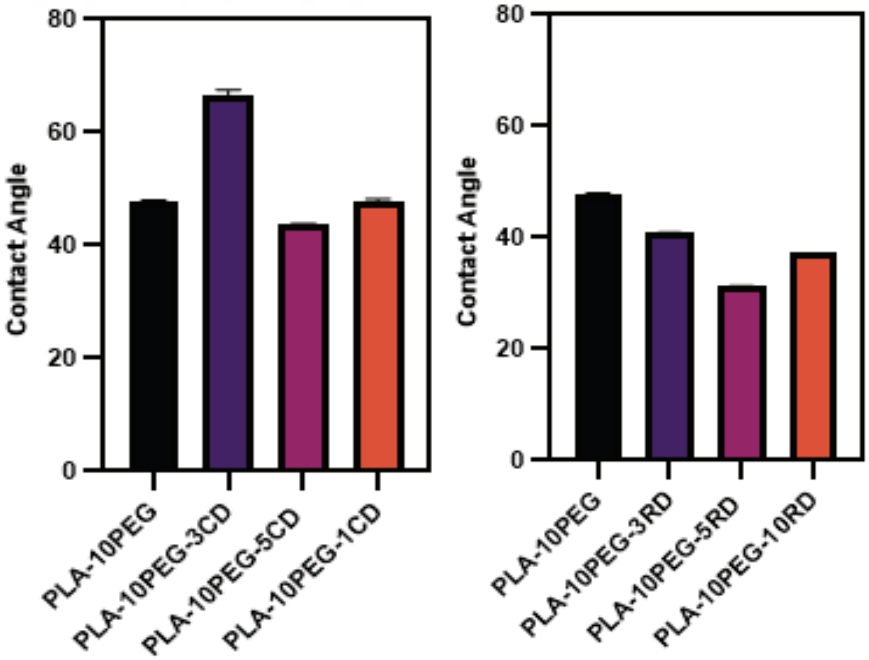


Figure 4.16. Contact angle results of PLA-10PEG-Diatom composites

In this work, the second type of plasticizer/compatibilizer used was PEG/POSS. Polyhedral oligomeric silsesquioxanes (POSS) with PEG functional groups is a hybrid nanosilica which could have synergic effect and both reinforce the PLA matrix and at the same time enhance interactions between the PLA matrix and diatoms. Figure 4.13 illustrates the contact angle change with respect to raw diatom content in PLA. The contact angle of all composites increased as it was also observed by 5 wt% PEG plasticizer addition. As a result, both plasticizer addition with the same amount showed an increasing trend with increasing diatom amount. The values are in the range of 60,61±0,21 to 79,23±0,06 for 3 to 10 wt% RD addition.

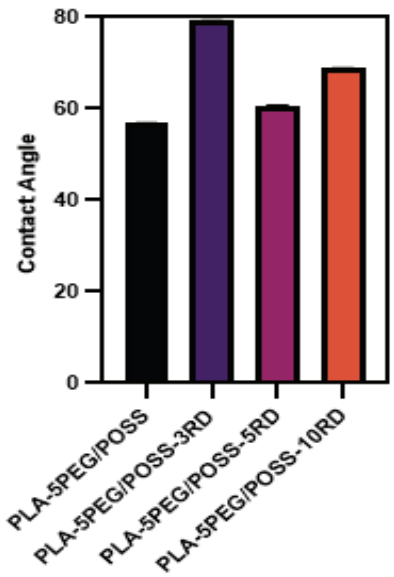


Figure 4.17. Contact angle results of PLA-5PEG/POSS-RD composites

Diatom addition can be arranged depending on the requirement of wettability character of PLA diatom composites. Contact angle behaviour of PLA-diatom composites with and without plasticizer affects the trend. Except PLA-10PEG samples, PLA-diatoms interactions are more dominant due to the reinforcing effect of diatoms than PLA-PEG interactions which cause plasticization effect, therefore contact angles values decreased for PEG and PEG-POSS plasticized samples. Plasticizers improved PLA surface activity and compatibility of pure PLA was increased with plasticizers [77].

### 4.2.3. Mechanical Properties

PLA has low glass transition temperature, biodegradable, processable, and no toxic gas emission. Despite the above positive features, PLA has drawbacks that limits its well and utilization in certain applications, mainly; poor toughness, low thermal stability and brittle character [21]. Generally, plasticizer blending, or micro /nanocomposites formulations are used to improve PLA property. In this work, bio silica source, diatom, as a filler, and PEG and PEG/POSS as plasticizers were utilized to investigate the mechanical property change of PLA. In literature, it was found that semicrystalline PLA has an approximate tensile strength of 21–60 MPa, tensile modulus of 0.35- 3 GPa, and an elongation at break of about 3-10 [109]. Both types of diatom incorporation enhanced the ultimate tensile strength of PLA. The values are almost twice as tensile strength in the range of 51,51-58,50 MPa compared to pure PLA (32,72±0,27 MPa). The highest strength value was observed for 3% raw diatom incorporated samples (PLA-3RD). However, the higher concentrations of diatoms caused a slight decrease in the tensile strength for PLA-5CD as 52,61 ± 2,50 MPa and for PLA-10CD as 51,51 ± 4,15 MPa. Because there are too many discontinuities exist due to rigid filler in the polymer, higher filler content led to a reduction in the tensile strength. Similar behaviour was observed for raw diatom cases, PLA-3RD, PLA-5RD and PLA-10RD had tensile strength as 58,50±1,46, 56,21±3,37 and 51,66±0,98 MPa, respectively. Increasing concentration can cause diatom agglomeration, thus cannot disperse in PLA matrix properly. In the study of Dobrosielska et al. (2020) 1-2.5wt% of diatoms was found to be an optimum concentration in PLA matrix. In our study, 3wt% diatom addition gave the best results in the enhancement of tensile strength of PLA [21].

The comparison of tensile strength was illustrated in Figure 4.18. Table 4.6 lists all mechanical properties for PLA-diatom composites. Pure PLA sample has an elongation break value of 5,60±0,73. Elongation at break values of all composites decreased with an increase in diatom content in the range of 2,72±0,34 – 4,94±0,54. However, as seen in Figure 4.18, Young Modulus was at a similar level for the composites containing less than 10 wt% diatom. Only the composites containing 10 wt% of diatoms (PLA-10CD and PLA-10RD) showed an increase in the value of Young Modulus (Table 4.6 and Figure 4.18).

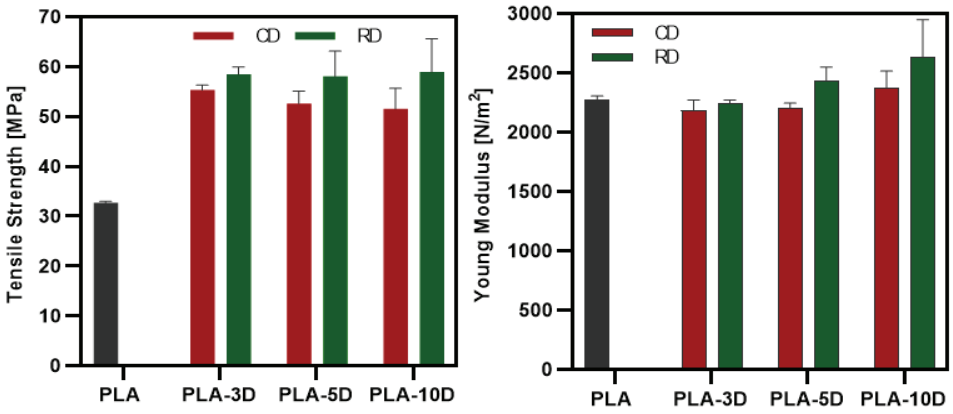


Figure 4.18. Ultimate tensile strength and Young Modulus results of PLA/Diatom composites

Table 4.6. Summary of mechanical property data for PLA-diatom composites

| | Stress [MPa] | Strain at break [%] | Young Modulus [MPa] |
|---|---|---|---|
| PLA | 32,72±0,27 | 5,60±0,73 | 2277,26±45,65 |
| PLA-3CD | 55,33±0,97 | 4,94±0,54 | 2183,11±78,81 |
| PLA-5CD | 52,61±2,50 | 3,58±0,44 | 2205,27±50,96 |
| PLA-10CD | 51,51±4,15 | 3,73±0,27 | 2376,41±138,80 |
| PLA-3RD | 58,50±1,46 | 3,76±0,10 | 2246,43±24,19 |
| PLA-5RD | 56,21±3,37 | 3,19±0,41 | 2435,44±113,97 |
| PLA-10RD | 51,66±0,98 | 2,72±0,34 | 2629,02±318,50 |

PEG is a common plasticizer used to improve the ductility of PLA polymers. Generally, the addition of PEG decreased the tensile behaviour as resulted a decrease in tensile strength and an increase in elongation at break values. Depending on the molecular weight and concentration of PEG, the mechanical properties are tailored by changing brittle nature of PLA to a more ductile fracture. This is mainly because the addition of PEG creates a plasticization effect by entering into amorphous PLA chains, and weaking the intermolecular forces between PLA chains. For semi-crystalline PLA, however, plasticizer effect was behaved differently in the tensile behaviour probably due to the cold crystallization effect of that diminish the elongation of PLA [110]. Our tensile stress-strain results showed an increase in the tensile strength of PLA which showed that our PLA is semi-crystallline (proven also by DSC analysis in Section 4.2.3.) Both

concentration (5 and 10%) levels of PEG 4000 decreased the elongation at break values up to 2,86±1,86. Increasing in tensile strength and decreasing in strain with PEG addition was observed due to increasing in toughness, consequently both PEG addition increases the absorbed energy of the material during the load [35]. In the study of Kulinski et.al (2005), they found an increase of 300% elongation at break as PEG 400 (5wt%) was used in amorphous PLA[110], however this value was 4.5% in semi crystalline PLA due to the more dominant crystallization effect that led to an increase in tensile strength and decrease in elongation as expected [110]. PEG as plasticizer directly decreased modulus of pure PLA. PLA-5PEG and PLA-10PEG had modulus as 1979,2 ± 48,3 and 1690,53 ± 75,31 MPa, respectively as stated in Figure 4.19, thus increasing plasticizer concentration decreased modulus of composites sharply, as expected [81].

PEG/POSS plasticizer/modifier, POSS with PEG functional groups is a type of nano silica, was used to investigate the synergic effect that could both reinforce the PLA matrix and enhance interactions between the PLA matrix and PEG. From the stress-strain results (Figure 4.19), obviously reinforcing effect of PLA with 5wt% PEG/POSS addition was seen. Comparing to PEG plasticizer addition, simultaneous toughening and strengthening of PLA was observed. Tensile test strength value (64,14±1,12 MPa) of PLA-5PEG-POSS almost doubled with the addition of 5 wt.% PEG/POSS to PLA matrix. Elongation at break value is almost close to each other around 3.5 as compared to PEG.

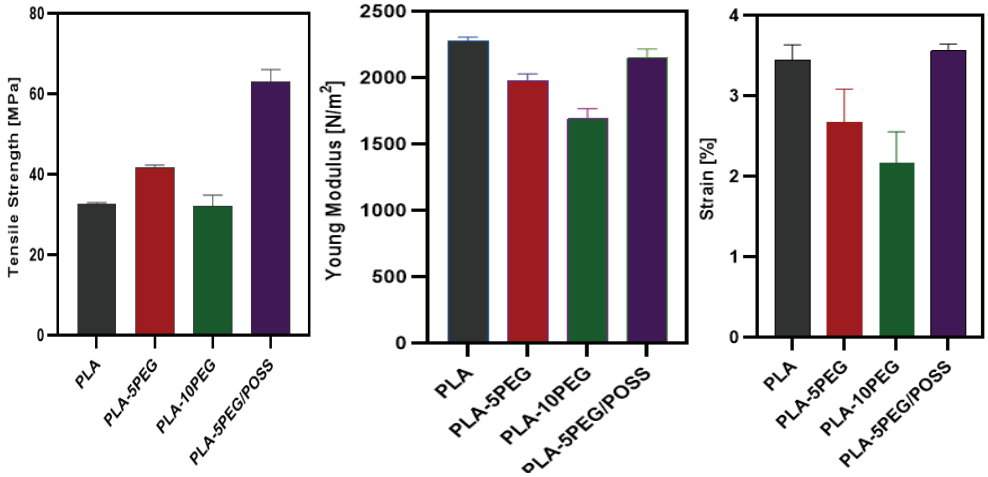


Figure 4.19. Ultimate tensile strength, Young Modulus and strain results of PLA-Plasticizer composites

Tensile Stress and Young Modulus data of PEG modified (5%) PLA-diatom composites are shown in Figures 4.20 and 4.21 for CD and RD filled composites, respectively. Overall tensile results are given in Table 4.7. The results showed that diatom addition into PLA-PEG matrix increased the strength initially. PLA-5PEG-3CD and PLA-5PEG-3RD showed the highest tensile strength as 42,97±2,60 MPa and 41,99±2,03 MPa. Silica content reinforcing effect was seen with PLA-5PEG composites. Increasing in diatom concentration decreased the strength, probably agglomeration effect as expected but this decrease is smaller for calcinated diatom than raw diatom. Mohapatra et al, (2014) indicated with different organoclay at 3% concentration with PLA-PEG composites showed increasing trend, it is due to the good dispersion quality which results better interaction in PLA-PEG layers [105]. However, as the PEG concentration is increased to 10%, the tensile strength of plasticized PLA even further decreased, as expected, but did not change much with incorporation of the calcinated diatoms. Raw diatom incorporation, on the other hand, showed higher strength values for all concentrations in contrast to calcinated diatom applied on PLA-10PEG. PLA-10PEG-3RD showed the best performance in strength as 40,41±2,49 MPa. There was slight decrease in PLA-10PEG-5RD as 39,33±1,95 MPa but PLA-10PEG-10RD had the lowest value as 31,72±3,006 MPa. Increasing in raw diatom concentration decreased strength value as expected due to some agglomerations as seen earlier in the SEM images (Figures 4.8). In order to compare both diatom types, RD addition had more strengthened character than CD. It can be explained that organic residues in raw diatom can affect the dispersion into the matrix due to the better interactions' organic groups with PLA- PEG.

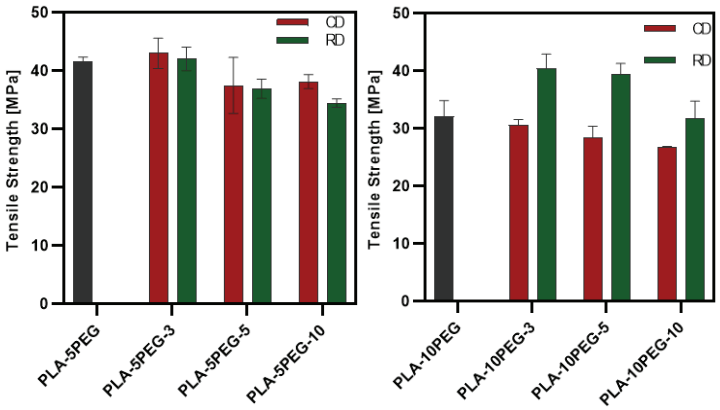


Figure 4.20. Ultimate tensile strength results of PLA-PEG-Diatom composites

As seen in Figure 4.21, Young modulus of PEG plasticized PLA decreased with 5% PEG addition and increasing PEG concentration up to 10% lowered the modulus significantly. For RD incorporated composites, significant increase in young modulus (YM) was observed with diatom addition into PLA-PEG matrix, however, CD incorporated ones, YM did not change much. As also expected, PLA-5PEG composites had higher YM values than PLA-10 PEG ones. Mohapatre et al. (2014) obtained the same results with 10% PEG application into PLA, this may be related to the phase separation caused by the absence of cohesiveness between the matrix polymer and PEG [105].

Increasing diatom concentrations of both diatom type, the best mechanical performance of the blend nanocomposites made with PLA-5PEG. This might be due to the strong contact of the -OH group in the surfactant of RD with the carbonyl groups of PLA and the -OH groups in PEG at the interface [105]. Additionally, PEG can more effectively pass through the matrix layers due to its greater flexibility than PLA, giving PLA chains more space to interact with lower PEG concentration [111].

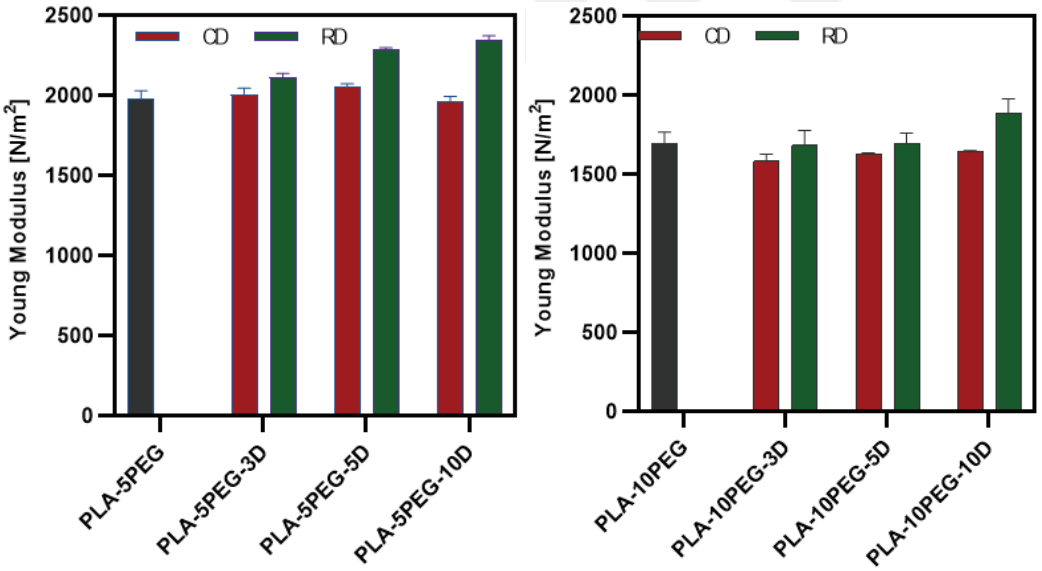


Figure 4.21. Young modulus results of PLA-PEG-Diatom composites

PLA-5PEG and PLA-10PEG had strain values as 3,56±0,33 and 2,86 ± 1,86 %, respectively as stated in Table 4.7. Increasing in tensile strength and decreasing in strain with PEG addition was observed due to increasing in toughness, consequently both PEG addition increases the absorbed energy of the material during the load. Both diatom type

addition increased the strain initially up to 6,66±1,59 % for PLA-5PEG-3RD composites, but after certain diatom content decreased the strain. Regarding the drawbacks of PLA, PLA-5PEG-5RD composites enhanced the PLA's both tensile strength and elongation at break values 41,99 ± 2,03 MPa and 6,66±1,59 %, respectively.

Table 4.7. Summarized results of PLA/PEG/Diatom composites

| | Tensile Strength [MPa] | Strain [%] | Young Modulus [MPa] |
|---|---|---|---|
| **PLA-5PEG** | 41,62 ± 0,71 | 3,56±0,33 | 1979,27±48,33 |
| **PLA-5PEG-3CD** | 42,97 ± 2,60 | 4,34±0,33 | 2004,02±41,11 |
| **PLA-5PEG-5CD** | 37,45 ± 4,80 | 3,02±1,18 | 2050,97±20,88 |
| **PLA-5PEG-10CD** | 38,11 ± 1,20 | 3,07±0,66 | 1958,31±34,90 |
| **PLA-5PEG-3RD** | 41,99 ± 2,03 | 6,66±1,59 | 2111,32±25,07 |
| **PLA-5PEG-5RD** | 36,89 ± 1,65 | 4,33±0,07 | 2281,27±14,84 |
| **PLA-5PEG-10RD** | 34,42 ± 0,72 | 4,65±0,22 | 2341,26±30,68 |
| **PLA-10PEG** | 32,08 ± 2,74 | 2,86±1,86 | 1690,53±75,31 |
| **PLA-10PEG-3CD** | 30,56 ± 0,98 | 5,13±0,49 | 1581,88±45,12 |
| **PLA-10PEG-5CD** | 28,34 ± 2,02 | 5,83±0,16 | 1630,71±3,65 |
| **PLA-10PEG-10CD** | 26,70 ± 0,15 | 7,71±1,29 | 1641,42±6,73 |
| **PLA-10PEG-3RD** | 40,41 ± 2,49 | 2,17±0,64 | 1683,55±92,40 |
| **PLA-10PEG-5RD** | 39,33 ± 1,95 | 3,55±1,49 | 1690,48±68,64 |
| **PLA-10PEG-10RD** | 31,72 ± 3,006 | 3,08±1,65 | 1888,75±86,70 |

The second plasticizer/modifier's (PEG-POSS) effect on tensile properties of PLA-RD composites was studied. PEG/POSS, is a type of nano-silica, functionalized with PEG molecules, was used to investigate the synergic effect that could both reinforce the PLA matrix and enhance interactions between the PLA matrix and PEG [124]. Comparing to PEG plasticizer addition, strength value increased greatly, however, simultaneous toughening and strengthening of PLA was not observed (Figure 4.22, Table 4.8). Tensile test strength value of PLA-5PEG-POSS almost doubled with the addition of 5wt. % PEG/POSS (64,14±1,12 MPa) as compared to pure PLA matrix (32,72±0,27 MPa). Elongation at break value decreased to 3,77±0,09 % (Table 4.8). Addition of

diatoms slightly decreased to tensile strength, however YM increased at higher RD concentrations due to the stiffing effect of diatoms as expected.

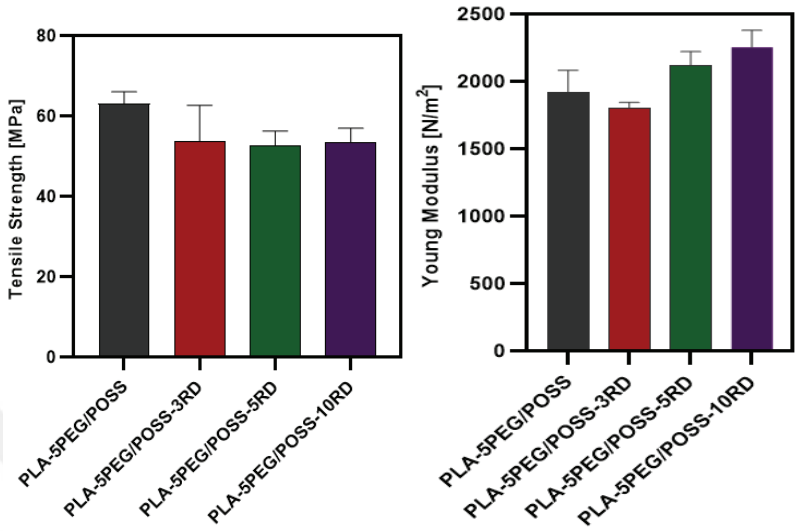


Figure 4.22. Ultimate tensile strength and Young Modulus results of PLA-5PEG/POSS – Raw diatom composites

Table 4.8. Summary of the results of PLA/PEG/POSS/Raw diatom composites

| | Tensile Strength [MPa] | Strain [%] | Young Modulus [MPa] |
|---|---|---|---|
| PLA-5PEG/POSS | 64,14±1,12 | 3,77±0,09 | 1922,17±160,03 |
| PLA-5PEG/POSS-3RD | 53,61±9,02 | 3,40±0,75 | 1804,52±41,13 |
| PLA-5PEG/POSS-5RD | 52,63±3,58 | 2,94±0,30 | 2121,61±99,26 |
| PLA-5PEG/POSS-10RD | 53,49±3,50 | 2,82±0,111 | 2253,527±126,46 |

### 4.2.4. Thermal Properties

Differential Scanning Microscopy (DSC) and thermal gravimetric analysis (TGA) were used to examine the thermal properties of PLA and PLA/Diatom composites.

### 4.2.4.1 Thermo-Gravimetric Analysis (TGA)

For the purpose of determining how diatom additives affect PLA's thermal stability, thermogravimetric analysis was carried out under nitrogen atmosphere at a heating rate of 10°C/min. Discussions and comparisons of thermal stability of PLA-Diatom composites have been done based on the yield of char residue (char%), the temperature of thermal degradation ($T_{onset}$).

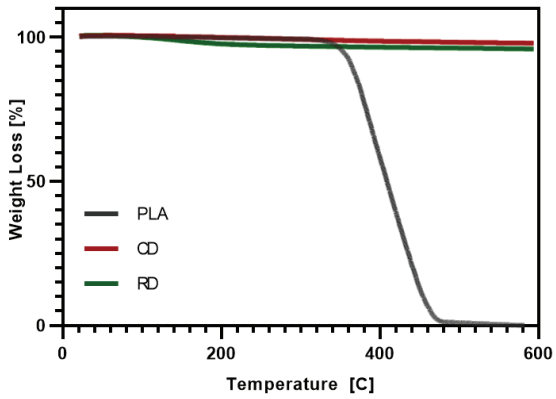


Figure 4.23. Thermal degradation of PLA, CD and RD

Figure 4.23 displays the thermogravimetric loss of weight curves of PLA, and both calcinated and raw diatoms from room temperature to 600°C. As seen, diatoms did not show any thermal decomposition up to 600°C, thermal stable, due to the mostly presence of silica content. Thermal decomposition behaviour of PLA-Diatom composites also showed a single step decomposition pattern (Figure 4.23).

As seen from thermograms (Figure 4.24), PLA-CD and PLA-RD composites showed almost similar degradation temperature during TGA. The degradation temperature of PLA with both diatoms addition decreased, for 5% weight loss, PLA started to degrade at 350,5°C. Depending on the results, it was clearly seen that diatom addition decreased the pure PLA decomposition temperature from 383,43°C to 368,85°C, 364,86°C and 364,49°C for PLA-3CD, PLA-5CD, and PLA-10CD composites, respectively. Same behaviour was also observed for PLA-RD composites. Generally, thermal decomposition temperature of thermoplastic polymer is retarded with inorganic particle addition such as boron nitride and clay [112] [113]. However, in our study, initial

thermal decomposition temperature is reduced almost 30 °C at high loadings of calcinated diatom addition. In these circumstances, diatom shells had a role as thermal breakdown [114].

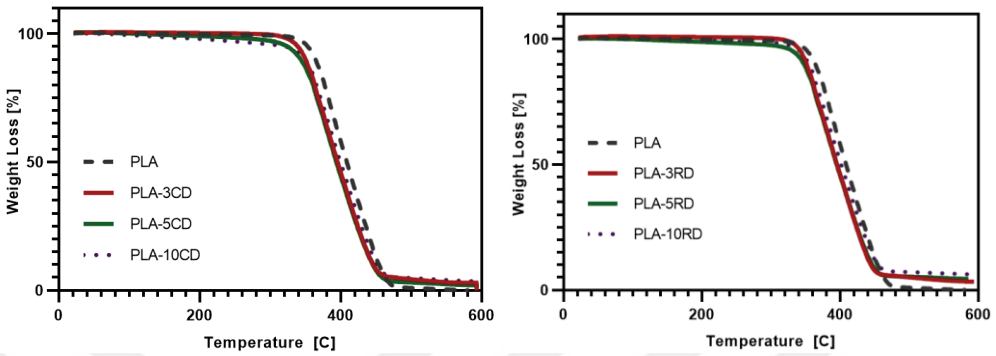


Figure 4.24. PLA-Diatom composites TGA results

For 5% mass loss, PLA started to degrade at 350,5°C. At the same manner 5% mass loss temperature of PLA for 5% mass loss decreased to 341,5°C for PLA-3RD, 326,21°C for PLA-5RD and 338,2°C for PLA-10RD. It was because of that during the melting process of composite preparation, diatoms and PLA matrix were subjected into friction force and heat at the same time. It was caused degradation temperatures changing[115].

The sample of pure PLA exhibited the highest degradation temperature between all samples. Increasing the concentration of both calcinated and raw diatom had different TGA results but decreased thermal stability. 3% CD and RD addition separately had the higher initial degradation temperature for 5% mass loss, but still lower than pure PLA. In this case thermal stability could be stated as higher degradation temperature. For diatom addition with 3% with the aid of porous structure of them blocked the movement of matrix in contrast to 5% and 10% diatom addition for both diatom types. All results were summarized in Table 4.9. The variation in pure PLA and PLA-Diatom composites' residue were occurred because of the thermal degradation behaviour. It can be concluded that the optimum diatom concentration for both CD and RD was 3% addition into PLA matrix.

Table 4.9. TGA results of PLA and PLA-Diatom composites

| | T at 5% Weight loss [°C] | T at max weight loss [°C] | Residue [%] |
|---|---|---|---|
| PLA | 350,5 | 383,4 | 0,0001± |
| PLA-3CD | 335,9 | 368,8 | 2,85±0,4 |
| PLA-5CD | 316,8 | 364,8 | 1,88±0,4 |
| PLA-10CD | 292,4 | 364,4 | 3,39±0,4 |
| PLA-3RD | 341,5 | 369,4 | 3,11±0,4 |
| PLA-5RD | 326,2 | 367,1 | 4,38±0,4 |
| PLA-10RD | 338,2 | 364,6 | 5,21±0,4 |

It was generally stiff and brittle characteristics with low elongation at break can be modified by altering PLA's physical characteristics with utilization of a biocompatible plasticizer. Figure 4.25 shows effect of plasticizer on thermograms of PLA. Addition of plastizer/compatibilizer decreased slightly the initial decomposition temperature. Similar decreasing trend in thermal stability of plasticized PLA has been reported in the literature[116] In this case PEG and PEG/POSS with different concentration. 5% and 10% PEG addition were applied into PLA matrix, then both diatoms were added to form composites. Thermogram indicated that PLA have the highest thermal stability and it can be result of crystalline structure.

PLA-5PEG content decreased 5% mass loss temperature to 328,5°C and at the same concentration for PLA-5PEG/POSS had higher 5% mass loss temperature value than PLA-5PEG and it was 334,2°C. Cage structure of PEG/POSS can create more stabilized thermal character but the difference was not too high. But 10% PEG concentration had the lowest 5% mass loss temperature as 305,1°C. Plasticizer concentration should be optimized and it was clearly seen that 5% plasticizer concentration had better than 10% plasticizer content as PEG. In addition to that, 5% PEG/POSS showed higher thermal stability than 5% PEG plasticizer composites.

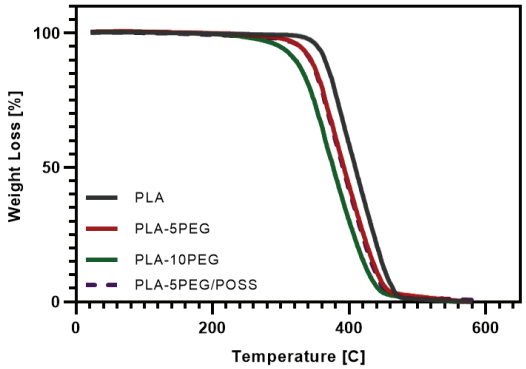


Figure 4.25. TGA curves of plasticized PLA

Firstly 5% PEG plasticizer was explained as plasticizer and both diatom types with 3% concentration were applied and investigated, as well. PLA-5PEG composites TGA curves were indicated in Figure 4.26 below.

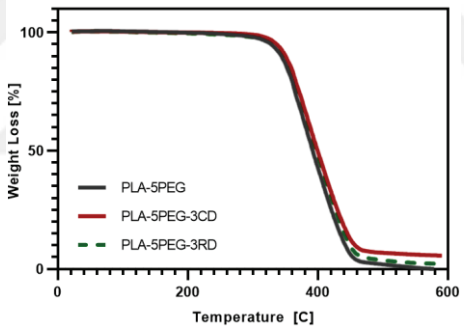


Figure 4.26. TGA curves of PLA-5PEG-3Diatom composites

The pure PLA begins to break down due to the loss of end group off the primary chain or an ester change at approximately 273°C [117]. 5% PEG incorporation into PLA matrix directly decreased the 5% mass loss temperature of PLA from 350,5°C to 322,5°C. Since PEG 5% mass loss temperature is only 290,6°C, which is significantly lower than that of pure PLA, this behaviour is mostly caused by the material's weak thermal stability. Additionally, PEG's plasticization of PLA has the tendency to lower the polymer's overall crystallinity. The polymer may be more susceptible to degrade at higher temperatures due to the lower crystallinity. Additionally, it was discovered that the PLA/PEG blend's burned residue was minimal. The thermal stability is improved with the addition of CD

and RD into PLA matrix, though. A higher temperature of 5% mass loss was observed in the blend nanocomposites made with PLA-5PEG-3CD and PLA-5PEG-3RD at 332.5°C and 327.5°C, respectively. In thermal decomposition of PLA-PEG composites are slightly enhanced with the incorporation of both type of diatoms. As a result, in the case of PLA-PEG-composite systems, the delayed thermal decomposition of blend has been observed, however unplasticized PLA-composite system, the opposite behaviour was observed. Mass loss data for PLA-5PEG-diatom composites was summarized in Table 4.10 below.

Table 4.10. TGA results of PLA-5PEG-3Diatom composite systems

| | T at 5% Weight loss [◦C] | T at max weight loss [◦C] | Residue [%] |
|---|---|---|---|
| PLA | 350,5 | 383,4 | 0,0001± |
| PLA-5PEG | 322,5 | 378 | 0 |
| PLA-5PEG- 3CD | 332,5 | 390 | 5,6±0,40 |
| PLA-5PEG- 3RAW | 327,5 | 386 | 2,1±0,41 |

Depending on the results stated in Table 4.10 above, it can be said that 3% calcinated diatom added PLA-5PEG had higher thermal stability than PLA-5PEG-3RD composite systems. Calcination process includes thermal treatment in order to get rid of the organic residues of the raw diatom. But there wasn't a significant degradation in 5% mass loss temperature, but char residue percent of PLA-5PEG-3RD was approximately half of PLA-5PEG-3CD composites. It can be result of an organic content inside of raw diatom, which burned more than calcinated diatom.

Plasticizer concentration was increased with each composite sample in order to investigate and compare the difference and the effect of plasticizer concentration. 10% PEG addition was applied to polymer matrix and PLA-diatom composites and the results are indicated in Figure 4.27 below.

There were slightly decreased in 5% mass loss temperature with PLA-10PEG. 5% mass loss temperature of PLA-10PEG-Diatom composites have lower value than 5% PEG added PLA-Diatom composites, as expected. But same behaviour that 3% both diatom addition enhanced the thermal stability of PLA-10PEG composites. 5% mass loss temperature of PLA-10PEG-Diatom composites were increased on the contrary to PLA-

10PEG 5% mass loss temperature. Thermal stability of pure PLA and PLA-10PEG were enhanced because of better dispersion of layered silicate molecules. Additionally, polymer chains and diatom particles have high molecular interaction. This interaction contributes the improvements of thermal stability [118]. The results of 10% PEG added composites were summarized in Table 4.11.

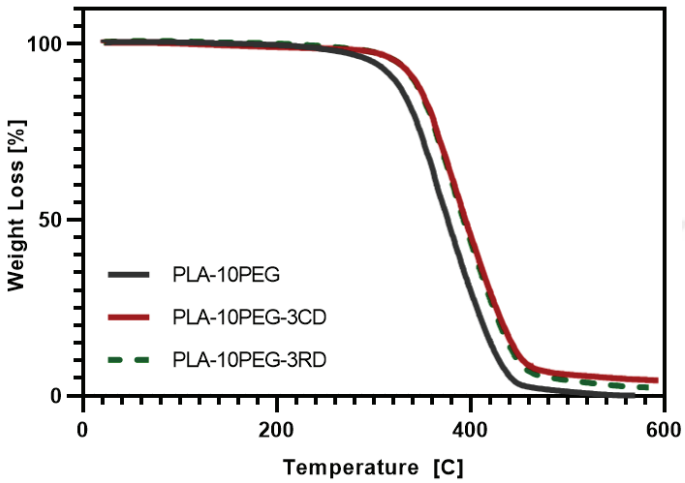


Figure 4.27. TGA results of 10% PEG added PLA-Diatom composites

Table 4.11. TGA results of PLA-10PEG-Diatom composites

| | T at 5% Weight loss [°C] | T at max weight loss [°C] | Residue [%] |
|---|---|---|---|
| PLA | 350,5 | 383,4 | 0,0001± |
| PLA-10PEG | 296 | 366 | 0 |
| PLA-10PEG- 3CD | 330 | 392 | 4,3±0,4 |
| PLA-10PEG- 3RD | 331 | 388 | 2,2±0,41 |

Plasticizer effected polymer thermal stability in negative way, because PEG has lower thermal stability. Furthermore, PEG's plasticization of PLA has a tendency to lower polymer's overall crystallinity. The polymer may be favourable to degrade at higher temperatures due to the lower crystallinity. Additionally, it was discovered that PLA-PEG blends had very small amount of char. Diatom addition increases char amount, and PLA-10PEG-3RD composites had 2,29% residue and PLA-10PEG-3CD composites had lower

char as 4.36 %. As previously mentioned, organic content of raw diatom could be accepted as burnt more than calcinated diatom composites.

Both calcinated and raw diatom composites had lower thermal stability than pure PLA and higher thermal stability than 5% and 10% PEG added pure PLA. Plasticizers directly affect pure crystal character polymer but silica content additives increase plasticized polymer molecular interaction, thus thermal stability. Concentration difference of PEG into PLA was investigated but at the same time PEG-POSS plasticizer effect was performed, as well. PEG-POSS cage structure had relatively different behaviour, but just one diatom type used, raw diatom. The reason for that raw diatom had improved PLA' s composite properties and there were very small changes between calcinated and raw diatom addition into PEG plasticized PLA composites. In this part, PEG-POSS plasticized PLA with raw diatom addition were discussed.

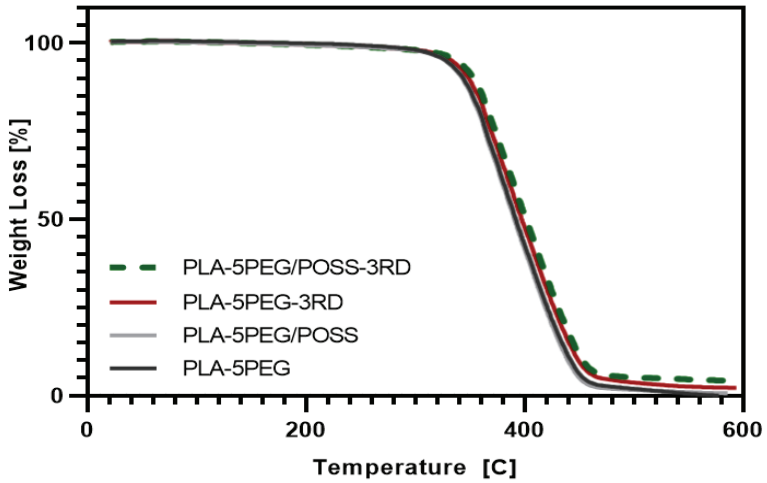


Figure 4.28. TGA curves of PLA-5PEG-3RD and PLA-5PEG/POSS-3RD composites

As in the case of PEG-POSS addition to PLA, decomposition slightly increased (from 383,43° for PLA to 386° PLA-5PEG/POSS) as seen in Figure 4.28, similarly RD incorporation increased decomposition temperature to 392°C for PLA-5PEG/POSS-3RD. It is also noted that PLA-5PEG/POSS-5RD and PLA-5PEG/POSS-10RD incorporated composites might have agglomerations due to the residual amount result (Table 4.12). Meyva et al (2020) indicated the similar results for PLA-POSS composite system manufactured with compound mixing, POSS application increased decomposition

temperature and increasing POSS content increased the degradation temperature again (PLA-%1POSS 365°C and PLA-%3POSS 368°C)[119].

Table 4.12. TGA results of PLA-5PEG/POSS-RD composites

| | T at 5% Weight loss [°C] | T at Max Weight loss [°C] | Char [%] |
|---|---|---|---|
| PLA | 350,5 | 383,4 | 0,0001± |
| PLA-5PEG/POSS | 334,2 | 386 | 0,6±0,4 |
| PLA-5PEG/POSS-3RD | 336,1 | 392 | 4,1±0,3 |
| PLA-5PEG/POSS-5RD | 343,2 | 414 | 3,7±0,4 |
| PLA-5PEG/POSS-10RD | 331,2 | 409,2 | 8,7±0,3 |

### 4.2.4.2 Differential Calorimetric Scanning (DSC)

Figure 4.29 shows the DSC thermograms of PLA and diatoms under heating mode from room temperature to 600°C. It can be seen that there are 3 thermal transition points of PLA:

I. Glass transition temperature ($T_g$),
II. Melting temperature ($T_m$) and
III. Thermal degradation temperature ($T_d$)

$T_g$ of PLA was determined as 63,39°C. Melting and thermal decomposition temperatures are determined as 152,52 and 383,43°C, respectively. Figure 4.29 shows the thermograms of PLA-Diatom composites. Incorporation of diatoms did not significantly change the $T_g$'s of PLA-CD composites, however, slight decrease approximately of 1-2 $^{o}$ C in PLA-RD composites was observed. Melting temperature of PLA decreased with diatom incorporation and increased even further with an increase in diatom content (Table 4.13). In addition, except lower concentration of PLA-CD composites, crystallinity of PLA composites generally improved by diatom incorporation as seen in Table 4.13. This finding can be attributed to the possibility that diatom shells serve as crystallization nuclei and promote the crystal formation. This behavior was also observed in the study of Dobrosielska et.al (2020) [21].

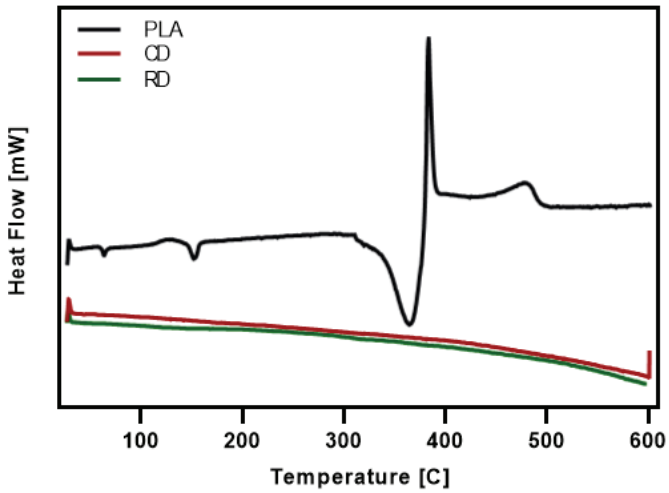


Figure 4.29. DSC thermograms of pure PLA, Calcinated and Raw Diatoms

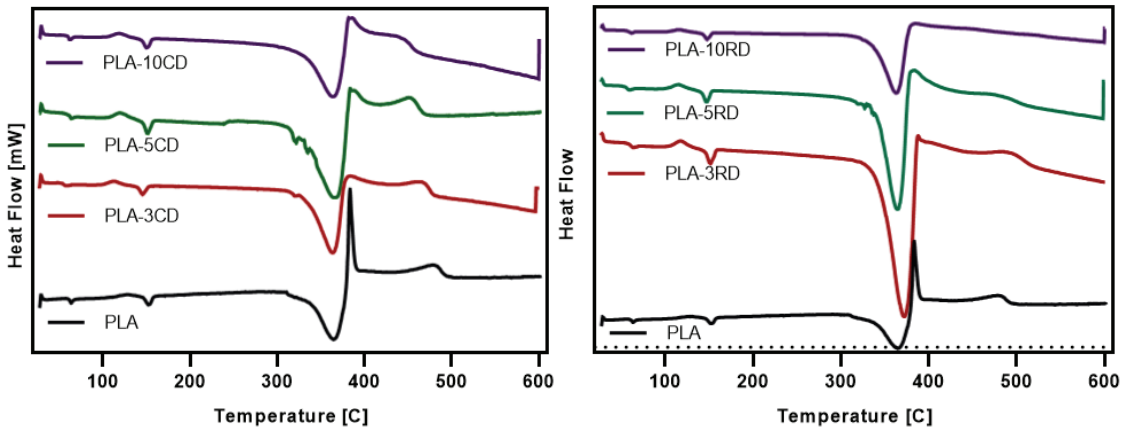


Figure 4.30. DSC thermograms of pure PLA-Diatoms

Table 4.13. DSC results of PLA-Diatom composites

| | Tg [°C] | Tcc [°C] | Tm [°C] | ΔHm [J/g] | Xc [%] |
|---|---|---|---|---|---|
| PLA | 63,39 | 126,20 | 152,52 | 15,39 | 16,54 |
| PLA-3CD | 63,21 | 114,40 | 150,52 | 10,22 | 10,22 |
| PLA-5CD | 64,16 | 118,33 | 151,22 | 16,22 | 16,22 |
| PLA-10CD | 63,41 | 116,37 | 151,36 | 19,62 | 19,62 |
| PLA-3RD | 61,28 | 118,33 | 149,26 | 26,01 | 26,01 |
| PLA-5RD | 62,11 | 116,30 | 156,22 | 11,45 | 11,45 |
| PLA-10RD | 63,33 | 114,42 | 149,34 | 25,12 | 25,12 |

Plasticizer effects on thermal behaviour were investigated, as well (Figure 4.31). $T_g$ values decreased from 63,39 º to 55,4°C, 57,09°C and 55,36°C, respectively for PLA-5PEG, PLA-10PEG and PLA-5PEG/POSS. Plasticisers directly affected PLA's processability with decreasing $T_g$ values; thus; plasticiser concentration had an importance and limiting character. PEG-POSS had almost similar effect on the $T_g$'s of PLA that was measured very close to PLA-5PEG blend.

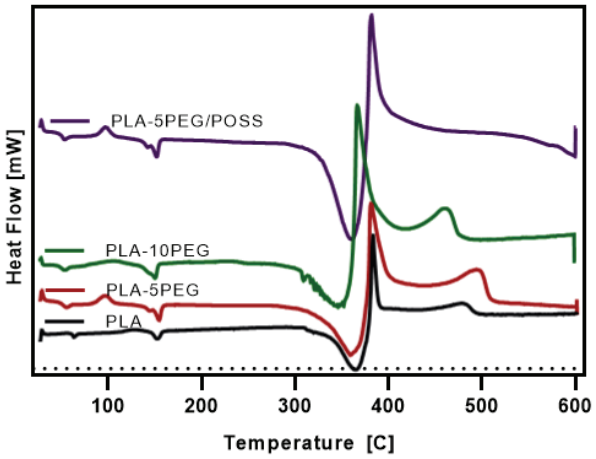


Figure 4.31. DSC Thermograms of PLA and plasticizers

Effect of PEG plasticization on thermal behaviour of 3wt% diatom incorporated PLA composites was shown in Figure 4.32 and all results are tabulated in Table 4.14. PEG plasticization decreased the $T_g$, and increased the $T_m$ and $X_c$% values of PLA. As diatoms were incorporated in PLA-PEG, it was found that diatoms did not change much $T_g$'s, however, $T_m$ and crystallinity percentage decreased slightly with diatom content from 154 to 153°C and 21 to 15 %, respectively. This could be due to the size difference of CD and RD diatom that can affect on nucleation of crystals differently.

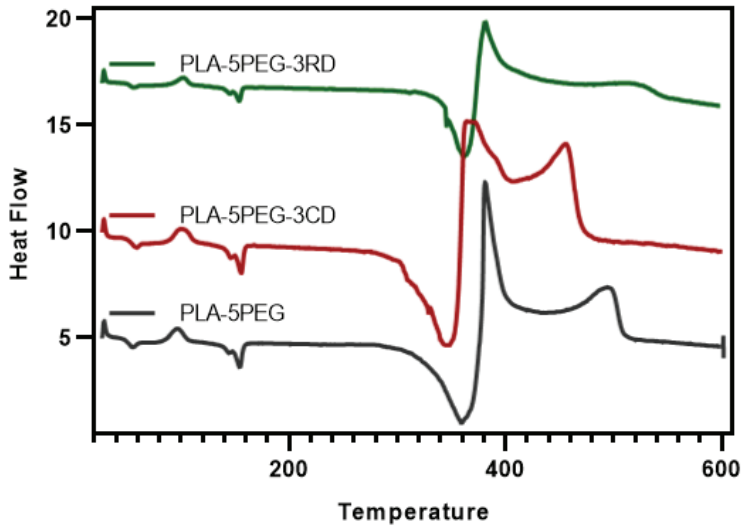


Figure 4.32. DSC thermograms of PLA-5PEG-3D composites

Table 4.14. DSC results of PLA-5PEG-3Diatoms composites

| | Tg [◦C] | Tcc [◦C] | Tm [◦C] | ΔHm | Xc [%] |
|---|---|---|---|---|---|
| PLA | 63,99 | 126,20 | 152,52 | 15,39 | 16,54 |
| PLA-5PEG | 55,40 | 100,63 | 154,33 | 20,97 | 20,97 |
| PLA-5PEG- 3CD | 57,52 | 102,60 | 154,09 | 19,52 | 19,52 |
| PLA-5PEG- 3RAW | 55,74 | 103,91 | 153,42 | 14,63 | 14,63 |

In the case of PLA-10PEG, $T_g$ value is greater than the value of PLA-5PEG, but crystallinity is improved with an increase in PEG concentration from 21 to 38%. This behaviour was also explained by Toncheva et al (2016) that cold crystallization ($T_{cc}$) peak shifted lower and the degree of polyester crystallization [7]. On the other hand, diatom addition decreased the $T_g$ values of PLA-10PEG. PLA-10PEG-3CD, PLA-10PEG-3RD had $T_g$ values as 51,23°C, 53,08°C and 52,43°C respectively. $T_m$ values did not change with diatom incorporation.

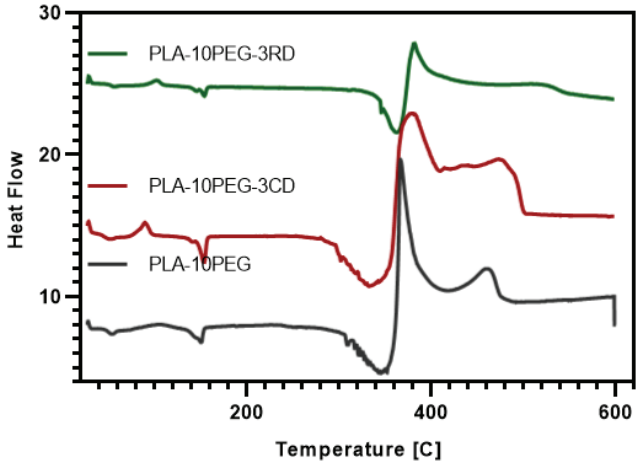


Figure 4.33. DSC thermograms of PLA-10PEG-3Diatom composites

Table 4.15. DSC results of PLA-10PEG-3Diatom composites

| | Tg [°C] | Tcc [°C] | Tm [°C] | ΔHm | Xc [%] |
|---|---|---|---|---|---|
| PLA | 63,39 | 126,20 | 152,52 | 15,39 | 16,54 |
| PLA-10PEG | 57,09 | 94,73 | 153,49 | 32,09 | 37,95 |
| PLA-10PEG- 3CD | 51,23 | 90,80 | 152,55 | 24,16 | 24,16 |
| PLA-10PEG- 3RD | 52,43 | 88,83 | 153,71 | 22,36 | 22,36 |

Crystallinity of PLA were increased with an increase in PEG concentration from 16.5 to 37,95%. Semicrystalline PLA had more crystalline structure than PLA-10PEG, With the melt mixing process, PEG may pass in the spaces between PLA macromolecules and create atomic-level physical interactions such as hydrogen bonds or dipole-dipole interactions. This will lead to a partial replacement of the rigid homogeneous PLA-PLA contact by heterogeneous PLA-PEG interaction. This effect might improve macromolecular mobility, resulting in less energy being used during the glass transition or lowering the $T_g$ [7]. In the case of the diatom addition, PLA-5PEG-3CD, PLA-5PEG-3RD PLA-10PEG-3CD, and PLA-10PEG-3RD blend nanocomposites, respectively, the degree of virgin matrix crystallinity changed from 16% to 19%, 14%, 24% and 22%. It is clear that the increase in $\Delta H_m$ caused $X_c$ to rise in the case of the mixture and its nanocomposites. Sungsanit et al. (2012) also noted the blend's improved crystallinity by enhancing the mobility of the PLA molecule, PEG as a plasticizer has the potential to boost the ductility of virgin material[120]. Figure 4.34 shows the DSC thermograms of

PLA-PEG/POSS and RD incorporates composites. $T_g$ values of PLA-5PEG/POSS was determined as 55,36°C. PEG/POSS addition decreased the $T_g$ of PLA as expected and at the same time, like PEG, crystallinity percentage increased. Turan et al (2011) declared the same finding as POSS particles served as the PLA's nucleating agent and plasticized PLA were shown to have increased % crystallinity in the presence of POSS [81]. RD addition did not change the $T_g$'s however slight decrease in crystallinity occurs first, but reach the same value of PLA-PEG/POSS (25%) at the higher loadings of RD.

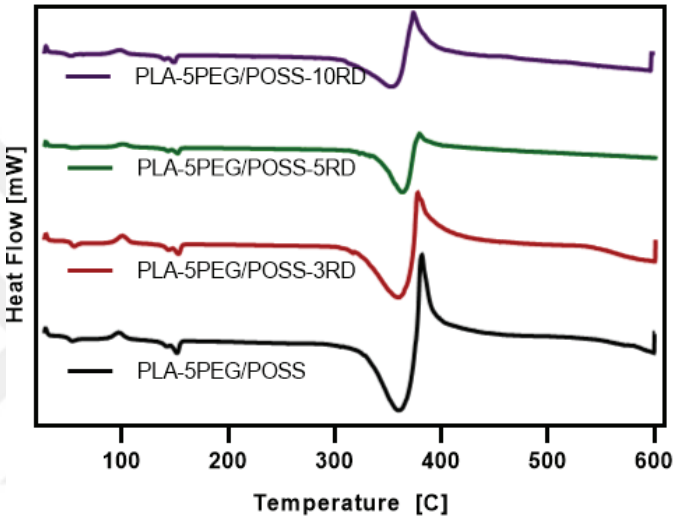


Figure 4.34. DSC thermograms of PLA-5PEG/POSS-RD

Table 4.16. DSC results of PLA-5PEG/POSS-RD composites

| | $T_g$ [°C] | Tcc [°C] | $T_m$ [°C] | $\Delta H_m$ | $X_c$ [%] |
|---|---|---|---|---|---|
| PLA | 63,39 | 126,20 | 152,52 | 15,39 | 16,54 |
| PLA-5PEG/POSS | 55,36 | 96,70 | 153,63 | 22,21 | 25,07 |
| PLA-5PEG/POSS-3RD | 55,41 | 100,63 | 153,41 | 21,99 | 18,92 |
| PLA-5PEG/POSS-5RD | 55,37 | 102,60 | 153,39 | 18,28 | 20,96 |
| PLA-5PEG/POSS-10RD | 58,14 | 98,66 | 152,49 | 19,98 | 24,16 |

### 4.2.5. Fourier Transform Infrared (FTIR) Analysis of Composites

PLA/Diatom composites were subjected to FTIR spectroscopy to investigate the differences in bond structure.

Figure 4.35 shows the infrared spectra of pure PLA. PLA has ester groups and peak values at 2988, 2950, 1716 and 1119 $cm^{-1}$ correspond to antisymmetric of the $–CH_2$ group, symmetric stretching vibration of $–CH_2$ group, stretching vibration of the C = O bonds and symmetric stretching vibration of the C–O–C groups, respectively [121].

Diatomite reactivity is expressed by the existence of primary active sites on its surface. The -OH groups and oxygen bridges on the diatomite surface serve as an adsorption site., additionally, -OH groups are bounded by Hydrogen bonds. On the surface of diatom, there are siloxane groups (Si-O-Si) that makes bridges with oxygen atoms. Main characteristic bands of diatoms have been reported as 467, 799, and 1093 $cm^{-1}$ correspond to the bending vibration and symmetric stretching vibration of the Si–O bonds and antisymmetric stretching vibration of the Si–O-Si bonds, respectively,[122].

It is observed that typical infrared absorption characteristic peaks of pure PLA were all present in the spectrum of the PLA-diatom composites (Figure 4.36). There is no new bond formed, however, it was challenging to detect the main characteristic peaks of the diatoms in the spectrum of PLA composites due to coinciding of PLA and diatoms peaks in the range of 1000-500 $cm^{-1}$. It was also observed some shifts in the specific bands of the spectrum of PLA-Diatom composites at the bending frequencies of $–CH_3$ symmetric peak from 1360 to 1350 $cm^{-1}$, at similarly 1140 $cm^{-1}$ peak for PLA shifted to 1089 $cm^{-1}$ and bending frequencies of $–CH_3$ asymmetric peak broadened from 1440 to 1470 $cm^{-1}$.

Since diatom has OH groups and they can interact with PLA ester groups. The adsorption sites of diatoms are Si-OH, Si $(OH)_2$ and Si-O-Si. Si-O stretching peaks were expected in the spectrum of PLA-Diatom composites at around 1050-1090 $cm^{-1}$. It can be concluded that PLA-Diatom composites separately showed main characteristic peaks, but shifting and broadening the peaks indicate the secondary interactions between PLA-Diatoms.

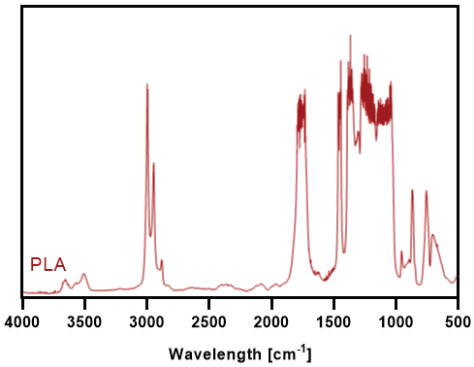


Figure 4.35. FTIR spectra of pure PLA

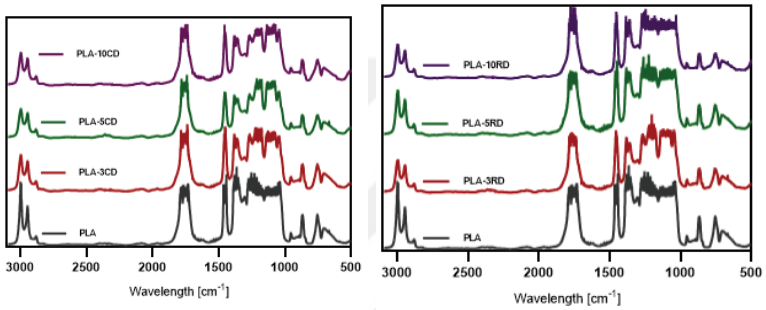


Figure 4.36. FTIR spectra of PLA-CD and PLA-RD composites

Similar spectrum was also observed in the spectrum of PLA-RD composites. However, intensity in the spectrum of PLA-RD composite at 1450 $cm^{-1}$ was stronger than PLA-CD composites. It can be said that surface chemistries resembled, but at the same concentrations (PLA-5CD & PLA-5RD) RD showed greater interaction than CD [123]. Increasing diatom concentrations indicated stronger interactions like broadened peak but CD showed more resemble peaks at 1000-1300 $cm^{-1}$ to RD composites (Figure 4.37).

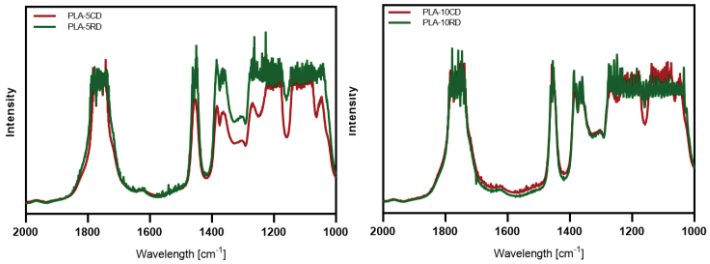


Figure 4.37. FTIR spectra of PLA-5Diatom and PLA-10Diatom composites between 1000-2000 $cm^{-1}$

FTIR spectrum of PLA-PEG exhibited characteristic peaks similar to those of pure PLA as seen in Figure 4.38. Additionally, C-H stretching peak observed at 2880 $cm^{-}$ was broadened compared to pure PLA. Also, the intensity of characteristic peaks of PLA at 2988 $cm^{-1}$ (asymmetric of the $–CH_2$ group) and 1765 $cm^{-1}$ (C=O stretching ) was reduced TO 1758 $cm^{-1}$ with PEG addition. Strong hydrogen bonding between the C=O group in PLA and the -OH group in PEG is responsible for the displacement of the peak that has been attributed to PLA's C=O stretching. This indicates good chemical interactions between PLA and PEG. PLA-5PEG also showed the most intensive absorbance at 1365 – 1375 $cm^{-1}$ wavelength range (C-H deformation) compared to PLA-10PEG.

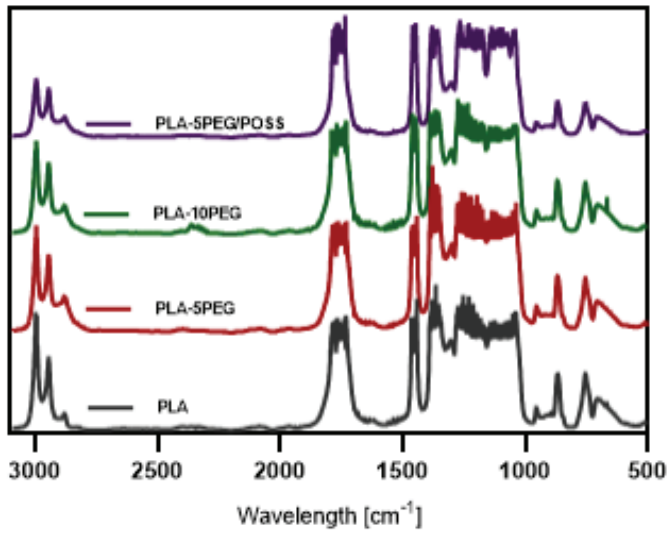


Figure 4.38. FTIR spectra of PLA-Plasticizer blends

FTIR analyses of PLA-PEG/POSS composites were also illustrated in Figure 4.38 and showed the characteristic main peaks of PLA as reported earlier and Si–O–Si and Si–C peaks of POSS observed at 1080 $cm^{-1}$ and 1250 $cm^{-1}$, respectively as found in good agreement with the literature [119]. Slight shifts in some peaks were observed as C–O stretching peaks at 1080 $cm^{-1}$ and broadened. These changes could be accepted as the certain level of secondary interactions between PEG/POSS and PLA.

In addition, -C–H bending peak at 1363 $cm^{-1}$, $CH_3$ bending absorption peak at 1453 $cm^{-1}$; C=O stretching peak at 1745 $cm^{-1}$, and asymmetrical and symmetrical stretching of C-H peak at 2943 and 2993 $cm^{-1}$ were observed, respectively. However,

distinguishing discrepancies in the IR spectrum of the PLA-PEG/POSS was not easy due to the overlap of typical PLA peaks with POSS peaks.

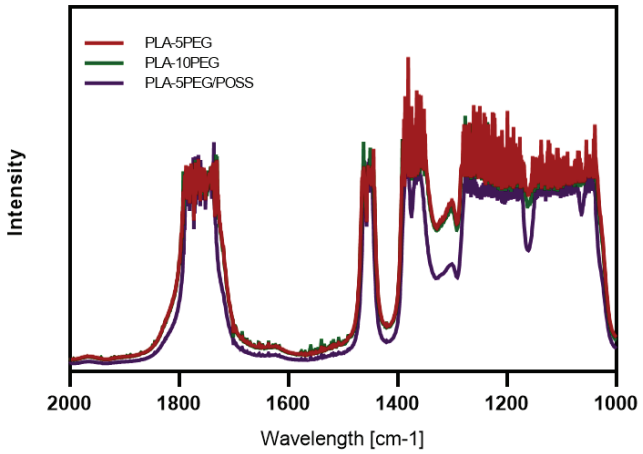


Figure 4.39. FTIR spectra of PLA-Plasticizer composites between 1000-2000 $cm^{-1}$

Effect of diatom addition on FT-IR spectrum results of PLA-PEG blends was demonstrated in Figure 4.40.

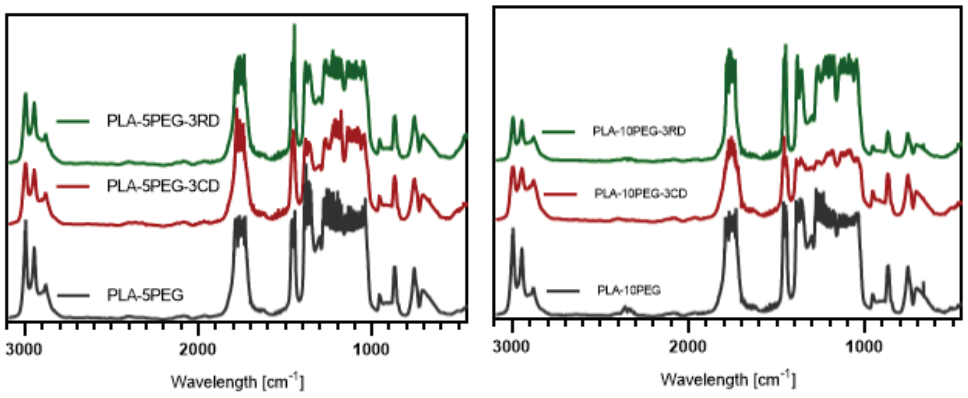


Figure 4.40. FTIR spectra of PLA-5PEG-3Diatom and PLA-10PEG-3Diatoms blends

Apparently seen from the spectrum of composites, the stretching vibrations of the siloxane (-Si-O-Si-) groups are responsible for the large bands seen 1200-900 $cm^{-1}$ respectively, while the bending vibrations of the -OH and Si-O groups are responsible for

the small bands appeared at 1635 $cm^{-1}$ and 748 $cm^{-1}$ [123]. $CH_3$ peak at 1453 $cm^{-1}$ was observed and RD showed more intense peak in contrast to CD composites.

Lastly, PEG/POSS was used in order to compatibilizer PLA/Diatom composites. Figure 4.41 indicated the spectra of PLA-5PEG/POSS-RD below.

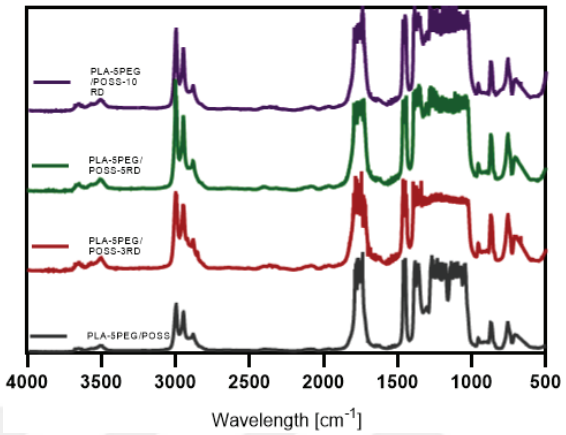


Figure 4.41. FTIR spectra of PLA-5PEG/POSS-RD composites

The stretching vibration peaks of siloxane (Si-O-Si) between 1040 and 1120 $cm^{-1}$, the peak of Si-C vibration at 1250 $cm^{-1}$ and the bending vibration of C-H in the band of 1295-1365 $cm^{-1}$ were reported as the distinctive IR bands for the fundamental POSS structure [119]. FTIR results showed that the Si-O-Si and Si-C peaks were found at 1080 cm1 and 1180 cm1, respectively, and the C-H bending vibration was shown in the band of 1332 $cm^{-1}$ to 1366 $cm^{-1}$. PLA-5PEG/POSS-RD composites had same bond vibrations as the stretching vibrations of the silanol (Si-OH) and siloxane (-Si-O-Si-) groups, respectively, raw diatom has wide bands at the range of 1200–900 $cm^{-1}$, while the little bands at 1635 $cm^{-1}$ and 748 $cm^{-1}$ represent the bending vibrations of -OH and Si-O groups, respectively.

## 4.2.6. Rheological Properties of Composites

A common method for assessing the internal structure of PLA-composites in a fluid state is dynamic rheological analysis. The viscoelastic behaviour of the sample is

basically described by the storage modulus G' (in Pa), which stands for the elastic component and the loss modulus G'' (in Pa), which stands for viscous component of the viscoelastic behaviour. Compatibility of composites can be obtained with decreasing G', G'' and η* values [85].

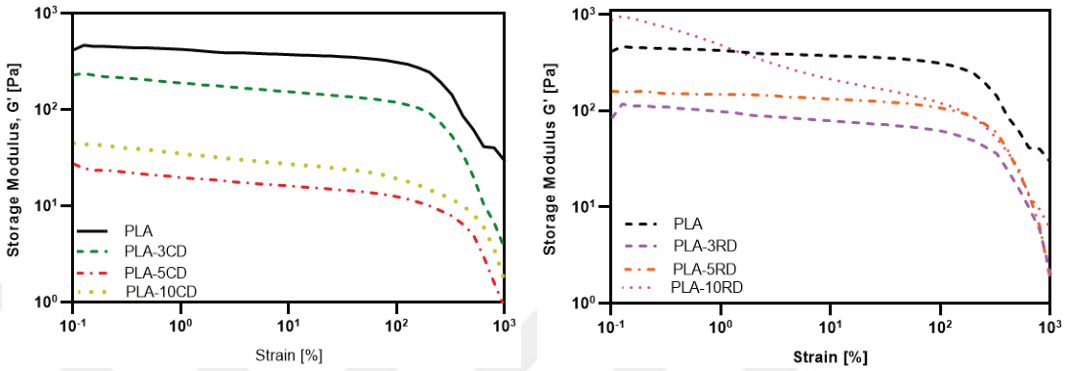


Figure 4.42. Storage Modulus (G') and Strain (%) of PLA-CD and PLA-RD

PLA has the highest G' value as 423,30 Pa diatom addition directly decreased G' value of PLA. PLA-3CD, PLA-5CD and PLA-10CD had G' value as 188,9 Pa, 19,69 Pa and 35,26 Pa respectively (Figure 4.42). Increasing diatom concentration decreased G' value up to 5% calcinated diatom, then there was a slight increase on PLA-10CD, but still lower than pure PLA. Raw diatom had the same effect on pure PLA, however increasing raw diatom concentration resulted in slight increase proportionally in G'. PLA-3RD, PLA-5RD and PLA-10RD had G' value as 97,81 Pa, 148,20 Pa and 480,30 Pa respectively. G' stated to the solid-like behaviour and both diatom types decreased G' value of PLA, thus decreased solid-like behaviour of PLA and increase in liquid-like behaviour. The PLA-Diatom composite is becoming more viscous due to the addition of diatoms. It was ascribed to the diatom and PLA matrix interactions. Because diatoms are porous, they helped with internal friction and energy dissipation in PLA-Diatom composites. As strain grows, this action can cause the materials' capacity to store elastic energy to decrease.

Liquid-like behaviour is related to the G'' loss modulus. Loss modulus of PLA-Diatom composites was investigated, as well (Figure 4.43).

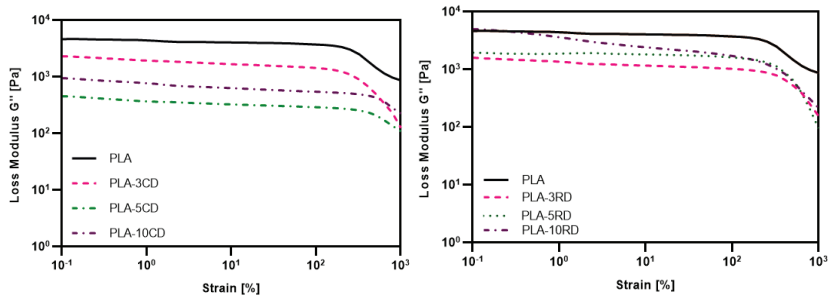


Figure 4.43. Loss Modulus (G'') and Strain (%) of PLA-Diatoms

PLA had 4395 Pa G'' value at 1% strain. Calcinated diatom composites showed similar trend with storage modulus (G'). PLA-3CD, PLA-5CD and PLA-10CD had G'' values as 1930 Pa, 366,60 Pa and 769,20 Pa respectively. Raw diatom composites had similar trends as storage modulus (G'), as well. G'' values were increased proportional to the concentration of raw diatom, but still lower than pure PLA. Rheological analysis was performed in molten phase, thus G'' values of all samples are greater than G' values. The results indicated that both diatom addition increased the liquid-state behaviour of the PLA. When diatoms were added to PLA, the loss modulus was lower than when PLA was pure. It highlighted the PLA-Diatom composites' capacity to recover deformation energy and suggested that they responded more elastically. Pure PLA's elastic qualities were strengthened by the addition of diatoms. When the concentration of diatoms increased, the composites exhibited a decreased tendency to release energy as heat during deformation. This decrease in viscous dissipation may be linked to increased stiffness of the material. Diatoms also served as a reinforcing ingredient, which helped the composites resist deformation without suffering a large energy loss. Consequently, loss modules decreased, particularly at greater strain values.

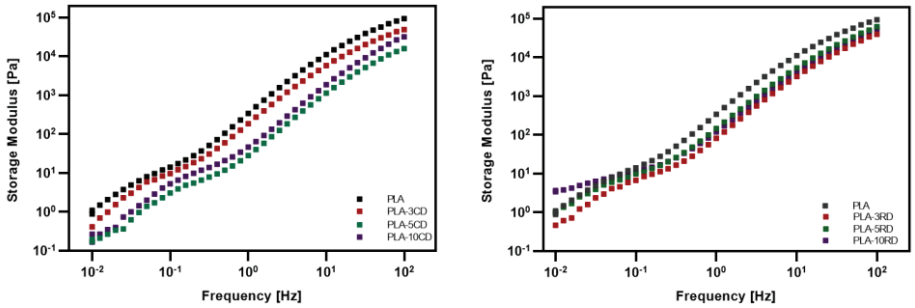


Figure 4.44. Storage Modulus (G') and Frequency (Hz) of PLA-CD and PLA-RD

The results of strain sweep tests of pure PLA, and its composites with CD (3, 5 and 10 wt. %) and with RD (3, 5 and 10 wt. %) were given in Figure 4.42 and 4.43. Pure PLA has the highest G' value and the addition of CD directly decreased G' value of PLA (Figure 4.42). Increasing diatom concentration decreased G' value up to 5% CD, then there was a slight increase on PLA-10CD, but still lower than pure PLA. The addition of CD decreased the ability of holding its structure up against incremental in frequency and became more deformable at 175°C.

It was observed that the G' of pure PLA were higher than the samples of PLA-CD composites, even though, the addition of RD into PLA decreased the G' of the sample as well when compared with pure PLA. The addition of 10 wt. % RD into PLA made the sample more sensitive to applied frequency. It was observed by a decreasing trend of G' and G'' with incremental frequency.

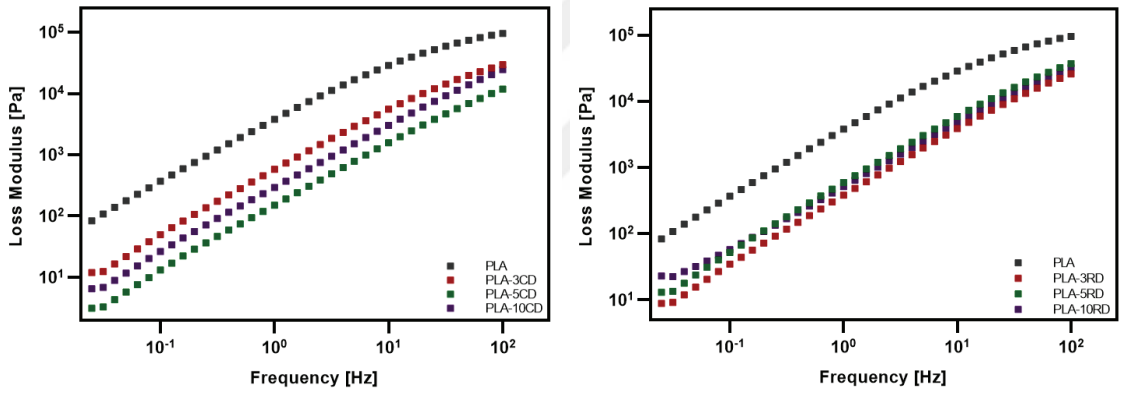


Figure 4.45. Loss Modulus (G'') and Frequency (Hz) of PLA-Diatoms

The distribution of G'' of PLA-Diatom composites were given in Figure 4.43. The distribution of G'' of CD and RD composites showed similar trend with storage modulus (G'). The G'' values were increased proportional to the concentration of RD, but still lower than pure PLA. Both types of diatoms decreased modulus of pure PLA but RD showed approximately similar behaviour for all concentrations.

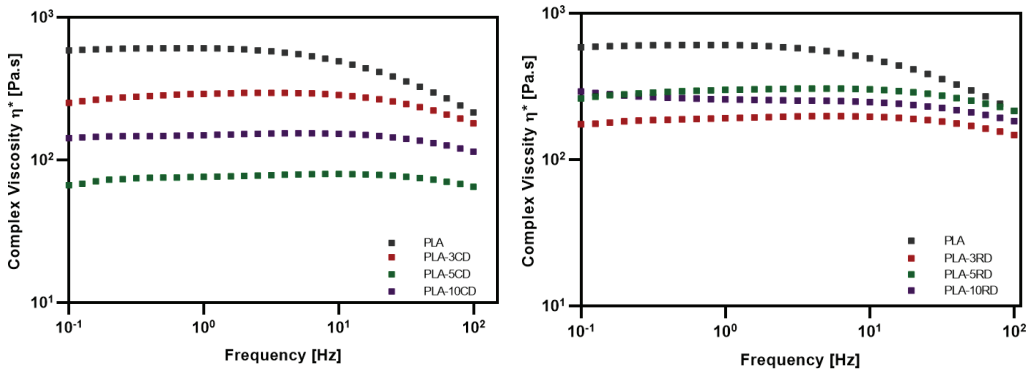


Figure 4.46. Complex viscosity (η*) and Frequency (Hz) of PLA-Diatom composites

Complex viscosity is another important property of rheological analysis which was investigated for all PLA composites. Blending character is important which was preferable with lower viscosities [105]. Diatom addition decreased complex viscosity; it is indicated that blending properties of PLA improved with diatom addition. Increasing concentration of calcinated diatom reduced complex viscosity of composites up to 5% calcinated diatom concentrations. However, PLA-10CD showed higher complex viscosity than PLA-5CD. It could be the reason for stiffness of higher concentration due to the agglomeration of additives. Ding et al. (2021) indicated that diatom addition decreased complex viscosity of PLA-Diatom composites [85]. All composites showed shear thinning behaviour that was observed with decreasing the viscosity while increasing angular frequency. Especially CD addition had greater decrease in complex viscosity than RD addition. Particle size of CD is lower than RD, according to Dobrosielska et al. (2020), the viscosity was reduced by the incorporation of diatomaceous earth in a smaller range of particle sizes [125]. Among different concentration of CD, PLA-3CD had higher complex viscosity than PLA-10CD and the lowest complex viscosity was observed with PLA-5CD. However, different concentration of RD addition showed totally different trend in contrast to CD which PLA-5RD had the highest complex viscosity and PLA-10RD showed greater complex viscosity than PLA-3RD. RD have different size of frustules and different shapes, thus fluctuations of complex viscosity value was obtained [126].

PEG and PEG/POSS were utilized with PLA and its effects on the rheological properties was investigated. G' value of plasticized PLA was decreased; thus, plasticity of PLA was improved. Choi et al. (2013) reported the improved plasticity of PLA with PEG addition [127]. PEG addition with two different concentrations (PLA-5PEG and

PAL-10PEG) had almost similar G' values but PLA-10PEG deformed easier than PLA-5PEG (Figure 4.58). PEG-POSS addition had similar behaviour as PLA-5PEG, but it had higher G' value than PLA-5PEG. PLA-5PEG/POSS showed liquid-like behaviour PLA-5PEG did. As a result, compatibility of PLA was improved with the addition of all plasticizers.

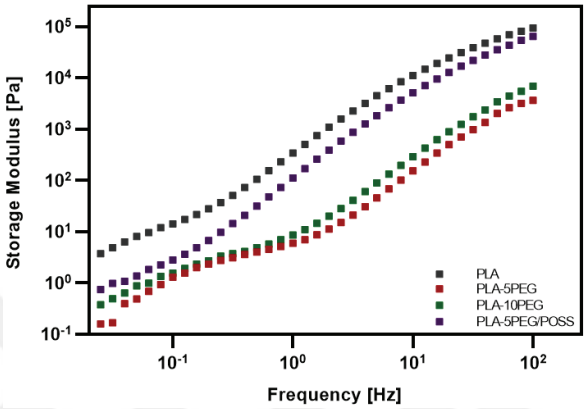


Figure 4.47. Storage Modulus (G') and Frequency (Hz) of PLA-Plasticizer

Loss Modulus of PLA-5PEG was higher than PLA-10PEG and PLA-5PEG/POSS in lower frequency, thus liquid-like character was higher than those composites. 5% PEG addition created more stiff character with PLA due to cold crystallization effect and increasing frequency decreased G'' value of PLA-5PEG.

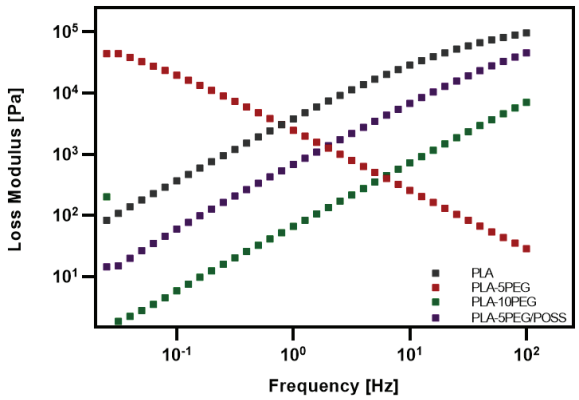


Figure 4.48. Loss Modulus (G'') and Frequency (Hz) of PLA-Plasticizer

Lower value of complex viscosity was obtained for all plasticized PLA in comparison to pure PLA. But complex viscosity of plasticized PLA remained approximately constant with increasing frequency. PLA-5PEG/POSS showed the highest complex viscosity value compared to PLA-5PEG and PLA-10PEG. PEG addition with higher concentration had reduced complex viscosity significantly. Linear region of PEG plasticized composites was extended, which indicated the adsorbed energy of PEG – plasticized PLA composites were higher than those PLA and PLA-5PEG/POSS samples.

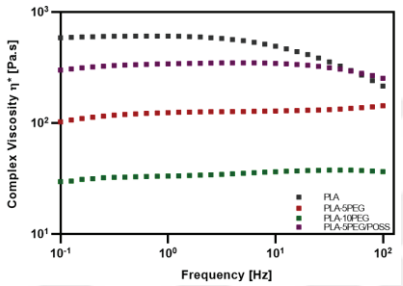


Figure 4.49. Complex Viscosity (η*) and Frequency (Hz) of PLA-Plasticizer

After plasticising PLA with PEG, diatom addition was applied in 3% wt. concentration to all plasticised PLA composites. Storage Modulus G' of PLA-5PEG-3RD and PLA-5PEG-3CD had resembled trend (Figure 4.48). On the other hand, PLA-5PEG-3RD had the highest G' value with increasing frequency than PLA-5PEG and PLA-5PEG-3CD. It would be result of the different particle size of diatomite particles [83]. RD particles contains more micro- and sub-micro fractions, thus showed a greater modulus because [19]. Increasing modulus in 5% plasticized composited referred the increasing compatibility of composites with both diatom addition, especially in higher frequencies.

The G'' of PLA-5PEG was the highest value than PLA-5PEG-3CD and PLA-5PEG-3RD. Since G'' represents liquid-like behaviour, it was seen that both CD and RD addition results in a reduction effect on G'. This result was consistent to the literature: the PLA composite samples gradually changed from the initial liquid-like response to a solid-like behaviour [128]. PLA-5PEG-3CD had lower G'' value than PLA-5PEG-3RD.

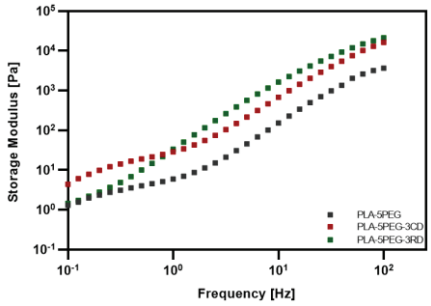


Figure 4.50. Storage Modulus (G') and Frequency (Hz) of PLA-5PEG-3Diatoms

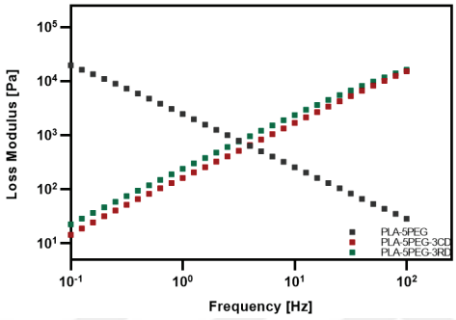


Figure 4.51. Loss Modulus (G'') and Frequency (Hz) of PLA-5PEG-3Diatoms

Complex viscosities of PLA-5PEG, PLA-5PEG-3RD and PLA-5PEG-3CD showed similar behaviour. PLA-5PEG-3CD had lower complex viscosity with increasing frequency when it is compared to other two samples. This behaviour was observed with PLA-5PEG-3RD as well. Linear region (Newtonian plateau) of PLA-5PEG was reduced with both diatom addition. The complex viscosity of the bio-composite materials systems in the melt is not dramatically worsened by a small amount of diatomite [125].

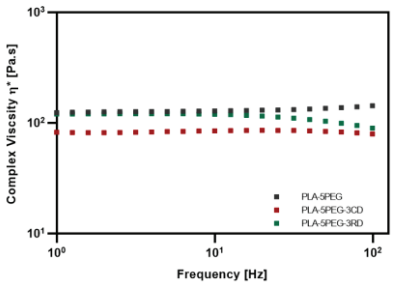


Figure 4.52. Complex viscosity (η*) and Frequency (Hz) of PLA-5PEG-3Diatom

PLA-10PEG had the highest G' value compared to PLA-10PEG-3RD and PLA-10PEG-3CD, thus solid-like behaviour was decreased with diatom content. PLA-5PEG-3CD promoted liquid-like behaviour more than PLA-3RD.

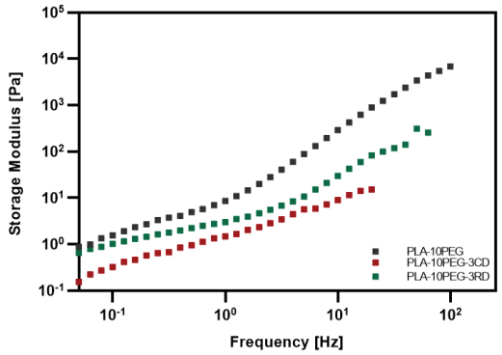


Figure 4.53. Storage Modulus (G') and Frequency (Hz) of PLA-10PEG -3Diatoms

PLA-10PEG-3CD had the lowest loss modulus G'' value but PLA-10PEG-3RD had greater loss modulus than PLA-10PEG-3CD as well. As a result, both diatom addition increased liquid-like trend of PLA-10PEG contrarily to the PLA-5PEG. Interestingly, this indicated the PEG concentration effects on modulus of PLA that increasing PEG concentration dominated the solid-like to liquid-like transition of composites. It is predicted that PLA-10PEG had more free volume in polymer chains.

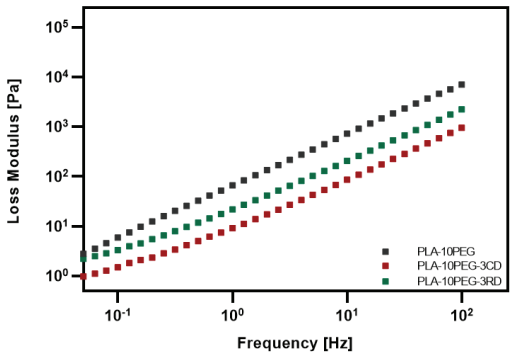


Figure 4.54. Loss Modulus (G'') and Frequency (Hz) of PLA-10PEG -3Diatoms

PLA-10PEG showed the greatest complex viscosity than PLA-10PEG-3RD and PLA-10PEG-3CD. Plasticizers penetrated into PLA matrix and interrupt the chain order, thus decreased the complex viscosity [125]. Diatom addition showed the similar behaviour as penetrating into the PLA-10PEG matrix, and lower the chain order more. Addition of both diatom addition with same concentrations decreased the complex viscosity of PLA-10PEG, CD reduced complex viscosity of PLA-10PEG more than RD did. It can be reason for different frustules and particle sizes [83].

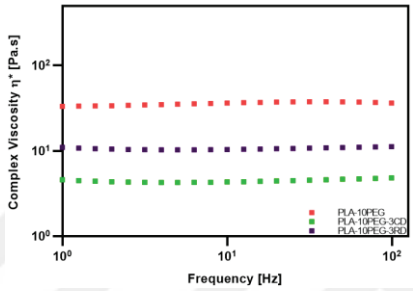


Figure 4.55. Complex viscosity (η*) and Frequency (Hz) of PLA-10PEG-3Diatoms

The last plasticiser/compatibilizer was PEG/POSS. Storage Modulus G' of PLA-5PEG/POSS showed similar trend and closer storage modulus. On the other hand, PLA-5PEG/POSS-3RD had the highest G' value than PLA-5PEG/POSS. It would be result of the different particle size of diatomite particles [83]. PLA-5PEG composites had similar behaviour as storage modulus. PEG/POSS plasticized PLA composites had increased storage modulus RD added composites, consequently improved solid-like behaviour of composites.

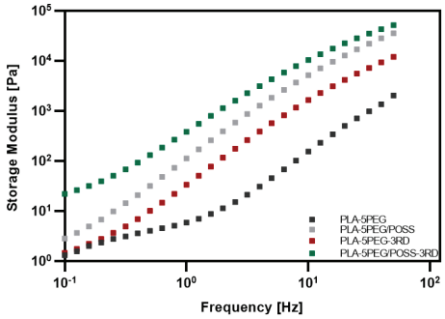


Figure 4.56. Storage Modulus (G') and Frequency (Hz) of PLA-5PEG/POSS-3Diatoms

Loss Modulus of G'' of PLA-5PEG/POSS was indicated, but RD addition increased G'' value of PLA-5PEG/POSS. Liquid-like behaviour was improved with PLA-5PEG/POSS-3RD. Additionally, PLA-5PEG-3RD had similar behaviour in loss modulus. Yet, the loss modulus considerably increased when diatom was added to PLA-5PEG/POSS, which might be attributed to the formation of an improved interaction between PLA and the PEG/POSS cage structure [129].

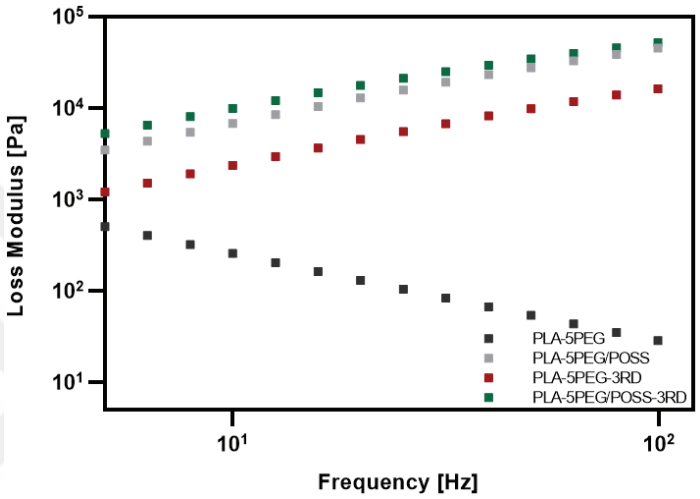


Figure 4.57. Loss Modulus (G'') and Frequency (Hz) of PLA-5PEG/POSS-3Diatoms

Complex viscosity of PLA-5PEG/POSS was increased after both diatom addition. PLA-5PEG/POSS-3CD had greater Newtonian plateau than PLA-5PEG/POSS and PLA/5PEG/POSS-3RD. It promotes the shear thinning behaviour and easy to be processibility [128]. In contrast to PEG addition into PLA, PEG/POSS compatibilizer acted as not only for plasticizer with PEG functionalized part but also reinforcing with POSS particles. Diatom promoted this reinforcing behaviour of POSS particles and increased the stiff character of PLA-5PEG/POSS in contrast to PLA-5PEG composite and PLA-5PEG-Diatom composite systems. Storage modulus of PLA-5PEG/POSS was increased with both type of diatom addition (Figure 4.54).

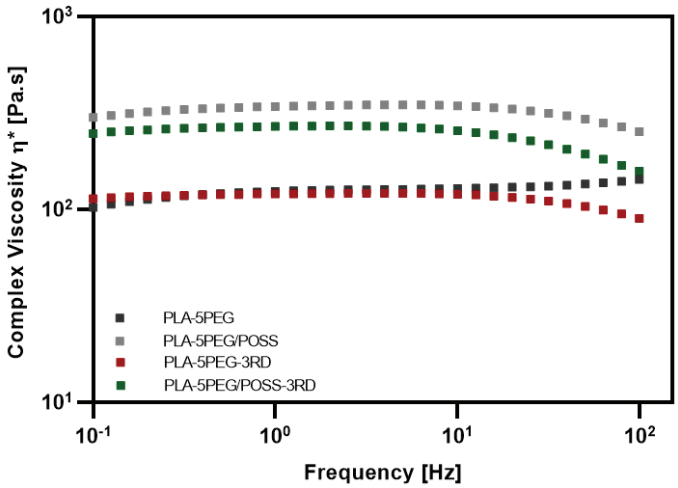


Figure 4.58. Complex viscosity (η*) and Frequency (Hz) of PLA-5PEG-3Diatom

Semicrystalline behaviour of PLA showed more solid-like character and brittleness of PLA was previously explained. Both diatom addition promoted the transition of solid-like behaviour to liquid-like behaviour. Plasticizers promoted this character, as well. Silica based diatomaceous earth, however, penetrated into PEG/POSS plasticised PLA matrix more appropriate than PEG did and increased the solid-like behaviour. According to the process requirements, PLA-based composites can be designed and fabricated.

## 4.2.7. Water Sorption Capacity of Composites

A biomaterial's ability to absorb water is essential when dealing with bodily fluids. To enable a chemical interaction with the contents of physiological fluids, such as proteins, biomaterial must have a hydrophilic nature. In this work, swelling ratio (SR) was calculated together with water uptake measurement to obtain the scaffolds' capacity to absorb water. Scaffolds have been immersed in PBS solution at 25°C for 48 hours to mimic body fluid conditions. Using Eq. 3.1, the amount of swelling of PLA composite was calculated, and the results are shown in Tables 16 and Table 17. The capacity of scaffolds to absorb water increased as diatomite concentration increased due to the hydrophilic nature of diatomite frustules.

Table 4.17. Water uptake weight and % of PLA-Diatom composites

| | Dry weight | 48 hours | 48hr % |
|---|---|---|---|
| PLA | 55,1±0,0051 | 55,21±0,003 | 0,170 |
| PLA-3CD | 59,02±0,0008 | 59,82±0,001 | 0,448 |
| PLA-5CD | 43,85±0,0005 | 44,082±0,000 | 0,516 |
| PLA-10CD | 54,32±0,018 | 54,78±0,000 | 0,840 |
| PLA-3RD | 54,35±0,007 | 54,51±0,022 | 0,297 |
| PLA-5RD | 55,54±0,002 | 55,82±0,041 | 0,513 |
| PLA-10RD | 36,70±0,053 | 36,92±0,034 | 0,613 |

The silica frustules that make up diatomite have a hydrophilic nature. As a result, the ability of the chitosan matrix to absorb water is improved by the insertion of diatomite particles. The swelling behaviour of scaffolds was favourably impacted by the changes in pore size and pore surface area that were obtained with increasing silica content [130]. PLA has hydrophobic character and diatom content increased water swelling properties the effect of swelling properties wasn't significant.

Surface modifications were applied and the water sorption capacity were investigated as well. PLA-5PEG, PLA-10PEG and PLA-5PEG/POSS had incubated and the results were stated in Table 4.17 below.

Table 4.18. Water uptake weight and % of PLA-Plasticizer composites

| | Dry weight | 48 hours | 48hr % |
|---|---|---|---|
| PLA | 55,1±0,0051 | 55,21±0,003 | 0,170 |
| PLA-5PEG | 43,37±0,009 | 43,73±0,003 | 0,829 |
| PLA-10PEG | 42,35±0,009 | 44,082±0,000 | 1,27 |
| PLA-5PEG/POSS | 52,61±0,000 | 53,19±0,000 | 1,10 |

Plasticizers increased water sorption property of pure PLA. PLA-10PEG absorbed more water than PLA-5PEG, thus increasing plasticizer content increased the absorbed water amount of PLA composites. Additionally, PEG/POSS had absorbed more water

than PEG at the same concentration. Silica content of POSS structure interacted water molecules easily, consequently PLA-5PEG/POSS absorbed more water than PLA-5PEG.

Calcinated and raw diatom were subjected to plasticized PLA, the diatom concentration and type effects were investigated as well. For the sake of simplicity, 48 hours weight measurement were indicated for both diatoms added plasticized composites. The results were summarized in Table 4.18 below.

Table 4.19. Water uptake weight and % of PLA-PEG-Diatoms composites

| | Dry weight | 48 hours | 48hr % |
|---|---|---|---|
| PLA-5PEG | 43,37±0,009 | 43,45±0,02 | 0,19 |
| PLA-5PEG-3CD | 61,04±0,007 | 61,16±0,004 | 0,92 |
| PLA-5PEG-5CD | 57,05±0,001 | 58,56±0,006 | 2,65 |
| PLA-5PEG-10CD | 51,02±0,001 | 52,39±0,004 | 2,68 |
| PLA-5PEG-3RD | 40,64±0,005 | 40,86±0,004 | 0,53 |
| PLA-5PEG-5RD | 57,59±0,005 | 58,11±0,000 | 0,89 |
| PLA-5PEG-10RD | 50,48±0,003 | 51,47±0,000 | 1,95 |
| PLA-10PEG | 42,35±0,009 | 42,89±0,001 | 1,27 |
| PLA-10PEG-3CD | 60,70±0,005 | 61,60±0,000 | 1,47 |
| PLA-10PEG-5CD | 52,89±0,002 | 53,94±0,001 | 1,98 |
| PLA-10PEG-10CD | 54,78±0,001 | 55,92±0,000 | 2,08 |
| PLA-10PEG-3RD | 66,81±0,002 | 67,11±0,001 | 0,43 |
| PLA-10PEG-5RD | 53,52±0,000 | 54,02±0,000 | 0,93 |
| PLA-10PEG-10RD | 53,68±0,002 | 54,62±0,004 | 1,72 |

Diatom addition into PLA-5PEG and PLA-10PEG was improved swelling properties at the end of 48 days. Increasing PEG concentration affected water uptake significantly. Additionally, increasing diatom concentration directly increased water uptake ability, as well.

The material swelled more after POSS integration, showing that the microstructural network had greatly expanded as a result of the chemical interaction between the functional group of POSS and the polymer's constituents. POSS content had unique molecular structure and silica content of POSS had significant effect on swelling properties of PLA, raw diatom and PEG/POSS included composites were analysed in water uptake ratio. The results were indicated below in Table 4.19.

Table 4.20. Water uptake weight and % of PLA-5PEG/POSS-RD composites

| | Dry weight | 48 hours | 48hr % |
|---|---|---|---|
| PLA-5PEG/POSS | 52,64±0,000 | 53,19±0,000 | 1,10 |
| PLA-5PEG/POSS-3RD | 42,90±0,001 | 43,49±0,000 | 1,36 |
| PLA-5PEG/POSS-5RD | 53,72±0,002 | 54,52±0,000 | 1,49 |
| PLA-5PEG/POSS-10RD | 50,95±0,009 | 51,83±0,000 | 1,71 |

Both the diatomite and POSS are made up of silica particles, and adding silica to PLA increases the ability of the composites to absorb water. The water absorbing capacity of scaffolds was favourably impacted by the variations in size of pores and pore surface area acquired with increasing silica content. Pore diameters and surface areas were larger in composites with increasing silica content. As a result, the ability to absorb water increased.

# CHAPTER 5

# CONCLUSION

The focus of tissue engineering research has been on the fabrication of adaptable 3D scaffolds that can promote tissue regeneration naturally while providing structurally robust reinforcement. Synthetic polymer-based composites have received interest recently for hard tissue engineering applications due to their biocompatibility and biodegradability. In this study, a customisable biomaterial for bone tissue engineering purposes was created by mixing the synthetic polymer PLA with natural silica Diatomaceous earth. Melt mixing and hot-press techniques were used to create PLA-Diatom composites using two different types of diatoms: calcined and raw diatoms. To increase PLA's compatibility, plasticizers PEG and PEG/POSS were used. Different concentrations of plasticizers and reinforcing agents were added to PLA matrix to optimize the properties for biomaterial applications.

Our comprehensive characterization involved SEM for morphology, mechanical testing, rheological analysis, AFM for roughness, contact angle analysis for surface wettability, swelling property, and FTIR for chemical structure.

The results demonstrated that the incorporation of both types of diatoms improves the ultimate tensile strength of PLA. The values are nearly twice as strong, with a range of 51.51-58.50 MPa compared to pure PLA (32.72±1.08 MPa). The highest strength value was observed for samples with 3% raw diatom incorporation (PLA-3RD). However, higher concentrations of diatoms led to a slight reduction in tensile strength due to their agglomeration, observed through SEM and TGA analyses. An enhancement in tensile strength and reduction in strain was detected by adding up to 5% PEG because of the cold crystallisation phenomenon that occurs in our semi-crystalline PLA. This was established by means of DSC analysis. To elaborate on the morphology of the fabricated composites, SEM, FTIR, AFM, surface roughness, surface wettability (measured by contact angle), swelling characteristics, and chemical structure were employed. The addition of diatoms improved the mechanical strength of PLA. In particular, PLA-3CD and PLA-3RD, which had 3% diatom content, demonstrated the greatest strength. Furthermore, mechanical properties were improved by the inclusion of up to 5% PEG or

a combination of PEG and POSS. Simultaneous toughening and strengthening of polylactic acid (PLA) were observed upon incorporation of PEG/POSS plasticizer/modifier. The tensile strength test value of PLA-5PEG-POSS nearly doubled upon the addition of 5wt% PEG-POSS to PLA matrix, with a value of 64.14 ± 1.12. Additionally, the elongation at break value was found to be higher than that of PEG's plasticization and slightly greater than that of PLA. For PEG plasticized PLA-diatom composites, the incorporation of raw diatom increased both the tensile strength and YM of the PLA-PEG composites. The highest tensile strength was observed at a diatom concentration of 3%.

However, the strain was reduced by both the incorporation of diatoms and the application of plasticisers. Rheological analyses revealed that the composites altered the solid-like behaviour of PLA to liquid-like, as evidenced by the increased loss modulus (G'') and decreased storage modulus (G') upon diatom addition. Additionally, the plasticizers reinforced this effect and sustained the viscosities of PLA-Diatom composites. Consistent grammar, spelling, and citation styles have been applied as per British English conventions. AFM analysis data shows that the addition of both calcinated and raw diatoms improved the surface roughness of pure PLA significantly. The PLA-RD composites with raw diatoms added displayed greater roughness than those with calcined diatoms. The larger particle size of raw diatoms, as proven by SEM and various frustule types, led to stronger molecular interaction and dispersion in the PLA interlayers compared to the calcined diatoms. The diatoms were more visible in the SEM pictures. At higher concentrations, phase separation was observed in the presence of diatoms. However, increasing the concentration of diatoms improved the selectivity of SEM pictures for diatom morphologies. Contact angle studies showed that the application of diatoms enhanced the wettability of hydrophobic PLA in all concentrations. Furthermore, surface wettability was found to increase with higher concentrations of diatoms. Swelling data demonstrated that incorporating diatomite particles enhances the water absorption capacity of the PLA matrix. Increasing silica content resulted in favourable changes to pore size and pore surface area, which in turn improved scaffold swelling behaviour [123]. PLA is hydrophobic, but diatom content increases water swelling properties.

In conclusion, the tuning of the properties of PLA diatom composites via the addition of plasticisers and a varying amount of diatom can be achieved, paving the way for personalised biomaterials to be developed using 3D printing technology in the future.

# REFERENCES


[1] K. Jamshidi, S.-H. Hyon, and Y. Ikada, "Thermal characterization of polylactides," *Polymer (Guildf)*, vol. 29, no. 12, pp. 2229–2234, Dec. 1988, doi: 10.1016/0032-3861(88)90116-4.

[2] S. Ebnesajjad, *Handbook of biopolymers and biodegradable plastics: properties, processing and applications*. 2012.

[3] J. Chen, T. Zhang, W. Hua, P. Li, and X. Wang, "3D Porous poly(lactic acid)/regenerated cellulose composite scaffolds based on electrospun nanofibers for biomineralization," *Colloids Surf A Physicochem Eng Asp*, vol. 585, p. 124048, Jan. 2020, doi: 10.1016/j.colsurfa.2019.124048.

[4] D. Mao, Q. Li, N. Bai, H. Dong, and D. Li, "Porous stable poly(lactic acid)/ethyl cellulose/hydroxyapatite composite scaffolds prepared by a combined method for bone regeneration," *Carbohydr Polym*, vol. 180, pp. 104–111, Jan. 2018, doi: 10.1016/j.carbpol.2017.10.031.

[5] S. Farah, D. G. Anderson, and R. Langer, "Physical and mechanical properties of PLA, and their functions in widespread applications — A comprehensive review," *Adv Drug Deliv Rev*, vol. 107, pp. 367–392, Dec. 2016, doi: 10.1016/j.addr.2016.06.012.

[6] H. Liu and J. Zhang, "Research progress in toughening modification of poly(lactic acid)," *J Polym Sci B Polym Phys*, vol. 49, no. 15, pp. 1051–1083, Aug. 2011, doi: 10.1002/polb.22283.

[7] A. Toncheva *et al.*, "Antibacterial PLA/PEG electrospun fibers: Comparative study between grafting and blending PEG," *Eur Polym J*, vol. 75, pp. 223–233, Feb. 2016, doi: 10.1016/j.eurpolymj.2015.12.019.

[8] L. Fan, X. Wang, and D. Wu, "Polyhedral Oligomeric Silsesquioxanes ( <scp>POSS</scp> )-based Hybrid Materials: Molecular Design, Solution <scp>Self-Assembly</scp> and Biomedical Applications," *Chin J Chem*, vol. 39, no. 3, pp. 757–774, Mar. 2021, doi: 10.1002/cjoc.202000536.

[9] O. Böstman and H. Pihlajamäki, "Clinical biocompatibility of biodegradable orthopaedic implants for internal fixation: a review," *Biomaterials*, vol. 21, no. 24, pp. 2615–2621, Dec. 2000, doi: 10.1016/S0142-9612(00)00129-0.

[10] A. Bozorgi, M. Khazaei, M. Soleimani, and Z. Jamalpoor, “Application of nanoparticles in bone tissue engineering; a review on the molecular mechanisms driving osteogenesis,” *Biomater Sci*, vol. 9, no. 13, pp. 4541–4567, 2021, doi: 10.1039/D1BM00504A.

[11] M. Milazzo *et al.*, “Additive Manufacturing Approaches for Hydroxyapatite-Reinforced Composites,” *Adv Funct Mater*, vol. 29, no. 35, p. 1903055, Aug. 2019, doi: 10.1002/adfm.201903055.

[12] J. A. Sanz-Herrera and A. R. Boccaccini, “Modelling bioactivity and degradation of bioactive glass based tissue engineering scaffolds,” *Int J Solids Struct*, vol. 48, no. 2, pp. 257–268, Jan. 2011, doi: 10.1016/j.ijsolstr.2010.09.025.

[13] W. Wu, X. Cao, Y. Zhang, and G. He, “Polylactide/halloysite nanotube nanocomposites: Thermal, mechanical properties, and foam processing,” *J Appl Polym Sci*, vol. 130, no. 1, pp. 443–452, Oct. 2013, doi: 10.1002/app.39179.

[14] M. Kong, G. Chen, S. Xi, Y. Huang, and G. Li, “Morphology Mapping of Nanoparticle-Filled Immiscible Polymer Blends in Flow: The Existence of a Critical Ratio between Nanoparticle Concentration and Droplet Concentration,” *ACS Omega*, vol. 3, no. 9, pp. 11550–11557, Sep. 2018, doi: 10.1021/acsomega.7b02072.

[15] C.-J. Wu, A. K. Gaharwar, P. J. Schexnailder, and G. Schmidt, “Development of Biomedical Polymer-Silicate Nanocomposites: A Materials Science Perspective,” *Materials*, vol. 3, no. 5, pp. 2986–3005, Apr. 2010, doi: 10.3390/ma3052986.

[16] E. H. Backes *et al.*, “Engineering 3D printed bioactive composite scaffolds based on the combination of aliphatic polyester and calcium phosphates for bone tissue regeneration,” *Materials Science and Engineering: C*, vol. 122, p. 111928, Mar. 2021, doi: 10.1016/j.msec.2021.111928.

[17] M. Kaseem, Z. Ur Rehman, S. Hossain, A. K. Singh, and B. Dikici, “A Review on Synthesis, Properties, and Applications of Polylactic Acid/Silica Composites,” *Polymers (Basel)*, vol. 13, no. 18, p. 3036, Sep. 2021, doi: 10.3390/polym13183036.

[18] A. Aguero, L. Quiles-Carrillo, A. Jorda-Vilaplana, O. Fenollar, and N. Montanes, “Effect of different compatibilizers on environmentally friendly composites from poly(lactic acid) and diatomaceous earth,” *Polym Int*, vol. 68, no. 5, pp. 893–903, May 2019, doi: 10.1002/pi.5779.

[19] M. Dobrosielska *et al.*, “A New Method of Diatomaceous Earth Fractionation—A Bio-Raw Material Source for Epoxy-Based Composites,” *Materials*, vol. 14, no. 7, p. 1663, Mar. 2021, doi: 10.3390/ma14071663.

[20] J. F. Mukerabigwi *et al.*, “Eco-friendly nano-hybrid superabsorbent composite from hydroxyethyl cellulose and diatomite,” *RSC Adv*, vol. 6, no. 38, pp. 31607–31618, 2016, doi: 10.1039/C6RA01759B.

[21] M. Dobrosielska *et al.*, “Biogenic composite filaments based on polylactide and diatomaceous earth for 3D printing,” *Materials*, vol. 13, no. 20, pp. 1–22, Oct. 2020, doi: 10.3390/ma13204632.

[22] S. Tamburaci and F. Tihminlioglu, “Diatomite reinforced chitosan composite membrane as potential scaffold for guided bone regeneration,” *Materials Science and Engineering: C*, vol. 80, pp. 222–231, Nov. 2017, doi: 10.1016/j.msec.2017.05.069.

[23] “Bio-economy and the sustainability of the agriculture and food system.”

[24] K. Jõgi and R. Bhat, “Valorization of food processing wastes and by-products for bioplastic production,” *Sustain Chem Pharm*, vol. 18, p. 100326, Dec. 2020, doi: 10.1016/j.scp.2020.100326.

[25] E. S. Place, J. H. George, C. K. Williams, and M. M. Stevens, “Synthetic polymer scaffolds for tissue engineering,” *Chem Soc Rev*, vol. 38, no. 4, p. 1139, 2009, doi: 10.1039/b811392k.

[26] K. Madhavan Nampoothiri, N. R. Nair, and R. P. John, “An overview of the recent developments in polylactide (PLA) research,” *Bioresour Technol*, vol. 101, no. 22, pp. 8493–8501, Nov. 2010, doi: 10.1016/j.biortech.2010.05.092.

[27] K. Hamad, M. Kaseem, M. Ayyoob, J. Joo, and F. Deri, “Polylactic acid blends: The future of green, light and tough,” *Prog Polym Sci*, vol. 85, pp. 83–127, Oct. 2018, doi: 10.1016/j.progpolymsci.2018.07.001.

[28] A. K. Mohanty, M. Misra, and L. T. Drzal, Eds., *Natural Fibers, Biopolymers, and Biocomposites*. CRC Press, 2005. doi: 10.1201/9780203508206.

[29] A. J. T. John C. Middleton*, “Synthetic biodegradable polymers as orthopedic devices,” *Biomaterials*, 2000.

[30] R. A. Auras, L. T. Lim, S. E. M. Selke, and H. Tsuji, “Poly (lactic acid): synthesis, structures, properties, processing, and applications,” in *Poly(lactic acid): Synthesis, Structures, Properties, Processing, and Applications*, Vol 10., 2011.

[31] S. Bhagia *et al.*, “Critical review of FDM 3D printing of PLA biocomposites filled with biomass resources, characterization, biodegradability, upcycling and opportunities for biorefineries,” *Appl Mater Today*, vol. 24, p. 101078, Sep. 2021, doi: 10.1016/J.APMT.2021.101078.

[32] C. Zhou *et al.*, “Electrospun Bio-Nanocomposite Scaffolds for Bone Tissue Engineering by Cellulose Nanocrystals Reinforcing Maleic Anhydride Grafted PLA,” *ACS Appl Mater Interfaces*, vol. 5, no. 9, pp. 3847–3854, May 2013, doi: 10.1021/am4005072.

[33] Z. U. Arif, M. Y. Khalid, R. Noroozi, A. Sadeghianmaryan, M. Jalalvand, and M. Hossain, “Recent advances in 3D-printed polylactide and polycaprolactone-based biomaterials for tissue engineering applications,” *Int J Biol Macromol*, vol. 218, pp. 930–968, Oct. 2022, doi: 10.1016/j.ijbiomac.2022.07.140.

[34] T. Malmgren, J. Mays, and M. Pyda, “Characterization of poly(lactic acid) by size exclusion chromatography, differential refractometry, light scattering and thermal analysis,” *J Therm Anal Calorim*, vol. 83, no. 1, pp. 35–40, Jan. 2006, doi: 10.1007/s10973-005-7066-0.

[35] M. Yasuniwa, S. Tsubakihara, K. Iura, Y. Ono, Y. Dan, and K. Takahashi, “Crystallization behavior of poly(l-lactic acid),” *Polymer (Guildf)*, vol. 47, no. 21, pp. 7554–7563, Oct. 2006, doi: 10.1016/j.polymer.2006.08.054.

[36] R. , Auras, L. T. , Lim, S. E. M. , & Selke, and H. (2010) Tsuji, *Polymer Engineering and Technology* . 2010.

[37] L. Bouapao, H. Tsuji, K. Tashiro, J. Zhang, and M. Hanesaka, “Crystallization, spherulite growth, and structure of blends of crystalline and amorphous poly(lactide)s,” *Polymer (Guildf)*, vol. 50, no. 16, pp. 4007–4017, Jul. 2009, doi: 10.1016/j.polymer.2009.06.040.

[38] A. Södergård and M. Stolt, “Properties of lactic acid based polymers and their correlation with composition,” *Prog Polym Sci*, vol. 27, no. 6, pp. 1123–1163, Jul. 2002, doi: 10.1016/S0079-6700(02)00012-6.

[39] R. Auras, B. Harte, and S. Selke, “An Overview of Polylactides as Packaging Materials,” *Macromol Biosci*, vol. 4, no. 9, pp. 835–864, Sep. 2004, doi: 10.1002/mabi.200400043.

[40] S. Farah, D. G. Anderson, and R. Langer, “Physical and mechanical properties of PLA, and their functions in widespread applications — A comprehensive review,” *Adv Drug Deliv Rev*, vol. 107, pp. 367–392, Dec. 2016, doi: 10.1016/j.addr.2016.06.012.

[41] Z. Rehman, K. Seong, S. Lee, and M. H. Song, “Experimental study on the rheological behavior of tetrafluoroethane (R-134a) hydrate slurry,” *Chem Eng Commun*, vol. 205, no. 6, pp. 822–832, Jun. 2018, doi: 10.1080/00986445.2017.1422494.

[42] B. E. Rapp, “Fluids,” in *Microfluidics: Modelling, Mechanics and Mathematics*, Elsevier, 2017, pp. 243–263. doi: 10.1016/B978-1-4557-3141-1.50009-5.

[43] M. Kontopoulou, Ed., *Applied Polymer Rheology*. Wiley, 2011. doi: 10.1002/9781118140611.

[44] G. Li, P. Sarazin, and B. D. Favis, “The Relationship between Starch Gelatinization and Morphology Control in Melt-Processed Polymer Blends with Thermoplastic Starch,” *Macromol Chem Phys*, vol. 209, no. 10, pp. 991–1002, May 2008, doi: 10.1002/macp.200700637.

[45] P. K. Penumakala, J. Santo, and A. Thomas, “A critical review on the fused deposition modeling of thermoplastic polymer composites,” *Compos B Eng*, vol. 201, p. 108336, Nov. 2020, doi: 10.1016/j.compositesb.2020.108336.

[46] G. Mensitieri *et al.*, “Processing and shelf life issues of selected food packaging materials and structures from renewable resources,” *Trends Food Sci Technol*, vol. 22, no. 2–3, pp. 72–80, Mar. 2011, doi: 10.1016/j.tifs.2010.10.001.

[47] G. Gautam, S. Kumar, and K. Kumar, “Processing of biomaterials for bone tissue engineering: State of the art,” *Mater Today Proc*, vol. 50, pp. 2206–2217, 2022, doi: 10.1016/j.matpr.2021.09.459.

[48] J.-S. Bow, S.-C. Liou, and S.-Y. Chen, “Structural characterization of room-temperature synthesized nano-sized β-tricalcium phosphate,” *Biomaterials*, vol. 25, no. 16, pp. 3155–3161, Jul. 2004, doi: 10.1016/j.biomaterials.2003.10.046.

[49] A. J. Salinas, P. Esbrit, and M. Vallet-Regí, “A tissue engineering approach based on the use of bioceramics for bone repair,” *Biomater. Sci.*, vol. 1, no. 1, pp. 40–51, 2013, doi: 10.1039/C2BM00071G.

[50] J. Jeong, J. H. Kim, J. H. Shim, N. S. Hwang, and C. Y. Heo, “Bioactive calcium phosphate materials and applications in bone regeneration,” *Biomater Res*, vol. 23, no. 1, p. 4, Dec. 2019, doi: 10.1186/s40824-018-0149-3.

[51] H. K. Kleinman, D. Philp, and M. P. Hoffman, “Role of the extracellular matrix in morphogenesis,” *Curr Opin Biotechnol*, vol. 14, no. 5, pp. 526–532, Oct. 2003, doi: 10.1016/j.copbio.2003.08.002.

[52] N. Tran and T. J. Webster, “Increased osteoblast functions in the presence of hydroxyapatite-coated iron oxide nanoparticles,” *Acta Biomater*, vol. 7, no. 3, pp. 1298–1306, Mar. 2011, doi: 10.1016/j.actbio.2010.10.004.

[53] Y. Huang *et al.*, “Silica nanoparticles: Biomedical applications and toxicity,” *Biomedicine & Pharmacotherapy*, vol. 151, p. 113053, Jul. 2022, doi: 10.1016/j.biopha.2022.113053.

[54] S. Rangaraj and R. Venkatachalam, “*In vitro* and *in vivo* characteristics of biogenic high surface silica nanoparticles in A549 lung cancer cell lines and *Danio rerio* model systems for inorganic biomaterials development,” *Artif Cells Nanomed Biotechnol*, vol. 46, no. 7, pp. 1415–1424, Oct. 2018, doi: 10.1080/21691401.2017.1369427.

[55] L. Khanna, G. Gupta, and S. K. Tripathi, “Effect of size and silica coating on structural, magnetic as well as cytotoxicity properties of copper ferrite nanoparticles,” *Materials Science and Engineering: C*, vol. 97, pp. 552–566, Apr. 2019, doi: 10.1016/j.msec.2018.12.051.

[56] X. Zhou, N. Zhang, S. Mankoci, and N. Sahai, “Silicates in orthopedics and bone tissue engineering materials,” *J Biomed Mater Res A*, vol. 105, no. 7, pp. 2090–2102, Jul. 2017, doi: 10.1002/jbm.a.36061.

[57] E. M. Carlisle, “Silicon: A Possible Factor in Bone Calcification,” *Science (1979)*, vol. 167, no. 3916, pp. 279–280, Jan. 1970, doi: 10.1126/science.167.3916.279.

[58] F. H. Nielsen and R. Poellot, “Dietary silicon affects bone turnover differently in ovariectomized and sham-operated growing rats,” *The Journal of Trace Elements*

*in Experimental Medicine*, vol. 17, no. 3, pp. 137–149, 2004, doi: 10.1002/jtra.20004.

[59] D. M. Reffitt *et al.*, "Orthosilicic acid stimulates collagen type 1 synthesis and osteoblastic differentiation in human osteoblast-like cells in vitro," *Bone*, vol. 32, no. 2, pp. 127–135, Feb. 2003, doi: 10.1016/S8756-3282(02)00950-X.

[60] S. Yan, J. Yin, Y. Yang, Z. Dai, J. Ma, and X. Chen, "Surface-grafted silica linked with l-lactic acid oligomer: A novel nanofiller to improve the performance of biodegradable poly(l-lactide)," *Polymer (Guildf)*, vol. 48, no. 6, pp. 1688–1694, Mar. 2007, doi: 10.1016/j.polymer.2007.01.037.

[61] W. Wu, X. Cao, Y. Zhang, and G. He, "Polylactide/halloysite nanotube nanocomposites: Thermal, mechanical properties, and foam processing," *J Appl Polym Sci*, vol. 130, no. 1, pp. 443–452, Oct. 2013, doi: 10.1002/app.39179.

[62] A. M. Alakrach *et al.*, "Thermal properties of PLA/HNTs composites: Effect of different halloysite nanotube," 2018, p. 020052. doi: 10.1063/1.5066693.

[63] Y. Dong *et al.*, "Polylactic acid (PLA)/halloysite nanotube (HNT) composite mats: Influence of HNT content and modification," *Compos Part A Appl Sci Manuf*, vol. 76, pp. 28–36, Sep. 2015, doi: 10.1016/j.compositesa.2015.05.011.

[64] K. Prashantha, B. Lecouvet, M. Sclavons, M. F. Lacrampe, and P. Krawczak, "Poly(lactic acid)/halloysite nanotubes nanocomposites: Structure, thermal, and mechanical properties as a function of halloysite treatment," *J Appl Polym Sci*, p. n/a-n/a, 2012, doi: 10.1002/app.38358.

[65] C. Venkatesh, E. Fuenmayor, P. Doran, I. Major, J. G. Lyons, and D. M. Devine, "Additive manufacturing of PLA/HNT nanocomposites for biomedical applications," *Procedia Manuf*, vol. 38, pp. 17–24, 2019, doi: 10.1016/j.promfg.2020.01.003.

[66] A. R. Boccaccini, J. A. Roelher, L. L. Hench, V. Maquet, and R. Jrme, "A Composites Approach to Tissue Engineering," pp. 805–816. doi: 10.1002/9780470294758.ch90.

[67] (2), J. E. Gough(1), A. R. Boccaccini(1), (2), L. L. Hench(1), V. Maquet(3), (4), R. Jérôme J. A. Roether(1), "Novel bioresorbable and bioactive composites based on bioactive glass and polylactide foams for bone tissue engineering ," *Journal of materials science: materials in medicine* , 2002.

[68] G. Ozkoc, S. Kemaloglu, and M. Quaedflieg, “Production of poly(lactic acid)/organoclay nanocomposite scaffolds by microcompounding and polymer/particle leaching,” *Polym Compos*, p. NA-NA, 2009, doi: 10.1002/pc.20846.

[69] M. Kodal, H. Sirin, and G. Ozkoc, “Investigation of relationship between crystallization kinetics and interfacial interactions in plasticized poly(lactic acid)/POSS nanocomposites: ‘Effects of different POSS types,’” *Polym Compos*, vol. 39, no. 8, pp. 2674–2684, Aug. 2018, doi: 10.1002/pc.24258.

[70] T. D. H. Le *et al.*, “Processing and characterization of diatom nanoparticles and microparticles as potential source of silicon for bone tissue engineering,” *Materials Science and Engineering: C*, vol. 59, pp. 471–479, Feb. 2016, doi: 10.1016/j.msec.2015.10.040.

[71] Hossam Elden Galal Morsy Mohamed Bakr, “Diatomite: Its Characterization, Modifications and Applications,” *Asian Journal of Materials Science*, 2010.

[72] T. D. H. Le *et al.*, “Processing and characterization of diatom nanoparticles and microparticles as potential source of silicon for bone tissue engineering,” *Materials Science and Engineering: C*, vol. 59, pp. 471–479, Feb. 2016, doi: 10.1016/j.msec.2015.10.040.

[73] Y. Wang, J. Cai, Y. Jiang, X. Jiang, and D. Zhang, “Preparation of biosilica structures from frustules of diatoms and their applications: current state and perspectives,” *Appl Microbiol Biotechnol*, vol. 97, no. 2, pp. 453–460, Jan. 2013, doi: 10.1007/s00253-012-4568-0.

[74] *, Kun-Ang Li1, An-Ke Du2 Jian-Bing Zeng1, “Compatibilization strategies in poly(lactic acid)-based blends,” *Royal Society of Chemistry*, 2003.

[75] K. M. Wee, T. N. Rogers, B. S. Altan, S. A. Hackney, and C. Hamm, “Engineering and Medical Applications of Diatoms,” *J Nanosci Nanotechnol*, vol. 5, no. 1, pp. 88–91, Jan. 2005, doi: 10.1166/jnn.2005.020.

[76] R. M. Rasal, A. V. Janorkar, and D. E. Hirt, “Poly(lactic acid) modifications,” *Prog Polym Sci*, vol. 35, no. 3, pp. 338–356, Mar. 2010, doi: 10.1016/j.progpolymsci.2009.12.003.

[77] T. Serra, M. Ortiz-Hernandez, E. Engel, J. A. Planell, and M. Navarro, “Relevance of PEG in PLA-based blends for tissue engineering 3D-printed scaffolds,”

*Materials Science and Engineering: C*, vol. 38, pp. 55–62, May 2014, doi: 10.1016/j.msec.2014.01.003.

[78] Y. Srithep and D. Pholharn, "Plasticizer effect on melt blending of polylactide stereocomplex," *e-Polymers*, vol. 17, no. 5, pp. 409–416, Aug. 2017, doi: 10.1515/epoly-2016-0331.

[79] R. Sothornvit and J. M. Krochta, "Plasticizer Effect on Oxygen Permeability of β-Lactoglobulin Films," *J Agric Food Chem*, vol. 48, no. 12, pp. 6298–6302, Dec. 2000, doi: 10.1021/jf000836l.

[80] M. S. Ullah, N. Yazıcı, A. A. Wis, G. Özkoç, and M. Kodal, "A review on polyhedral oligomeric silsesquioxanes as a new multipurpose nanohybrid additive for poly(lactic acid) and poly(lactic acid) hybrid composites," *Polym Compos*, vol. 43, no. 3, pp. 1252–1281, Mar. 2022, doi: 10.1002/pc.26483.

[81] D. Turan, H. Sirin, and G. Ozkoc, "Effects of POSS particles on the mechanical, thermal, and morphological properties of PLA and Plasticised PLA," *J Appl Polym Sci*, vol. 121, no. 2, pp. 1067–1075, Jul. 2011, doi: 10.1002/app.33802.

[82] C.-H. Jung, I.-T. Hwang, C.-H. Jung, and J.-H. Choi, "Preparation of flexible PLA/PEG-POSS nanocomposites by melt blending and radiation crosslinking," *Radiation Physics and Chemistry*, vol. 102, pp. 23–28, Sep. 2014, doi: 10.1016/j.radphyschem.2014.04.020.

[83] M. Dobrosielska *et al.*, "Influence of Diatomaceous Earth Particle Size on Mechanical Properties of PLA/Diatomaceous Earth Composites," *Materials*, vol. 15, no. 10, p. 3607, May 2022, doi: 10.3390/ma15103607.

[84] S. Aggarwal, S. Johnson, D. Saloni, and M. Hakovirta, "Novel 3D printing filament composite using diatomaceous earth and polylactic acid for materials properties and cost improvement," *Compos B Eng*, vol. 177, Nov. 2019, doi: 10.1016/j.compositesb.2019.107310.

[85] Y. Ding *et al.*, "Effect of talc and diatomite on compatible, morphological, and mechanical behavior of PLA/PBAT blends," *E-Polymers*, vol. 21, no. 1, pp. 234–243, Jan. 2021, doi: 10.1515/epoly-2021-0022.

[86] A. A. Stepashkin, D. I. Chukov, F. S. Senatov, A. I. Salimon, A. M. Korsunsky, and S. D. Kaloshkin, "3D-printed PEEK-carbon fiber (CF) composites: Structure

and thermal properties," *Compos Sci Technol*, vol. 164, pp. 319–326, Aug. 2018, doi: 10.1016/j.compscitech.2018.05.032.

[87] R. Zou *et al.*, "Isotropic and anisotropic elasticity and yielding of 3D printed material," *Compos B Eng*, vol. 99, pp. 506–513, Aug. 2016, doi: 10.1016/j.compositesb.2016.06.009.

[88] R. Pugliese, B. Beltrami, S. Regondi, and C. Lunetta, "Polymeric biomaterials for 3D printing in medicine: An overview," *Annals of 3D Printed Medicine*, vol. 2, p. 100011, Jun. 2021, doi: 10.1016/j.stlm.2021.100011.

[89] A. Valerga, M. Batista, S. Fernandez-Vidal, and A. Gamez, "Impact of Chemical Post-Processing in Fused Deposition Modelling (FDM) on Polylactic Acid (PLA) Surface Quality and Structure," *Polymers (Basel)*, vol. 11, no. 3, p. 566, Mar. 2019, doi: 10.3390/polym11030566.

[90] D. da Silva *et al.*, "Biocompatibility, biodegradation and excretion of polylactic acid (PLA) in medical implants and theranostic systems," *Chemical Engineering Journal*, vol. 340, pp. 9–14, May 2018, doi: 10.1016/j.cej.2018.01.010.

[91] B. Ádám and Z. Weltsch, "Thermal and Mechanical Assessment of PLA-SEBS and PLA-SEBS-CNT Biopolymer Blends for 3D Printing," *Applied Sciences*, vol. 11, no. 13, p. 6218, Jul. 2021, doi: 10.3390/app11136218.

[92] C. Schiller and M. Epple, "Carbonated calcium phosphates are suitable pH-stabilising fillers for biodegradable polyesters," *Biomaterials*, vol. 24, no. 12, pp. 2037–2043, May 2003, doi: 10.1016/S0142-9612(02)00634-8.

[93] X.-F. Wang, P.-J. Lu, Y. Song, Y.-C. Sun, Y.-G. Wang, and Y. Wang, "Nano hydroxyapatite particles promote osteogenesis in a three-dimensional bio-printing construct consisting of alginate/gelatin/hASCs," *RSC Adv*, vol. 6, no. 8, pp. 6832–6842, 2016, doi: 10.1039/C5RA21527G.

[94] J. Wu *et al.*, "3D printing mesoporous bioactive glass/sodium alginate/gelatin sustained release scaffolds for bone repair," *J Biomater Appl*, vol. 33, no. 6, pp. 755–765, Jan. 2019, doi: 10.1177/0885328218810269.

[95] H. Cui *et al.*, "Direct 3D printing of a tough hydrogel incorporated with carbon nanotubes for bone regeneration," *J Mater Chem B*, vol. 7, no. 45, pp. 7207–7217, 2019, doi: 10.1039/C9TB01494B.

[96] X. Zhai *et al.*, "3D-Printed High Strength Bioactive Supramolecular Polymer/Clay Nanocomposite Hydrogel Scaffold for Bone Regeneration," *ACS Biomater Sci Eng*, vol. 3, no. 6, pp. 1109–1118, Jun. 2017, doi: 10.1021/acsbiomaterials.7b00224.

[97] Y.-H. Lin, Y.-C. Chiu, Y.-F. Shen, Y.-H. A. Wu, and M.-Y. Shie, "Bioactive calcium silicate/poly-ε-caprolactone composite scaffolds 3D printed under mild conditions for bone tissue engineering," *J Mater Sci Mater Med*, vol. 29, no. 1, p. 11, Jan. 2018, doi: 10.1007/s10856-017-6020-6.

[98] M. Neufurth *et al.*, "3D printing of hybrid biomaterials for bone tissue engineering: Calcium-polyphosphate microparticles encapsulated by polycaprolactone," *Acta Biomater*, vol. 64, pp. 377–388, Dec. 2017, doi: 10.1016/j.actbio.2017.09.031.

[99] H. Yi, F. Ur Rehman, C. Zhao, B. Liu, and N. He, "Recent advances in nano scaffolds for bone repair," *Bone Res*, vol. 4, no. 1, p. 16050, Dec. 2016, doi: 10.1038/boneres.2016.50.

[100] W. Götz, E. Tobiasch, S. Witzleben, and M. Schulze, "Effects of Silicon Compounds on Biomineralization, Osteogenesis, and Hard Tissue Formation," *Pharmaceutics*, vol. 11, no. 3, p. 117, Mar. 2019, doi: 10.3390/pharmaceutics11030117.

[101] Y. Yang *et al.*, "Laser additive manufacturing of Mg-based composite with improved degradation behaviour," *Virtual Phys Prototyp*, vol. 15, no. 3, pp. 278–293, Jul. 2020, doi: 10.1080/17452759.2020.1748381.

[102] R. L. Simpson *et al.*, "A comparative study of the effects of different bioactive fillers in PLGA matrix composites and their suitability as bone substitute materials: A thermo-mechanical and in vitro investigation," *J Mech Behav Biomed Mater*, vol. 50, pp. 277–289, Oct. 2015, doi: 10.1016/j.jmbbm.2015.06.008.

[103] R. Han, F. Buchanan, L. Ford, M. Julius, and P. J. Walsh, "A comparison of the degradation behaviour of 3D printed PDLGA scaffolds incorporating bioglass or biosilica," *Materials Science and Engineering C*, vol. 120, Jan. 2021, doi: 10.1016/j.msec.2020.111755.

[104] M. Uy and J. K. Telford, "Optimization by Design of Experiment techniques," in *2009 IEEE Aerospace conference*, IEEE, Mar. 2009, pp. 1–10. doi: 10.1109/AERO.2009.4839625.

[105] A. K. Mohapatra, S. Mohanty, and S. K. Nayak, “Effect of PEG on PLA/PEG blend and its nanocomposites: A study of thermo-mechanical and morphological characterization,” *Polym Compos*, vol. 35, no. 2, pp. 283–293, Feb. 2014, doi: 10.1002/pc.22660.

[106] H. Pan and Z. Qiu, “Biodegradable Poly( <scp>l</scp> -lactide)/Polyhedral Oligomeric Silsesquioxanes Nanocomposites: Enhanced Crystallization, Mechanical Properties, and Hydrolytic Degradation,” *Macromolecules*, vol. 43, no. 3, pp. 1499–1506, Feb. 2010, doi: 10.1021/ma9023685.

[107] F. Noll, M. Sumper, and N. Hampp, “Nanostructure of Diatom Silica Surfaces and of Biomimetic Analogues,” *Nano Lett*, vol. 2, no. 2, pp. 91–95, Feb. 2002, doi: 10.1021/nl015581k.

[108] T. Qian, J. Li, and Y. Deng, “Pore structure modified diatomite-supported PEG composites for thermal energy storage,” *Sci Rep*, vol. 6, no. 1, p. 32392, Sep. 2016, doi: 10.1038/srep32392.

[109] S. Farah, D. G. Anderson, and R. Langer, “Physical and mechanical properties of PLA, and their functions in widespread applications — A comprehensive review,” *Adv Drug Deliv Rev*, vol. 107, pp. 367–392, Dec. 2016, doi: 10.1016/j.addr.2016.06.012.

[110] Z. Kulinski and E. Piorkowska, “Crystallization, structure and properties of plasticized poly(l-lactide),” *Polymer (Guildf)*, vol. 46, no. 23, pp. 10290–10300, Nov. 2005, doi: 10.1016/j.polymer.2005.07.101.

[111] Y. Hu, M. Rogunova, V. Topolkaraev, A. Hiltner, and E. Baer, “Aging of poly(lactide)/poly(ethylene glycol) blends. Part 1. Poly(lactide) with low stereoregularity,” *Polymer (Guildf)*, vol. 44, no. 19, pp. 5701–5710, Sep. 2003, doi: 10.1016/S0032-3861(03)00614-1.

[112] S. Kong *et al.*, “Improvement in mechanical and thermal properties of polypropylene nanocomposites using an extremely small amount of alkyl chain-grafted hexagonal boron nitride nanosheets,” *Polymer (Guildf)*, vol. 180, p. 121714, Oct. 2019, doi: 10.1016/j.polymer.2019.121714.

[113] V. Kumar and A. Singh, “Polypropylene clay nanocomposites,” *Reviews in Chemical Engineering*, vol. 29, no. 6, Jan. 2013, doi: 10.1515/revce-2013-0014.

[114] R. Miandad *et al.*, “Catalytic Pyrolysis of Plastic Waste: Moving Toward Pyrolysis Based Biorefineries,” *Front Energy Res*, vol. 7, Mar. 2019, doi: 10.3389/fenrg.2019.00027.

[115] Z. Zhu, C. Ye, W. Fu, and H. Wu, “Improvement in mechanical and thermal properties of polylactic acid biocomposites due to the addition of hybrid sisal fibers and diatomite particles,” *International Journal of Polymer Analysis and Characterization*, vol. 21, no. 5, pp. 365–377, Jul. 2016, doi: 10.1080/1023666X.2016.1160529.

[116] R. Masirek, Z. Kulinski, D. Chionna, E. Piorkowska, and M. Pracella, “Composites of poly( <scp>L</scp> -lactide) with hemp fibers: Morphology and thermal and mechanical properties,” *J Appl Polym Sci*, vol. 105, no. 1, pp. 255–268, Jul. 2007, doi: 10.1002/app.26090.

[117] Y.-P. Song, D.-Y. Wang, X.-L. Wang, L. Lin, and Y.-Z. Wang, “A method for simultaneously improving the flame retardancy and toughness of PLA,” *Polym Adv Technol*, vol. 22, no. 12, pp. 2295–2301, Dec. 2011, doi: 10.1002/pat.1760.

[118] Vikas Mittal, *Advanced Polymer Nanoparticles: Synthesis and Surface Modifications*. CRC Press, 2010.

[119] Y. M. Zeybek and C. Kaynak, “Behaviour of PLA/POSS nanocomposites: Effects of filler content, functional group and copolymer compatibilization,” *Polymers and Polymer Composites*, vol. 29, no. 9_suppl, pp. S485–S500, Nov. 2021, doi: 10.1177/09673911211008020.

[120] K. Sungsanit, N. Kao, and S. N. Bhattacharya, “Properties of linear poly(lactic acid)/polyethylene glycol blends,” *Polym Eng Sci*, vol. 52, no. 1, pp. 108–116, Jan. 2012, doi: 10.1002/pen.22052.

[121] J. Muller, C. González-Martínez, and A. Chiralt, “Poly(lactic) acid (PLA) and starch bilayer films, containing cinnamaldehyde, obtained by compression moulding,” *Eur Polym J*, vol. 95, pp. 56–70, Oct. 2017, doi: 10.1016/j.eurpolymj.2017.07.019.

[122] C. Zhang *et al.*, “Poly(lactic acid)/artificially cultured diatom frustules nanofibrous membranes with fast and controllable degradation rates for air filtration,” *Adv Compos Hybrid Mater*, vol. 5, no. 2, pp. 1221–1232, Jun. 2022, doi: 10.1007/s42114-022-00474-7.

[123] H. Sun *et al.*, “Comparative of diatom frustules, diatomite, and silica particles for constructing self-healing superhydrophobic materials with capacity for thermal energy storage,” *Appl Energy*, vol. 332, p. 120482, Feb. 2023, doi: 10.1016/j.apenergy.2022.120482.

[124] Y. Lyu, Y. Chen, Z. Lin, J. Zhang, and X. Shi, “Manipulating phase structure of biodegradable PLA/PBAT system: Effects on dynamic rheological responses and 3D printing,” *Compos Sci Technol*, vol. 200, p. 108399, Nov. 2020, doi: 10.1016/j.compscitech.2020.108399.

[125] M. Dobrosielska *et al.*, “Biocomposites Based on Polyamide 11/Diatoms with Different Sized Frustules,” *Polymers (Basel)*, vol. 14, no. 15, p. 3153, Aug. 2022, doi: 10.3390/polym14153153.

[126] M. Dobrosielska *et al.*, “Methodological Aspects of Obtaining and Characterizing Composites Based on Biogenic Diatomaceous Silica and Epoxy Resins,” *Materials*, vol. 14, no. 16, p. 4607, Aug. 2021, doi: 10.3390/ma14164607.

[127] K. Choi, M.-C. Choi, D.-H. Han, T.-S. Park, and C.-S. Ha, “Plasticization of poly(lactic acid) (PLA) through chemical grafting of poly(ethylene glycol) (PEG) via in situ reactive blending,” *Eur Polym J*, vol. 49, no. 8, pp. 2356–2364, Aug. 2013, doi: 10.1016/j.eurpolymj.2013.05.027.

[128] S. Singh, A. K. Ghosh, S. N. Maiti, S. Raha, R. K. Gupta, and S. Bhattacharya, “Morphology and rheological behavior of polylactic acid/clay nanocomposites,” *Polym Eng Sci*, vol. 52, no. 1, pp. 225–232, Jan. 2012, doi: 10.1002/pen.22074.

[129] X. Wang, S. Peng, H. Chen, X. Yu, and X. Zhao, “Mechanical properties, rheological behaviors, and phase morphologies of high-toughness PLA/PBAT blends by in-situ reactive compatibilization,” *Compos B Eng*, vol. 173, p. 107028, Sep. 2019, doi: 10.1016/j.compositesb.2019.107028.

[130] S. Tamburaci and F. Tihminlioglu, “Biosilica incorporated 3D porous scaffolds for bone tissue engineering applications,” *Materials Science and Engineering: C*, vol. 91, pp. 274–291, Oct. 2018, doi: 10.1016/j.msec.2018.05.040.